



ISTITUTO ITALIANO  
DI TECNOLOGIA



UNIVERSITÀ DEGLI STUDI  
DI GENOVA

# MiniHyQ- Development of a Lightweight Highly-Dynamic Hydraulic Quadruped Robot

Hamza Khan

University of Genoa, Italy

and

Department of Advanced Robotics  
Istituto Italiano di Tecnologia (IIT)

A thesis submitted for the degree of  
Doctor of Philosophy (Ph.D.)  
April 2015

**Thesis supervisor:**

**Dr. Claudio Semini** (Principle Adviser)  
Advanced Robotics Department  
Istituto Italiano di Tecnologia (IIT)

**Prof. Darwin G. Caldwell**  
Advanced Robotics Department  
Istituto Italiano di Tecnologia (IIT)

Copyright © 2015 by Hamza Khan  
All rights reserved

## Abstract

Legged robots have become a prominent field of robotics in recent years. This may be due to their potential versatility and capability of performing tasks that conventional vehicles are unable to do. Quadrupedalism is often observed in highly mobile terrestrial animals. We find it to be advantageous for mobile robots as well. For this reason, we expect that quadruped robots will be specifically engaged in a variety of tasks where access for humans is not easy or life threatening. The objective of this dissertation is to develop a hydraulically actuated lightweight highly dynamic quadruped robot. Hydraulic actuators have the potential for accurate torque control on a robotic system and have superior power density to their weight and size. This thesis seeks to make the technology for hydraulic control more accessible for smaller robots, as well as to analyze the scalability of construction and actuation on smaller robot form factors. Ultimately, this versatile platform is intended to serve as a tool to deepen the understanding of terrestrial locomotion. This thesis builds upon the work of numerous researchers in the fields of robotics. As mentioned above, this thesis presents the development of the lightweight hydraulic quadruped robot *MiniHyQ*.

Listed below are specific contributions that will be described in this thesis:

- A **lightweight hydraulic quadruped robot-MiniHyQ** with a compact, on-board power pack (shown in Fig. 5.1). A comparison of existing hydraulic quadruped robots has been made (Table 5.1), which demonstrates how MiniHyQ compares to hydraulic quadruped robots. MiniHyQ is around three times lighter than most existing hydraulic quadruped robots. It has almost 30% higher joint torque density (robot mass to joint torque ratio) and 40% wider joint range of motion in leg-sagittal plane comparing to *HyQ* [49].
- An **isogram joint mechanism** is proposed and implemented in the MiniHyQ knee. This enables a larger joint range and allows the optimization of the joint torque curves over the whole range of the linear actuator extension.

- **A study of linear-actuator-based knee joints for the hydraulic legged robots:** The kinematic and torque analysis are done. The isogram mechanism is compared against two traditional knee joint mechanisms (the hinge joint and four bar linkage). We studied the influence of these mechanisms' geometric parameters on the knee joint torque profile and joint range of motion by assuming the same cylinder size in each case.
- **An innovative compact strain gauge-based torque sensor design** is proposed and implemented. We propose a step-by-step generalized design methodology for this sensor, allowing it to be easily modified based on the desired requirements. We show the design's symmetric (clockwise and counterclockwise rotation) and linear behavior through virtual prototyping and experimental tests.
- **A study of actuator sizing for highly-dynamic quadruped robots without whole robot simulation:** The scaling tools are proposed and it helps to estimate torque limits for tasks like the squat jump, static self-balancing, and running trot at various jump heights, payloads, and forward velocities, respectively.

To the author's best knowledge, MiniHyQ is the lightest and smallest hydraulic quadruped robot that has been designed and constructed. MiniHyQ is a fully torque controlled robot and has a wide joint range of motion and an onboard compact power pack. MiniHyQ has nearly the same leg length as the previous robot (HyQ, build by our group), but has constantly changing upper and lower link lengths due to a changeable instantaneous center of rotation of its knee joint. The robot's legs are 15% shorter with knees fully retracted. It weighs only 35kg (24kg with an off-board pump unit), and is portable by a single person. To reach the lightweight and miniaturization we have achieved, miniature hydraulic actuators were carefully selected. This allowed us to reduce the required pump size inside the torso. By using a hydraulic rotary actuator for the hip and linear actuators with isogram mechanism for the knee joint, a wider range of motion is achieved, allowing a self-righting motion.

I would like to dedicate this thesis to my father, Khurshid Anwar Khan, my mother, Rabia Basri, beautiful wife, Mishal Niazi, and daughter, Anaya Khan. Without your love and support, this work would not have been possible.



## Acknowledgements

I used 'we' and 'our' throughout the text while writing this thesis. I strongly believe that the MiniHyQ robot is the result of the hard work of several people, who guided and supported me during the last three years of my PhD course in robotics. I would like start by paying my gratitude to Dr. Claudio Semini for his continuous support throughout my PhD. Without his help and experience in designing and constructing a high-performance platform like HyQ, it would have been hard to bring MiniHyQ into existence. I am sincerely thankful for all his support, time, patience and teaching during my time at the DLS lab. Special thanks to Satoshi kitano for the valuable six months of helping me with the MiniHyQ project and for designing the MiniHyQ's torso and power pack.

Thanks to Prof. Darwin Caldwell for his support and motivation. Michele Focchi, thank you for the help with my various doubts in control and electrical issues and all the great discussions we had. Special thanks to Roy Featherstone for helping me with the isogram mechanism for MiniHyQ's knee joint.

Jake Goldsmith, thank you for the thorough support in mechanical design and for proofreading my papers and this thesis. Thanks to Thiago Boaventura Cunha for his help with the hydraulics and low level control. Dr. Ferdinando Cannella and Mariapaola d'Imperio, thanks for your help on the FEM analyses of the torque sensor. Marco Frigerio Marco, thank you for helping me with software, etherCAT, electronics, debugging, and implementing MiniHyQ in SL. Victor Barasuol, thanks for teaching me control, crazy gain tuning and staying late helping me with experiments. Jonas Buchli, Nikos G. Tsagarakis, Ioannis Havoutis, Stephane Bazeille, Carlos Mastalli, Hiroaki Kuwahara, Tomoo Yoneda, and Jesus Ortiz thanks for the nice conversations and advice. Bilal-Ur Rehman, thank for the valuable company and support throughout. Thanks to Samuel R. Zapolsky and Nawid Jamali for their valuable feedback about this dissertation and proofreading it. Thanks to Marco Cumurri for helping me with debugging the MiniHyQ robot. I would also like to thank our team of technicians Marco Migliorini, Stefano Cordasco, Phil Hudson, Gianluca Pane, Giuseppe Sofia, and Alessio Margan, as well as the whole group of the Advanced Robotics Department of the Istituto

Italiano di Tecnologia. I would like to express my thanks also to all my friends from Genoa; thanks for making my stay pleasant in Genoa.

Last but not least, I would like to particularly thank to my brother Omer, my sister Annie, Arif bahi, Amjid bahi, Mina baji, and all my family for all the affection and happiness you provide me. I sincerely thank my beloved parents for keeping me motivated and for their unconditional love. And my wife Mishal Niazi thanks for your love, care and support. Again I would like to express my deep gratitude to the above mentioned people.

Thank you very much!!

# Table of contents

<b>List of figures</b>	<b>v</b>
<b>List of tables</b>	<b>xi</b>
<b>1 Introduction</b>	<b>1</b>
1.1 Motivation . . . . .	1
1.2 Project Objectives . . . . .	3
1.3 Contributions . . . . .	3
1.4 Outline . . . . .	4
<b>2 Related work</b>	<b>5</b>
2.1 Highly Dynamic Quadruped robots . . . . .	5
2.1.1 Electrically actuated robots . . . . .	5
2.1.2 Hydraulically actuated robots . . . . .	7
2.2 Related Work to Scaling Studies . . . . .	16
2.3 Related Work to Knee Joints for Legged Robots . . . . .	18
2.4 Related Work to Joint Torque Sensor . . . . .	19
<b>3 Scaling and Actuator Selection for Quadruped robot</b>	<b>21</b>
3.1 Robot Specifications and Objectives . . . . .	21
3.2 Scaling tool . . . . .	23
3.2.1 Scaling of the HAA Joint . . . . .	23
3.2.2 Squat Jump . . . . .	26
3.2.3 Running Trot . . . . .	30
3.2.4 The limitations of the scaling tool . . . . .	33
3.3 MiniHyQ Actuator Selection . . . . .	34
3.3.1 Actuators . . . . .	34

3.3.2	MiniHyQ actuator configuration . . . . .	36
3.4	Conclusion . . . . .	37
<b>4</b>	<b>Isogram Knee Joint</b>	<b>39</b>
4.1	Knee Joint Mechanisms . . . . .	39
4.1.1	Hinge joint Knee Mechanism . . . . .	40
4.1.2	Knee Joint Angle $q$ and Joint Torque $\tau$ . . . . .	41
4.1.3	Four bar Knee Mechanism . . . . .	43
4.1.4	Knee Joint Angle $q$ . . . . .	44
4.1.5	Knee Joint Torque $\tau$ . . . . .	46
4.2	Isogram Mechanism Based Knee Joint . . . . .	47
4.2.1	Knee Joint Angle $q$ . . . . .	47
4.2.2	Knee Joint Torque $\tau$ . . . . .	50
4.3	Optimization of Isogram Knee . . . . .	50
4.3.1	Parametric optimization problem . . . . .	50
4.3.2	The Objective Function . . . . .	51
4.3.3	The constraints . . . . .	52
4.3.4	Optimization result . . . . .	52
4.4	HyQ's knee vs Optimized Isogram knee vs Four Bar Knee . . . . .	54
4.5	Conclusion . . . . .	56
<b>5</b>	<b>Design of MiniHyQ</b>	<b>59</b>
5.1	Introduction . . . . .	60
5.2	MiniHyQ's Torso . . . . .	61
5.3	Mechanical Design Of The Leg . . . . .	62
5.3.1	Hip Abduction/Adduction (HAA) . . . . .	63
5.3.2	Hip Flexion/Extension (HFE) . . . . .	64
5.3.3	Knee Flexion/Extension (KFE) . . . . .	65
5.3.4	Leg Configuration on Torso . . . . .	67
5.4	Torque sensor design . . . . .	67
5.4.1	Design . . . . .	68
5.4.2	Simulations . . . . .	70
5.4.3	Validation . . . . .	74
5.5	MiniHyQ Control System . . . . .	75
5.6	Power Pack . . . . .	76
5.6.1	Estimation of required flow rate . . . . .	76

5.6.2	Selection of Servo Valve . . . . .	77
5.6.3	Selection of pump and motor . . . . .	78
5.6.4	Accumulator . . . . .	80
5.6.5	Filter and Oil cooler . . . . .	80
5.6.6	Reservoir . . . . .	81
5.6.7	Manifold . . . . .	81
5.7	Final Design of MiniHyQ . . . . .	82
5.8	Conclusion . . . . .	83
<b>6</b>	<b>Results and Discussion</b>	<b>85</b>
6.1	Experimental testing of First Prototype of Isogram Knee . . . . .	85
6.1.1	First Prototype vs. Final Prototype Isogram knee Joint . . . . .	85
6.2	Experimental testing of final version of MiniHyQ Leg . . . . .	87
6.3	Experimental validation of Torque Sensor Design . . . . .	88
<b>7</b>	<b>Conclusion and Future Work</b>	<b>91</b>
7.1	Conclusion . . . . .	91
7.2	Future Work . . . . .	92
<b>Appendix A</b>	<b>Publications</b>	<b>95</b>
<b>Appendix B</b>	<b>Definition of Joint Frames</b>	<b>97</b>
<b>References</b>		<b>99</b>



# List of figures

2.1 StarlETH robot . . . . .	6
2.2 Mit cheetah . . . . .	7
2.3 Early version of BigDog . . . . .	8
2.4 Upgraded version of BigDog . . . . .	9
2.5 A picture of Legged Squad Support Systems . . . . .	9
2.6 WildCat robot . . . . .	10
2.7 A snapshot of Spot Robot . . . . .	11
2.8 Scalf-1 robot . . . . .	11
2.9 Jinpoong robot . . . . .	12
2.10 Babyelepnt . . . . .	13
2.11 HyQ robot side view . . . . .	14
2.12 HyQ Blue . . . . .	15
2.13 Block diagram of HyQ low level control . . . . .	15
2.14 A family of the Boston Dynamics quadruped robots . . . . .	17
3.1 Kinematic Structure of the leg . . . . .	22
3.2 Simplified Robot Model . . . . .	24
3.3 The leg-sagittal plane view . . . . .	24
3.4 Plot of HAA joint . . . . .	25
3.5 Sketch of the robot during a vertical jump motion . . . . .	26
3.6 Sketch of side view of HyQ in squat posture . . . . .	28
3.7 Plot of experimental data . . . . .	29
3.8 Plot of experimental data . . . . .	30
3.9 Plot of maximum knee joint power . . . . .	31
3.10 (a) A quadruped robot with the equivalent virtual spring (connected to CoM) represents the virtual linear spring of a diagonal pair of legs. . . . .	32
3.11 A CoM trajectory (purple solid) of the legged robot during a running trot. .	32

3.12 A CoM trajectory (purple solid) of the legged robot during a running trot represented by the SLIP model. . . . .	33
3.13 Plot of stable SLIP parameters (Spring Stiffness and Angle of Attack) for different leg segment lengths and forward velocities at robot mass 73kg. . . . .	34
3.14 Plot of maximum hip joint torque scaled by BW . . . . .	35
3.15 Commercial motor . . . . .	36
4.1 Cylinder minimum eye-to-eye length . . . . .	40
4.2 Drawing of HyQ's Leg . . . . .	40
4.3 Traditional knee mechanism . . . . .	41
4.4 The influence of design parameter $L_{23}$ . . . . .	42
4.5 The influence of design parameter $L_{23}$ . . . . .	43
4.6 Hinge knee mechanism torque profile . . . . .	43
4.7 Traditional knee mechanism . . . . .	44
4.8 The influence of design parameter $L_{03}$ . . . . .	44
4.9 The influence of design parameter $L_{03}$ . . . . .	45
4.10 Four bar based knee mechanism . . . . .	45
4.11 Four bar based knee mechanism . . . . .	46
4.12 Schematic representation of the isogram mechanism applied to a legged robot's knee joint. The joint is shown in the fully extended configuration (joint angle $q = 0^\circ$ ). . . . .	47
4.13 Isogram mechanism: close-up view of the first half of the mechanism to illustrate angle $q_1$ . . . . .	48
4.14 Isogram mechanism: close-up view of the second half of the mechanism to illustrate angle $q_3$ . . . . .	49
4.15 Isogram mechanism: close-up view of the cover link. . . . .	51
4.16 ( <i>left</i> ) Isogram knee joint torque profile with respect to knee angle; ( <i>right</i> ) knee joint angle vs. piston position; where the blue solid line indicates the optimized results; the red dot dashed line is the result of an initial guess based on trial and error method; the green dashed line shows the quadratic function $q_l$ with respect to piston position. . . . .	54
4.17 Plot of experimental data of HyQ (red solid), simulated data (black dashed) for a squat jump motion of 0.2m jump height, where simulated data (blue dashed) is at 0.3m jump height. <i>Top</i> : knee joint angle; <i>middle</i> : knee torque; <i>bottom</i> : total ground reaction force. (Figure modified from [50]) . . . . .	55

4.18 Shows the comparison of the effective lever arm between HyQ's knee joint and scaled optimized isogram knee joint during knee extension . . . . .	56
4.19 Shows the comparison of the effective lever arm between HyQ's knee joint, four bar, and scaled optimized isogram knee joint during knee extension . . . . .	57
5.1 MiniHyQ picture . . . . .	61
5.2 MiniHyQ's Torso CAD . . . . .	62
5.3 CAD model of MiniHyQ Leg . . . . .	63
5.4 CAD model of HAA joint . . . . .	64
5.5 Torque profile of HAA joint . . . . .	64
5.6 CAD model of HFE . . . . .	65
5.7 The CAD model of MiniHyQ KFE joint. . . . .	65
5.9 Isogram knee joint torque profile . . . . .	66
5.10 Leg configurations of MiniHyQ with forward walking direction to the right:(a) forward/backward; (b) backward/forward; (c)backward/backward; (d) forward/forward. . . . .	67
5.11 A drawing of easily customizable and compact strain gauge based joint torque sensor. Smooth surfaces show where strain gauges are to be glued on both wings. . . . .	68
5.12 Torque Sensor with ( <i>left</i> ) four spokes; ( <i>right</i> ) two spokes. . . . .	69
5.13 Drawing of Torque Sensor. ( <i>left</i> ) CAD drawing, ( <i>right</i> ) Strain Gauges Positions	70
5.14 Simulated strain with counter clockwise . . . . .	70
5.15 Simulated strain with clockwise . . . . .	71
5.16 Finite Element Model: (top left) the contact constraint between the Sensor and the case, (top right) the fix constraint, (bottom left) the applied torque, (bottom right) the mesh. . . . .	72
5.17 The Simulated Von Mises Stress at maximum load (60Nm) demonstrates that the maximum stress value of Torque Sensor is more than 25% under the yield point (260MPa). . . . .	72
5.18 Relationship between the Torque and the Strain depending on the Material . . . . .	73
5.19 Relationship between the torque and the Strain depending on the Size Scale parameter: the 25% of variation influences Torque Sensor behavior. The reduction increases more than double the strain and the increment of the scale reduces it about an half. . . . .	74

5.20 Relationship between the torque and the strain depending on the Wing Width parameter: the 25% of variation is almost negligible. It is possible to notice that the reduction of the width has more influence than the increment. . . . .	74
5.21 Relationship between the torque and the strain depending on the wing thickness parameter: the 25% of variation influences torque sensor behavior. The reduction increases more than 40% the strain and the increment of the thickness reduces it about that 25%. That means the width reduction has more influence than the width increment. . . . .	75
5.22 Experimental result vs FEM . . . . .	75
5.23 MiniHyQ's control system architecture . . . . .	76
5.24 Schematic of a hydraulic system. . . . .	77
5.25 CAD model of MiniHyQ Power pack. . . . .	77
5.26 Estimated flow rate, blue line shows the total required flow rate of the robot for a running trot, red dotted line shows the total required flow rate for a squat jump, and the black line shows the average flow rate while running trot. . . . .	78
5.27 Picture of Micro Pump. . . . .	81
5.28 MiniHyQ's centralized manifold. . . . .	82
5.29 MiniHyQ CAD model . . . . .	83
5.30 Self-righting sequence, front view. From 1 to 6: After a fall, the robot lies on its top. To right itself, the robot first has to move the feet of the two legs at one side and push to the ground up to turn its torso. The HAA will then rotate to push the robot up until the Center of gravity (CoG) passes the pivot point of the frame. As a consequence, the robot will then roll back onto the bottom of the torso. The retracted legs will then extend to move the robot back onto its feet. . . . .	84
6.1 Hardware implementation. <i>Left:</i> Side view of the <i>isogram mechanism</i> based knee joint; <i>center:</i> close up view of load cell and encoders; <i>Right:</i> Experimental setup for performing push ups. . . . .	86
6.2 Plot of experimental measured data of isogram knee (red solid), reference data (black dashed) for push ups at 0.5Hz (with 12Kg payload). <i>Top:</i> knee joint angle; <i>middle:</i> knee velocity; <i>bottom:</i> Hip joint angle. . . . .	86
6.3 Picture sequence of the prototype leg during an experiment that moves the knee joint from extended to a completely retracted position. . . . .	87





# List of tables

2.1 Specifications of HyQ Robot . . . . .	16
2.2 A comparison of Hydraulic Quadruped Robots . . . . .	16
2.3 List of estimated locomotion parameters based on body weight . . . . .	18
3.1 Samll size commercial rotary motors specifications . . . . .	35
3.2 A List of Commercial Hydraulic Cylinders . . . . .	37
4.1 Optimized Design Variables . . . . .	53
5.1 A comparison of Hydraulic Quadruped Robots . . . . .	60
5.2 Simulations Plan . . . . .	70
5.3 Simulations Plan . . . . .	71
5.4 MiniHyQ Power Pack . . . . .	78
5.5 Miniature Hydraulic valves comparison . . . . .	79
5.6 Specifications of MiniHyQ Robot . . . . .	82



# **Chapter 1**

## **Introduction**

Nature can provide excellent examples of agility and balancing in locomotion, as seen in legged animals. Quadrupeds are good at balancing and moving on rough terrain and they have powerful legs that help them perform motions, like bounding and jumping. This inspired the emergence of legged robots as a prominent field of robotics in recent years. It is mostly due to the expected versatility and capability of legged robots performing tasks which conventional vehicles are unable to do. However, recently developed legged robots, lack the versatility of performing both precise navigation over rough terrain and the strong, fast motions that are necessary for dynamic tasks such as jumping and running. Furthermore, most high-performance legged robots are bulky and are thus difficult to work with. In order to advance research faster, legged robots must become more manageable. This way dynamic experiments can be performed faster and more easily. The simplest way to achieve this goal is by reducing the size and weight of the robot. Currently, it is still an area of great interest for designers to build a portable, highly dynamic and versatile quadruped robot capable at remaining fast on all terrain.

The next section describes the motivation of this thesis, which includes why do we need to build a medium size of highly dynamic hydraulic quadruped robot and what are its benefits.

### **1.1 Motivation**

Traditionally, electrically actuated legged robots suffer during highly-dynamic tasks due to the electric motors limitations. These motors tended to provide a small torque relative to their size and weight. In order to increase the torque, reduction drives were used with high ratios, which in turn reduced the maximum joint velocity. Systems such as these struggle

with motion on uneven terrain due to the high, near instant, torque peaks that tended to be generated during footfall. Exceeding the maximum torque limit eventually results in the breakdown of the gears. To avoid these peak forces, designers normally add passive spring assemblies in series to reduce the joint stiffness. Series elastic actuation (SEA) can also be used to measure the joint torque through the displacement of the spring. By tuning the stiffness of SEAs offline they can be used effectively for running robots [22, 24] but the inherent elasticity of SEA significantly reduces the closed loop control bandwidth [51]. Currently, there are very few electrically actuated quadruped robots exist that are capable of performing fast and powerful motions. The MIT cheetah [52] is a recent example that performs tasks like running and jumping. To achieve this they used high power, low geared electromagnetic motors with proprioceptive force control. Another common actuation method is pneumatic which allows low passive impedance; however, it is restricted to low control bandwidth [11].

Hydraulic actuation, on the other hand, is much more robust against impacts, allowing high-bandwidth control and the application of very large forces. For these reasons, most mainstream dynamic legged robots like HyQ [49] and the robots from Boston Dynamics (BigDog [44], LS3, Cheetah and ATLAS) use hydraulics. However the conventional hydraulic quadrupeds are currently facing four main issues.

- The existing hydraulically actuated quadruped robots tend to be bulky and it is clearly showed in a comparison made in Table 2.2 (discussed later in Chapter 2). This makes it difficult to conduct experiments with hydraulic quadruped robots. In addition, appropriate safety procedures require a large number of people.
- Many commercial hydraulic components are focused on heavy industrial applications, for example excavators and bulldozers. Small scale hydraulics are still largely absent from the mainstream hydraulic industry and can normally only be found in niche markets.
- Hydraulically actuated robots need a pump to provide oil pressure. In the case of BigDog [44] and JINPOONG [32], a combustion engine is used to actuate the pump inside the torso. However when using a combustion engine it is difficult to conduct experiments indoors, because of the noise and the exhaust fumes. Normally for indoor experiments, an external electric pump is used to supply hydraulic power to the robot by means of two hydraulic hoses. These hoses can negatively affect the dynamics of the robots causing unpredictable disturbances and restricting the working range of the robot to remain inside a circumference around the pump.

- The existing legged hydraulic robots often lack versatility to perform a wide range of different motions. Limited joint range of motion and torque limits are the key limitations. From our experience with HyQ, for example during one of our recent experiments where HyQ walked over obstacles with planned footholds in a 3D map [61], when stepping onto a pallet, stairs, or over obstacles, the limited hip joint range made it too difficult to retract the leg enough to avoid collisions.

The motivation for this work arose from the experience of our group (the DLS lab) with the quadruped robot HyQ[49]. The desire to resolve the above issues, whilst maintaining the abilities of a high performance platform, led us to build a lightweight hydraulic quadruped robot.

## 1.2 Project Objectives

The goal of this project is the development and evaluation of a small hydraulically actuated quadrupedal robot, MiniHyQ. The development of a smaller version of the current HyQ is done using smaller actuators, lighter materials, etc., but it will also be robust and easily portable. MiniHyQ will be the first torque-controlled versatile robot of this size that will be able to walk, climb over rough terrain, jump and run. A lighter and smaller version is much easier to work with and is therefore expected to become attractive for many research groups in the world. Future European projects might use MiniHyQ as a common platform to test their controllers, high-level locomotion algorithms, biomechanic hypothesis, etc. The design of the MiniHyQ platform is based on the experiences gained from HyQ and through modeling and simulation.

## 1.3 Contributions

The main contributions of this work are:

- The development of a lightweight hydraulic quadruped robot MiniHyQ with a compact on-board power pack (shown in Fig. 5.1). To the author’s best knowledge, MiniHyQ is the lightest and smallest hydraulic quadruped robot that has been built so far. A comparison of existing hydraulic quadruped robots has been made (Table 5.1), demonstrating how MinihyQ compares against the rest of the existing hydraulic quadruped robots. MiniHyQ is around 3 times lighter than most of the existing hydraulic quadruped

robots. It has almost 30% higher joint torque density (robot mass to joint torque ratio) and 40% wider joint range of motion in leg-sagittal plane comparing to HyQ.

- A special knee joint mechanism ( an *Isogram Mechanism*) is proposed and implemented in the MiniHyQ's knee. This enables a larger joint range and allows the optimization of the joint torque curves over the whole range of the linear actuator extension.
- The linear actuator based knee joints for the hydraulic legged robots are studied. The kinematic and torque analyses are done. The isogram mechanism is compared with two traditional knee joint mechanisms ( the hinge joint and four bar linkage). We study the influence of these mechanism's geometric parameters on the knee joint torque profile and joint range of motion by assuming the same cylinder size in each case.
- An innovative compact torque sensor design is proposed and implemented. A step by step generalized design methodology is proposed for this sensor. One can easily modify it as per desired requirements.
- We present a study of actuator sizing for highly-dynamic quadruped robots without the need of whole robot simulation. The scaling tools are proposed and it helps to estimate torque limits for tasks such as squat jump, static self-balancing, and running trots at various jump heights, payloads, and forward velocities, respectively.

## 1.4 Outline

This thesis is structured as follows: Chapter 2 presents the state of the art of highly dynamic legged robots with focus on the hydraulically actuated quadruped robots. Chapter 3 presents the specifications of the MiniHyQ robot, the scaling of quadruped robots, and actuator selection based on proposed scaling studies. Chapter 4 describes the Isogram mechanism based knee joint and compares the Isogram knee joint with the traditional knee joints. Chapter 5 explains the design of the MinihyQ robot. The custom designed torque sensor and MiniHyQ's on-board hydraulic system design are also discussed in Chapter 5. Chapter 6 shows the results of the experiments that were performed with the prototype legs. Chapter 7 concludes this dissertation and gives directions for future work.

# **Chapter 2**

## **Related work**

The area of legged robots research is very vast. Since it is not possible to give an exhaustive reference to all the work done, we focused mostly on the highly dynamic hydraulically actuated quadruped robots and give a detailed overview of existing contributions related to this project. This Chapter starts with describing the existing dynamic quadruped robots. We divide the literature into electrically actuated and hydraulically actuated quadruped robots. Since this dissertation describes the design of medium-size legged robot, the state-of-the-art of hydraulically actuated quadruped robots emphasizes on the weight and the size of the robots. The scaling studies and implementation of a special mechanism-based knee joint are the one of the main contributions of this work. Its related works are also described in this chapter. This chapter ends with a literature overview of strain gauge based torque sensors.

### **2.1 Highly Dynamic Quadruped robots**

Here, we consider highly dynamic quadruped robots as a four legged machines that can jump, walk, and run on different types of terrain. Mostly available dynamic quadruped robots are hydraulically actuated; however, but their electrically actuated impressive examples do exist.

#### **2.1.1 Electrically actuated robots**

Conventional electric motors are not most favorable at directly actuating a joint of highly dynamic quadruped robots, mainly due to their low output torque and necessity of reduction gears. However, it can be used by adding springs to the joints, which is done by several robots to achieve dynamic motion. The StarlETH [23] robot is a recent example of such a robot.

### Springy Tetrapod with Articulated Robotic Legs (StarlETH)

Figure 2.1 shows the StarlETH [23] robot and its dimensions. It has four identical legs that are arranged in an X configuration. Every leg has a total of 3 degrees of freedom. It is as big as a medium-sized dog and it weighs of 26 kg. This robot is driven by high compliant series elastic actuation that makes it torque controllable and robust against impact. Besides series elastic actuation, StarlETH also uses a chain transmissions to drive the knee joint. This is one of the weak points of this robot's mechanics.

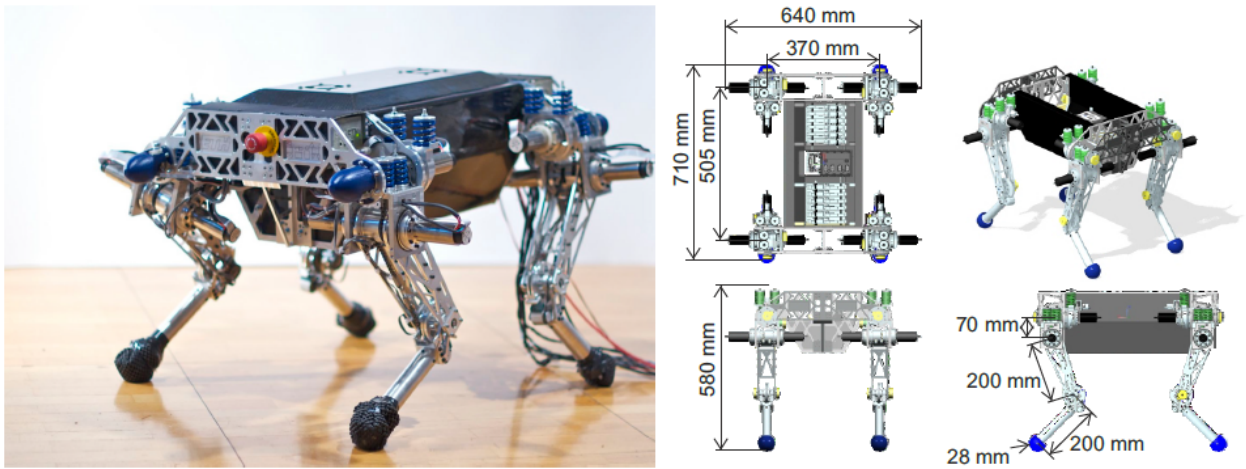


Fig. 2.1 StarlETH robot and its dimensions [23]

### MIT Cheetah

The MIT Cheetah's latest version is one the most impressive electric robots ever built in recent times. The MIT Biomimetic Robotics Laboratory named this version as MIT Cheetah Version 2 (shown in Fig. 2.2 (right)) and it is successor of its first version shown in Fig. 2.2 (left). The look of robot is like a *Cheetah*. The heart of Cheetah Version 2 is a custom high-torque-density electric motor, with amplifiers. These allow the Cheetah Version 2 to maintain balance on uneven ground without the use of force sensors. Researchers developed a custom designed three phase permanent magnet synchronous motor which is optimized for torque density (gap radius: 48.5 mm, torque constant: 0.6 Nm/A, weight: 1kg). The motor drivers are able to drive a three phase motor at a peak of 60 A from a supply of 100 V. The architecture of the motor driver is designed to act as a bidirectional buck boost converter [12]. It has 4 legs, each is programmed to exert a defined amount of force, in order to maintain a given speed: the faster the desired speed, the more force must be applied.

Thus, it allows the Cheetah Version 2 to run as fast as it does not by simply cycling its legs faster, but rather by generating more force in the fraction of a second when the robot's foot makes contact with the ground. MIT, were able to get their Cheetah to sustain speeds of 10 mph in indoor environments. Indoor track tests showed that the Cheetah could jump over a hurdle and continue running successfully. It was supposed to be able to reach 30mph in outdoor environments, uneven grassy terrain without any external support. To achieve a high

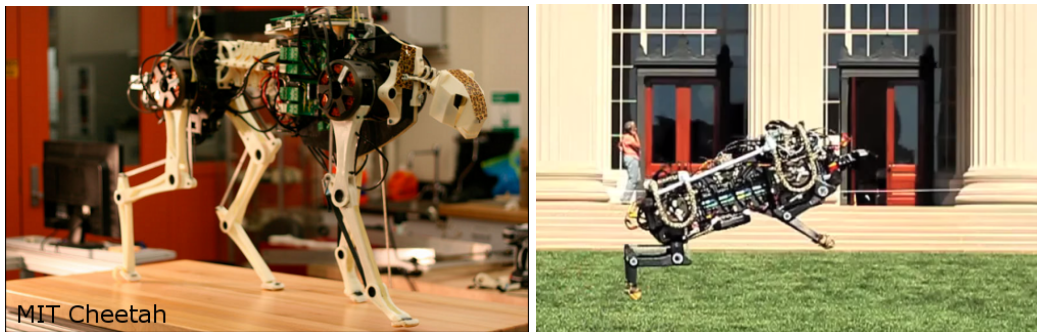


Fig. 2.2 Side view of the MIT Cheetah Robot.

running speed, the robot needs to have a high stride frequency and low a duty factor [35]. For better performances researchers decrease the individual leg inertia of the robot. To this end, the authors implemented the tendon-bone co-location architecture in the Cheetah robot in order to reduce the inertia of the legs [52]. This architecture makes effective use of the relative advantages of each part to achieve a strong and light structure. Thus, a Kevlar tendon was integrated into the design of the MIT Cheetah leg, linking the foot to the knee. Real experiments show that this architecture reduces the stress experienced by the bone during a stride by up to 59% [52]. The bone structure of the robot's leg also draws inspiration from biological structures. This is carried out by having a rigid and light polyurethane foam-core for the leg covered in a high stiffness polyurethane resin to form a composite with high strength but low inertia.

### 2.1.2 Hydraulically actuated robots

No doubt the recent development in high-torque-density electric motors has allowed the electric robots to compete with the hydraulically actuated robots. However, electric robots still have to cover the performance gap that is already set by strong and highly dynamic hydraulically actuated legged robots in recent years.

## BigDog

In 2005, the Boston Dynamic Inc. presented the first hydraulically actuated quadruped robot named as BigDog (Figure 2.3). The robot was 1m long, 1m tall and 0.3m wide, and it weighed 90kg. The robot had four legs each one had 4 DOFs; three were active rotational joints actuated by hydraulic cylinders and one was a passive linear joint in the foot based on a pneumatic spring. Boston Dynamics presented the BigDog robot with a new leg configuration in 2006 (shown in Fig. 2.4). In the new configuration, the front and hind knees pointed to each other, while the initial knees of the 4 legs were pointed to the front. The change was to increase the stability of the robot. Moreover, this allowed the robot to reach a velocity of 1.8m/s with a 25 degrees of inclines and walk over loose rock beds at a velocity of 0.7m/s while carrying of a payload of 50 kg.



Fig. 2.3 Early version of BigDog climbing a hill.

BigDog demonstrated a variety locomotion behaviors. It could stand, squat, do a crawling gait that lifted one leg at a time, walk with a trotting gait that lifted pairs of diagonal legs, trot with a running gait that included a flight phase, and bound in a special gallop gait. BigDog had about 50 sensors. For instance, inertial sensors measured the body's acceleration and the attitude, while joint sensors measured force and motion of the actuators. The on-board computer integrated all information coming from these sensors to provide accurate estimations of motion in the environment. Other sensors monitored BigDog's homeostasis: flow and temperature, hydraulic pressure, engine speed, and temperature.



Fig. 2.4 Upgraded version of BigDog.

### **Legged Squad Support Systems (LS3)**

The Legged Squad Support Systems (LS3) is shown in Fig. 2.5. It is also known as *AlphaDog*. It is a military robot that was developed by Boston Dynamics and like BigDog it was also funded by DARPA. LS3 is a rough-terrain robot that is designed to go anywhere marines and soldiers go on foot. It is meant to be of help in carrying their loads. Each LS3 can carry up to 400 lbs of gear for a mission of 20-miles long and a duration of 24 hours. LS3 is designed to automatically follow its leader using computer vision algorithms, thus it does not need a dedicated driver or tele-operators. In addition, it can travel autonomously to specific locations using GPS and terrain sensing. Continued work is being made to make the LS3 more mobile, like traversing a deep snow-covered hill, or avoiding bombs and gunfire on the battlefield.



Fig. 2.5 A picture of Legged Squad Support Systems (LS3).

The objective behind creating this robot was to develop an unmanned robotic platform to transport soldier equipment and charge batteries for their electronic gear. Requirements for the vehicle are to carry 1000 lb (450 kg) of gear, equal to the amount a nine-man infantry squad would need on a 72-hour motion. Cubic volume is seen as more of a problem for load-carrying unmanned vehicles, as their center of gravity changes when more gear has to be stacked. It has to travel 4 km/h for eight hour marches and speed up in bursts of up to 38 km/h for 200 meters. The vehicle needs to traverse forward and backward on slopes of up to 30% and descend on slopes of 60%.

### **WildCat**

Initially in late 2012, Boston Dynamics showed off Cheetah — a tethered quadruped robot that was capable of running at 28 mph (45 kph). Later on October 3, 2013, an untethered version, called WildCat was shown to be galloping around outside. It is seen in Fig. 2.6). WildCat, can run at 16 mph (26 kph), tested in an outdoor environment.

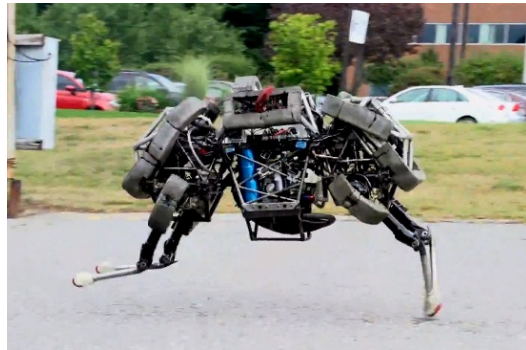


Fig. 2.6 A snapshot of WildCat while in an outdoor testing.

The BigDog (as one can see from online videos) is tuned for torque and stability, while, the WildCat is tailored towards pure speed. The ultimate goal is to produce a four-legged robot that is able to run at speeds of up to 50 mph on “all types of terrain”.

### **Spot**

Spot is the latest quadruped robot from Boston Dynamics, since it was purchased by Google back in 2013. Spot is 74kg robot that can navigate on a large variety of terrain. Two Spot robot's are shown in Fig. 2.7 and this robot is the fourth iteration of Boston Dynamics that started with BigDog just over 10 years ago. What we can see from the online video of Spot is that it is slightly smaller from BigDog but its exact sizing dimensions are not published

yet. It is also shown that Spot has the ability to withstand strong kicks, trot, and easily climb stairs.



Fig. 2.7 A snapshot of Spot while in an outdoor testing.

### **Scalf-1**

Fig.2.8 shows the Scalf-1 robot [46], developed by Shandong University, China. It has four legs. Each leg has two pitching rotary joints and a rolling rotary joint. All the joints are actuated by identical linear hydraulic servo cylinders. Each is composed of a single rod cylinder, one servo valve, two pressure sensors and one displacement sensor.



Fig. 2.8 Scalf-1 robot while testing.

The Scalf-1 weighs around 65 kg without a power pack. Its length, width, and height are 1 m × 0.4 m × 0.68 m respectively. The number of DOFs in each leg is 3 and all are active hydraulic actuators. The hydraulic pressure is about 21 MPa. The optimal stride frequency ranges from the value of 1Hz to 3Hz. Scalf-1 can walk with maximum load about of 120 kg at a maximum forward velocity of 1.5 m/s on flat ground.

### Jinpoong

Jinpoong [32] is a quadruped walking robot (Fig. 2.9) and it was developed by the Korea Institute of Industrial Technology, South Korea. The idea of this robot is for it to have dynamic motion such as carrying and moving a heavy load on a rough terrain. It has 4 legs in total 16 DOF, so each leg is designed to 4 DOF to utilize a broad workspace when walking on a rough terrain like an uneven surface. The size of the robot was chosen in order to consider the height of a person, speed, mobility and capability of transporting a relatively heavy load. The size of the robot is about 1.2 m in height, 0.4 m in width and 1.1 m in length, and the robot's weight is around 120 kg. It is slightly bigger and heavier than BigDog.

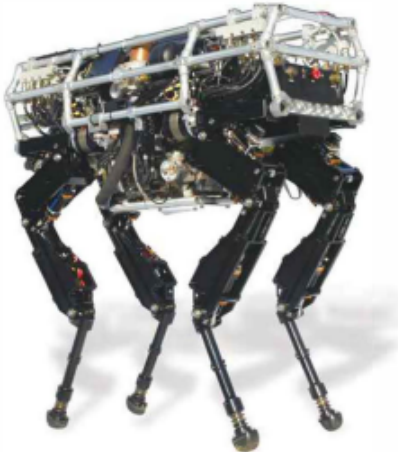


Fig. 2.9 Jinpoong robot.

It has designed a two-stroke cycle engine power pack to supply a maximum of 35 L/min at 21 Mpa. The robot's legs are constructed by linear hydraulic actuator on the hip by rolling joint and linear hydraulic actuator and on the hip, knee, and foot by a pitching joint. In the earlier version of the legs, the rotary hydraulic actuator is fixed on each joint so the mass distribution and spread over all the leg. In contrast, the new design of the leg has hydraulic actuators placed on the upper leg. Therefore, the lower part of the legs becomes much lighter. This design allows the overall center of gravity to be inward so that it is more stable and less affected by the dynamic effects while its swinging legs.

### Baby Elephant

Baby Elephant [17] (seen in Fig. 2.10) is designed to have heavy load capability and an elephant-like appearance. The robot has four legs, each leg is a serial-parallel hybrid mechanism. Considering the sagittal plane, the leg is a kind of parallel mechanism consisting

of two symmetrical crossed limbs. Each leg is constructed by three active DOFs, that are controlled by three hydraulic actuators fixed on the hip. In order to reduce the impact of the energy springs are attached to each leg. It is possible to estimate the ground forces by using the pressure sensors on hydraulic actuators. Legs developed for this robot have neither actuators nor sensors on the end part of the legs, as compared to serial mechanisms. This helps to protect the electronic circuit while walking on marshy terrain.



Fig. 2.10 Picture of the Baby Elephant robot.

Researchers have developed a new type of hydraulic actuator named the “Hy-Mo” to be used for this robot. It is a hydraulic actuator controlled by micro-motor simplified hydraulic system (it does not need filters, coolers, accumulators, or oil tanks). Its main principle is that the motion of the hydraulic cylinder is controlled by the motor while its power is supplied by hydraulic system. Through an inner mechanical feedback, servo motors control the opening of the valves, which is proportional to the piston velocity. Several trot experiments were carried out using “Baby Elephant” equipped with a Li-ion battery to supply the power. The robot’s net weight is about 130kg and it can carry a payload of 30kg and can reach a maximum speed of 1.8 km/h. The static gait experiment with the load given above was also conducted, which demonstrates that the robot can perform walk on different types of terrain, with a maximum load of 100kg. This robot is not joint force controlled yet.

## HyQ

HyQ is a quadruped robot developed at the Advanced Robotics Department of the Istituto Italiano di Tecnologia (IIT) [49]. The robot is about 1m long, weighs 80kg and is constructed with aerospace-grade aluminum alloy and stainless steel. More specifications are illustrated

in Table 2.1 . The robot has demonstrated its various abilities of motion ranging from highly dynamic motions like running and jumping, to careful walking over rough terrain. A side view of the robot is shown in Fig.2.11. It is a fully torque-controlled HyQ robot and has



Fig. 2.11 HyQ robot side view

four legs, each one has 3 joints (active DOFs) actuated by hydraulic cylinders and motors. The joints are controlled in position and force using high-performance Formula 1 Moog valves, which allows a smooth interaction of the hip abduction/adduction (HAA) joint, the hip flexion/extension (HFE) joint, the knee flexion/extension joint (KFE), and feet with the ground. High-speed servovalves connected to hydraulic asymmetric cylinders are used to actuate the HFE and KFE joints. These joints provide high speed and torque for motions in the robot sagittal-plane. In early versions of the HyQ robot, high-torque DC brushless electric motors are used in combination with a harmonic drive (e.g., reduction ratio of 1:100) to control the HAA joints. However, later the HAA electric motors are changed with hydraulic rotary motors.

HyQ is one of very few robots that has demonstrated such a wide range of behavior. Moreover, a version of this robot was sold to ETH Zurich in 2013. It is known as HyQ blue, as shown in Fig. 2.12.

Potential applications are targeted by this robot such as search and rescue, forestry technology, and construction. Figure 2.13 shows the low level control architecture of the HyQ for active compliance control [9].

The experience of our group (the DLS lab) with HyQ [49] was fundamental in building the MiniHyQ robot.

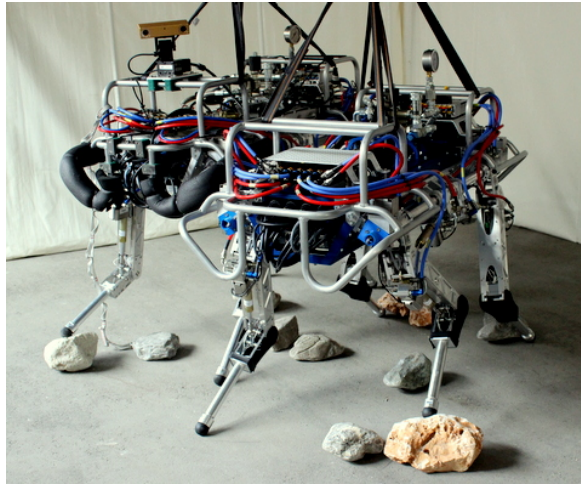


Fig. 2.12 A snapshot of HyQ Blue bought by ETH Zurich with HyQ in background.

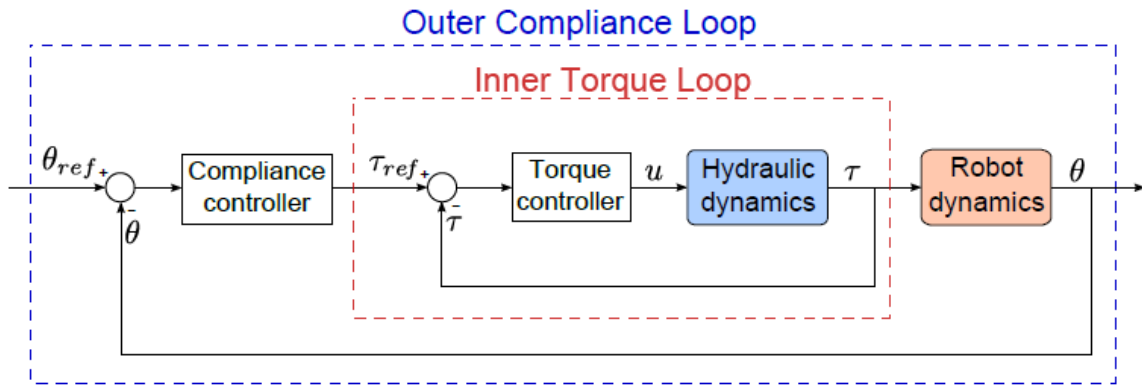


Fig. 2.13 Block diagram of HyQ low level joint control. [9]

## Summary

It is clearly noticed that since Boston Dynamics demonstrated their hydraulically actuated quadruped robot BigDog [44], the development of hydraulically actuated robots has been extensive [17], [46], [32], [25]. In Table 2.2 we show a comparison between the existing hydraulic quadruped robots. All are large and heavy. Only Jinpoong and BigDog have 4 DoF while of hydraulic quadruped robots exhibit 3 DoF per leg. The exact physical dimensions of the WildCat robot or any of Boston Dynamic robot are unpublished. We can only get an idea from the online videos published by Boston Dynamics. Figure 2.14 shows a family of Boston Dynamics quadruped robots and it gives a clear idea of the physical size each of robot relative to each other.

Table 2.1 Specifications of HyQ Robot

Dimensions (LxWxH) (Fully stretched legs)	1m x 0.5m x 1m
Weight (off-board/ Power Pack)	80kg
Degrees of Freedom	12 (3 per leg (2-linear 1-rotary hydraulic actuator))
Joint Torque/ Range of motion	120 Nm, 120° Hip AA 145 Nm, 120° Hip FE 145 Nm, 120° Knee FE
Sensors per Leg	2 Load cells, 1 Torque sensor 3 absolute/relative encoders
Hydraulic Valves	12 High performance servo valves
On-board Computing	1 computer (real time Linux)
Operating Pressure	16 MPa

Table 2.2 A comparison of Hydraulic Quadruped Robots

Name	Mass (offboard, onboard pump)	Dimensions (LxWxH)	DoF ( per leg)	Joint Torque Controlled
SCalf [46]	78kg,123kg	1.1m x 0.49m x 1m	3	Yes
HyQ [49]	75kg,98kg	1m x 0.5m x 1m	3	Yes
Baby Elephant [17]	90kg,130kg	1.2m x 0.6m x 1m	3	No
BigDog [44]	N.A,110kg	1.1m x 0.4m x 1m	4	Yes
JINPOONG [32]	80kg,120kg	1.1m x 0.4m x 1.2m	4	No
RLA-1 [25]	60.2kg,N.A	1.1m x 0.67m x 1m	3	No
LS3	N.A	Bigger than BigDog	3	N.A
Wildcat	N.A	N.A	3	N.A
Spot	N.A,74kg	Smaller than BigDog	3	N.A

## 2.2 Related Work to Scaling Studies

In the early 1980's in the field of applied zoology, a number of experiments were conducted to study the dynamic similarities in quadruped mammals [2–4]. The hypotheses formulated by these studies lay out the preliminary bio-inspired sizing guideline for the legged robot designers. Alexander[2] found that the legged animals of different sizes tend to move in



Fig. 2.14 A family of Boston Dynamics quadruped robots. The exact physical dimensions are not published for any of Boston Dynamic robot: we can only get an idea from the online videos published by Boston Dynamics. From right to left LS3: WildCat, BigDog, Spot, and LittleDog (the electric robot on the blue pillar)

dynamically similar fashion whenever their Froude numbers<sup>1</sup> are equal. In the light of the concept of dynamic similarity, it is also predicted that the geometrically similar animals of different sizes exhibit equal duty factors and equal relative stride lengths, when they are traveling with equal Froude numbers [4, 6]. To use these biologically inspired criteria for a legged robot design, a quadruped robot designer needs to solve an optimization problem by taking care of desired goals of the machine. Some biologically inspired criteria are useful to define robot specifications and design parameters such as Heglund and Taylor studied how speed and stride frequency change with body size [21]. They observed animals from 0.030kg mice to 200kg horses on a treadmill. They measured their speed and stride frequencies at so-called equivalent speeds for trotting, trot-gallop transition, and gallop. Table 2.3 lists the estimated forward speeds and stride frequencies for different body weights according to the estimation of [21].

Similar studies were conducted for the electric DC motor sizing of a bounding robot[13] and a hopping monopod robot[20]. However, these studies were limited to quadruped robots

<sup>1</sup>The Froude number is a dimensionless ratio used to study trends in animal gait patterns where the gravitational forces are important[15] and it is defined as  $\frac{v^2}{gh}$ , where  $v$  is forward velocity,  $g$  is the acceleration of free fall and  $h$  is the height of the hip joint from the ground.

Equivalent Speed	20kg	30kg	40kg	50kg	60kg	Unit
Minimum trotting speed	1.25	1.38	1.48	1.57	1.64	$\frac{m}{s}$
	1.84	1.78	1.73	1.70	1.67	$\frac{1}{s}$
Preferred trotting speed	2.12	2.32	2.47	2.60	2.70	$\frac{m}{s}$
	2.27	2.15	2.07	2.01	1.97	$\frac{1}{s}$
Trot-gallop transition speed	2.94	3.21	3.42	3.56	3.73	$\frac{m}{s}$
	2.67	2.51	2.41	2.33	2.27	$\frac{1}{s}$
Preferred galloping speed	4.71	5.06	5.32	5.53	5.71	$\frac{m}{s}$
	2.78	2.61	2.50	2.41	2.34	$\frac{1}{s}$
Maximum sustained galloping speed	6.29	6.75	7.10	7.39	7.63	$\frac{m}{s}$
	2.89	2.71	2.58	2.49	2.42	$\frac{1}{s}$

Table 2.3 List of estimated locomotion parameters for equivalent speeds based on body weight, according to [21].

with telescopic legs or a specific type of actuator. Another scaling study is done for the Oncilla-robot (a slightly bigger version and successor of CheetahCub-robot) [55] but the study is only limited to pantograph-based leg quadruped robots. However, the scaling studies (later shown in Chapter 3) in this work is for quadruped robots with articulated legs and it is not restricted to only one type of actuator.

## 2.3 Related Work to Knee Joints for Legged Robots

To build a highly dynamic and versatile legged robot, it is essential to have lightweight legs with optimized design and suitable actuators for the desired robot performance and tasks. The design goals are to achieve 1) a wide range of motion for bigger foot workspace which will increase rough terrain walking performance by increasing the number of reachable footholds for each step, 2) an optimized joint torque curve, since torque output is related to joint angle if linear actuators like pistons are used. As shown in one of our most recent works [51], hydraulic actuation is robust against impacts whilst also allowing high-bandwidth control. For this reason, most main-stream highly dynamic legged robots like HyQ and Boston Dynamics' machines (BigDog, LS3, Cheetah and ATLAS) use hydraulic actuators instead of electric motors to avoid breakage of reduction gears (an exception is the work presented in [53] where high-torque DC brushless motors with low gear ratio are used to actuate the joints of a highly dynamic quadruped robot). These actuators are installed directly at the joint and therefore no power transmission systems are required. However, these existing dynamic legged robots with linear hydraulic actuators for knee joints lack large range of motion and optimal joint

torque curves over the whole range of the linear actuator extension. HyQ and BigDog's knee joint has a range of motion of around  $120^\circ$ <sup>2</sup>, which makes a successful implementation of tasks like climbing over very rough terrain and self-righting difficult. A few existing legged robots are able to self-right after falling, e.g. NAO [19], Boston Dynamics' LS3, and ETH's ALOF [45] thanks to large joint ranges.

In this thesis, we propose the adaptation and optimization of the so-called *isogram* mechanism (more details in Chapter 4). It exhibits a changeable *instantaneous center of rotation* (CICR), similar to a human knee joint. The mechanisms that utilize a CICR like human joints, are based on a classic representation of the crossed four-bar linkage [58]. But there are also other possible ways of representing it, as Oberg showed in a summary of knee mechanisms with a CICR [37]. Here we are focused on the crossed four-bar linkage for a knee joint, which has also been named in literature as a polycentric four-bar linkage [40]. Most of its uses are in prosthetics [43] and human exoskeletons[40]. The mechanism which is proposed in this work is called an *Isogram Mechanism*. It uses a cross four-bar linkage driven by a linear hydraulic actuator. In another work, CICR based knee joint for legged robot showed superior performance when compared to a single axis joint in terms of stiffness and mechanical advantage [16]. There are also some examples that exist for quadruped robots that use additional mechanisms for a knee joint like WildCat, LS3 by Boston Dynamics, and the Cheetah-cub robot by Sprowitz et al. [56]. However, the resulting knee joint suffers from a small range of joint motion, which causes a lack of versatility.

## 2.4 Related Work to Joint Torque Sensor

The development of torque sensor for robots has been of great interest for decades [60] [1] [62] [59], as the commercially available torque sensors are expensive, need extra space in joints, and are difficult to customize. Thus, a variety of sensors were designed and developed for robotics systems with acceptable performance by different researchers [54]. It is understood that the torque sensor used with these actuators must be able to detect the maximum torque produced in the robot joint and bear the axial and shear loading. Otherwise, it may lead to the insufficient locomotion of robot due to torque sensor failure. Considering that in this work we will apply the aforementioned torque sensor to a hydraulically quadruped, the high stresses and shocks push to take in account only the first ones and essentially them that are associated with strain gauges. Further developments were targeted towards the

<sup>2</sup>To the best knowledge of the author, BigDog's knee range of motion has not been published. Here it is roughly estimated to be less than  $120^\circ$  based on online videos.

human-robot interaction [38], the motion stabilization [33], or miniaturization [18]. Till now, despite to the different applications, the basic design was not improved too much, because the non-linearity and the non-symmetrical behavior (in CWR and CCWR) was not guaranteed [14].

The high-performance torque-controlled robots control performance is highly dependent on the feedback of its joint torque. However, they mostly lack symmetric behavior and/or linearity. It gets more complicated, when it is needed to be customized for smaller and compact applications. Later, it is shown in Chapter 5, when we scale down traditional torque sensor designs to measure a joint torque for MiniHyQ. Finally, we develop a new innovative design of strain gauges based torque sensor; via virtual prototyping design and experimental tests. The final design gives symmetric behavior in the rotations (clockwise and counterclockwise) and provides linear output.

# **Chapter 3**

## **Scaling and Actuator Selection for Quadruped robot**

This chapter presents the scaling and actuator selection for quadruped robots. The scaling studies are done to scale the quadruped robots peak joint torques while robot performing template motions i.e jumping and running. The aim of these studies are to build a scaling tool that helps the quadruped robot designers to select actuators that fulfill the desired requirements. Most of this chapter is taken from our published work in [50] [26].

This chapter is started with the estimation of peak Hip Adduction and Abduction (HAA) joint torque for a quadruped robot.

This joint mainly plays a role in the robot balancing when, We continued this scaling study with the squat jump as a characteristic motion for highly dynamic robots, obtaining peak values of joint velocity and torque in relation to robot mass, leg segment length and desired jump height [50]. The study is extended with a running trot to get peak torques and velocities in relation to forward velocity, robot mass, and leg segment length [26]. This chapter ends with the selection of MiniHyQ's actuators on the bases of proposed criteria.

### **3.1 Robot Specifications and Objectives**

It is not straight forward to specify the initial physical specifications for designing a new robot. Mainly it is strongly influenced by commercial components. But the initial specifications are essential to start designing a robot. We already discussed the motivation and objective of this robot in the Section 1.1 (Chapter 1). Below a list of the objectives and physical specification of the MiniHyQ robot.

- To keep MiniHyQ easily manageable and lightweight in its category of robots, it is targeted to weigh around 22-25 kg. MiniHyQ needs to be light and powerful at the same time.
- Each joint of MiniHyQ should be hydraulically actuated and it should be fully joint torque controlled.
- This robot should be capable of performing versatile tasks like walking, running, and jumping. It should have the ability to move easily on rough terrain.
- It should be configured into a possible leg configurations, that includes forward/backward, backward/forward, backward/backward and forward/forward.
- Each of MiniHyQ's legs should have 3 DoF and each joint must give wide range of motion which allows motions like self-righting.
- MiniHyQ should have two hip joints with zero offset (where HyQ robot has 8 cm offset between the two hip joints axes). The naming of joints are the same as HyQ's leg-sagittal plane joints hip flexion/extension (HFE) and knee flexion/extension (KFE). The third joint is called as hip abduction/adduction (HAA). The desired MiniHyQ leg kinematic structure is shown in Fig. 3.1.

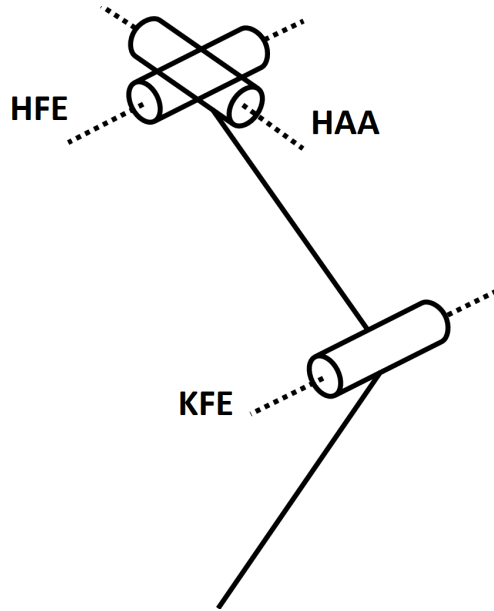


Fig. 3.1 Kinematic structure of the leg including two joints in the leg-sagittal plane hip flexion/extansion (hip f/e or HFE) and knee flexion/extansion (knee f/e or KFE).

- Each leg's KFE joint should have a wide range angle of around 0 to 180° and HFE joint that has targeted more than 0 to 200°.
- Each leg segment length should be around 25 -30 cm.
- Keep the manufacturing cost of MiniHyQ as low as possible without comprising on its performance.
- MiniHyQ is designed to have an on-board power pack that will be powered by off-board electric power.

## 3.2 Scaling tool

To design such machines, the designer has to define the tasks that the robot should accomplish, then choose the actuator that satisfies the task requirements in terms of joint velocity and torque. It is easier for a designer to narrow down the desired dimensions and mass of the robot. However, when it comes to the selection of actuators, it is not trivial to obtain appropriate joint velocity and torque limits without correctly modeling the whole robot in simulation and implementing stable locomotion controllers. The aim of this work is to build a scaling tool that helps the quadruped robot designers to select actuators that fulfill the desired requirements.

### 3.2.1 Scaling of the HAA Joint

The HAA joint is important for a quadruped robot to support its weight when robot legs are not parallel to its leg-sagittal plane and it needs to react quickly to keep its balance. It is less involved in the creation of forward propulsion of the robot. It is not straight-forward to define any template motion for scaling the HAA joint torque and velocities of the quadruped robots. We started with estimation of the required torque in the HAA joint. It is done by doing a static torque analysis, we considered extreme static posture where the robot needs to balance statically at maximum HAA joint angle. It is assumed that the robot's mass  $m_{robot}$  is evenly spread on its four legs and that the feet experience no friction on the ground. The vertical ground contact force acting on each leg is seen in Fig. 3.2 and it is expressed in Equation (3.1) as

$$F_Z = \frac{1}{4} L_{leg} m_{robot} g \quad (3.1)$$

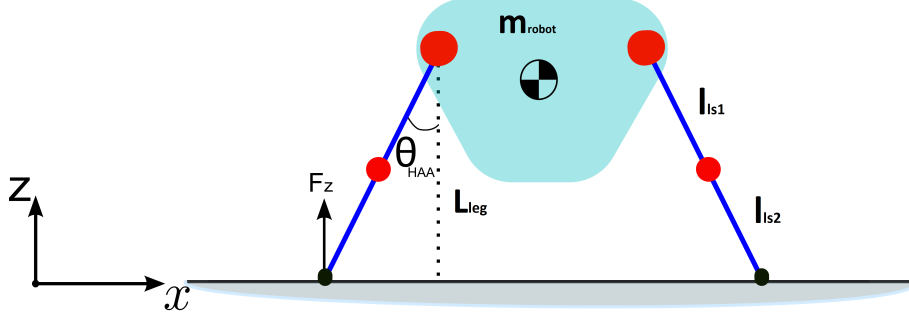


Fig. 3.2 Sketch of the front view of the simplified robot model with definition of variables used for Hip Abduction/adduction torque scaling.

Where the leg length in leg-sagittal plane depends on the knee angle  $\theta_{KEF_{max}}$  as it is shown in Fig. 3.3, therefore the leg length is written as

$$L_{leg}^2 = l_{ls1}^2 + l_{ls2}^2 - 2 * l_{ls1} * l_{ls2} * \cos(\pi - \theta_{KEF_{max}}) \quad (3.2)$$

$$L_{leg} = \sqrt{l_{ls1}^2 + l_{ls2}^2 - 2 * l_{ls1} * l_{ls2} * \cos(\pi - \theta_{KEF_{max}})} \quad (3.3)$$

At peak case leg is fully extended as seen in Fig 3.3, its knee angle  $\theta_{KEF_{max}}=180^\circ$  then Equation (3.3) becomes

$$L_{leg} = l_{ls1} + l_{ls2} \quad (3.4)$$

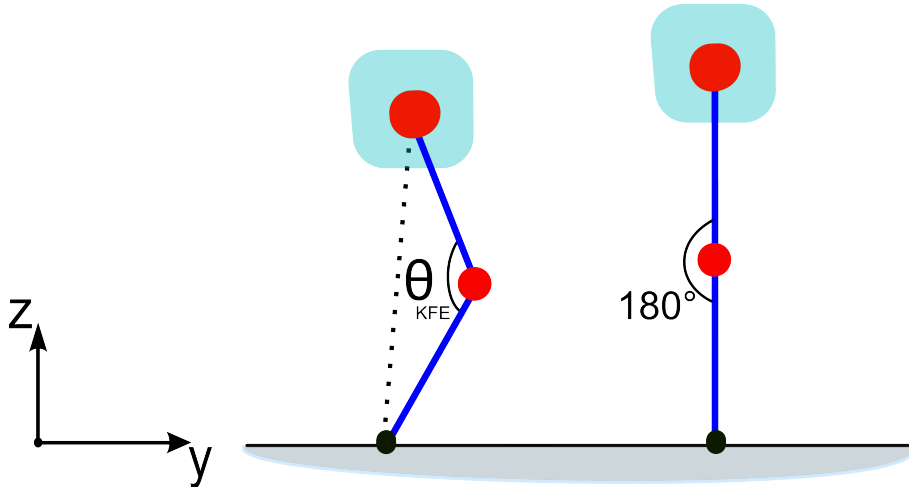


Fig. 3.3 The leg-sagittal plane view.

When the robot has vertical legs ( $\theta_{HAA} = 0^\circ$ ) then the torque in the HAA joint  $\tau_{HAA} = 0Nm$ . The more the legs spread outside, the more torque is by the HAA joint required to keep the robot. Therefore, HAA peak static torque at  $\theta_{HAA_{max}}$  is expressed as

$$\tau_{HAA_{max}} = F_Z L_{leg} \sin(\theta_{HAA_{max}}) \quad (3.5)$$

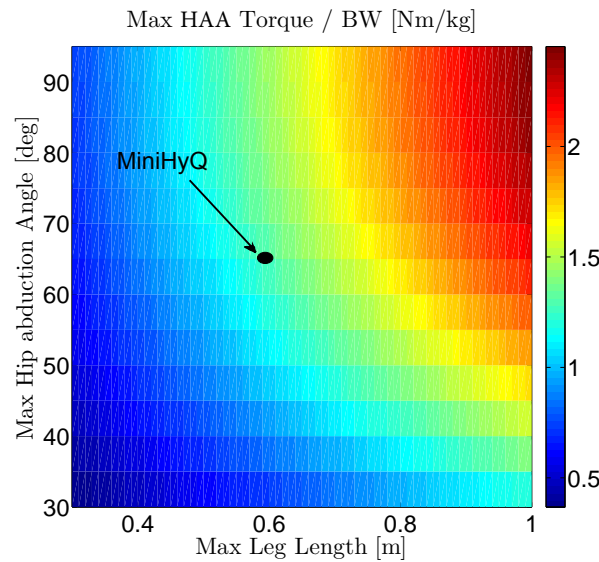


Fig. 3.4 Plot of HAA joint for different leg segment lengths and maximum angle.

Fig. 3.4 shows a scaling plot of the resulting maximum HAA joint torque scale with body weight(BW) of robot in relation to the HAA maximum outside joint angle for a series of leg lengths.

### Estimation for MiniHyQ

The HAA joint torque estimations for MiniHyQ are:

- At maximum HAA joint angel  $65^\circ$
- Leg length is 0.6 m
- Robot mass is 25 kg
- Estimated MiniHyQ maximum HAA joint torque equals to 36.2 Nm ( $1.45\text{Nm/kg} * 25\text{kg}$ ), as Shown in Fig. 3.4.

### 3.2.2 Squat Jump

We selected the squat jump as a characteristic motion for a highly dynamic robot. Such a *squat jump* is composed of several phases: first, a vertical **acceleration phase** from a squatting posture until **lift-off** (when the feet loose contact with the ground); then, a parabolic **flight phase** with the legs moving to a suitable landing posture [48]. It is shown in Fig. 3.5.

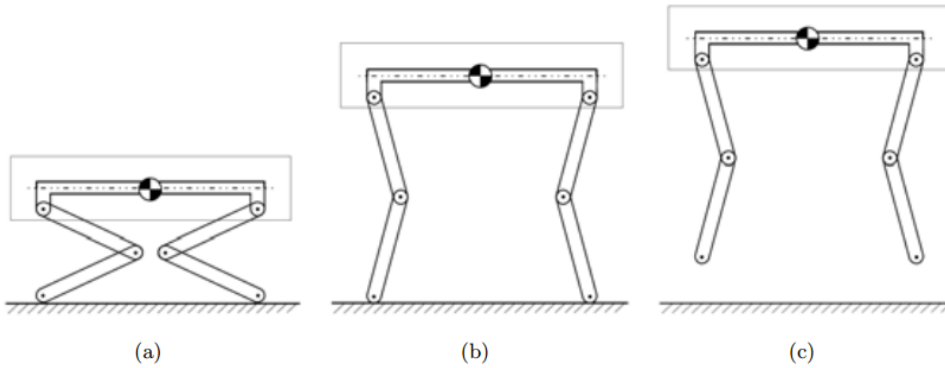


Fig. 3.5 Sketch of the robot during a vertical jump motion: (a) the robot in a squat posture at the start of the motion; (b) in a posture with almost fully stretched legs at foot lift-off, and (c) during the parabolic flight phase.(This figure was taken from [48])

To reduce the amount of tunable parameters, we made several assumptions: the legs are massless, all weight is equally distributed in the robot's torso, and the vertical acceleration is constant during the whole acceleration phase. Furthermore, the lengths of the upper and lower leg segments (distance between the hip and knee joint axis (upper) and knee joint axis and foot (lower)) are equal and the hip joint axes are always vertically above the contact point of their corresponding feet, as shown in Fig. 3.6. This leads to the following relationship between the hip and knee joint angles  $\theta_1$  and  $\theta_2$ :

$$\theta_1 = -\frac{\theta_2}{2} \quad (3.6)$$

Furthermore, these assumptions lead to ground reaction force vectors  $F_{zf}$  that intersect (*point through*) the hip axes during the whole acceleration phase, resulting in zero required hip torque. Section 3.2.4 will address the consequences of these assumptions and discuss the limitations of this approach.

The jump height is the crucial input to our simulation and is measured as the vertical distance that the COM travels from the time the body lifts off the ground to the end of the

upward motion. The maximum jump height  $h_{max}$  of any object undergoing a parabolic flight phase is directly related to its lift-off velocity  $v_{lo}$ :

$$v_{lo} = \sqrt{2gh_{max}} \quad (3.7)$$

and can be obtained by equating the kinetic energy  $E_{kin}$  at lift-off with the potential energy  $E_{pot}$  at the maximum jump height:

$$E_{kin} = \frac{1}{2}mv_{lo}^2 = mgh_{max} = E_{pot} \quad (3.8)$$

where  $g$  is the gravity constant and  $m_{robot}$  the robot mass. Note that  $v_{lo}$  is independent from  $m_{robot}$ .

The next step is to calculate the constant vertical acceleration  $a_z$  necessary to reach the velocity  $v_{lo}$ . To further reduce the number of input parameters, we defined the distance  $z_{ap}$  of vertical travel of the COM before lift-off to be equal to the length of the leg segments  $l_{ls}$ .

$$a_z = \frac{1}{2} \frac{v_{lo}^2}{z_{ap}} = \frac{1}{2} \frac{v_{lo}^2}{l_{ls}} \quad (3.9)$$

This results in the required vertical force  $F_{ap}$  during the acceleration phase:

$$F_{ap} = (a_z + g)m_{robot} \quad (3.10)$$

This force should be equally spread over the four legs and, therefore, results in a vertical ground reaction force of  $F_{zf} = \frac{1}{4}F_{ap}$  at each foot. The required torque in the knee joint depends on the momentary joint angles during the motion and is obtained as follows:

$$\tau_2 = \frac{1}{4}F_{ap}l_{ls} \sin(-\theta_1(t)) = \frac{1}{4}F_{ap}l_{ls} \sin\left(\frac{\theta_2(t)}{2}\right) \quad (3.11)$$

with the joint angles and torques as defined in Fig.3.6. The joint angle trajectories are obtained through the foot trajectory in Cartesian coordinates and the leg Jacobian [48]. Using Eq. (3.7) and (3.9)-(3.11), we get the following result:

$$\tau_2 = \frac{1}{4}gm_{robot}l_{ls} \sin\left(\frac{\theta_2(t)}{2}\right)\left(\frac{h_{max}}{l_{ls}} + 1\right) \quad (3.12)$$

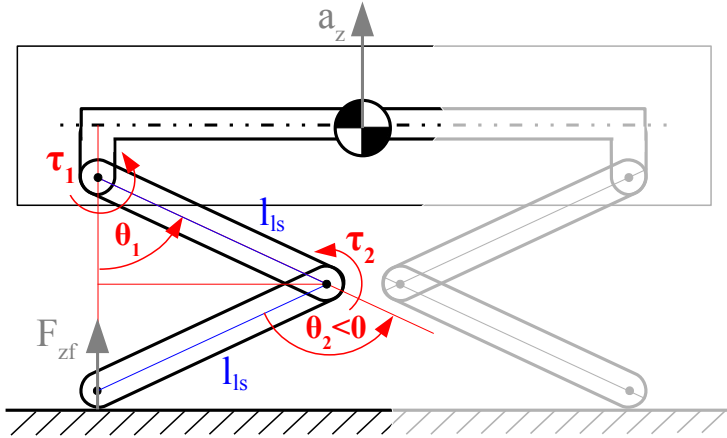


Fig. 3.6 HyQ: Hydraulic Quadruped robot, sketch of the side view of robot in squat posture, defining the centre of mass (CoM); acceleration vector  $a_z$ ; joint angles  $\theta_{1,2}$  and torques  $\tau_{1,2}$  of the hip and knee joint, respectively; leg segment lengths  $l_{ls}$  and ground reaction force vector at the foot  $F_{zf}$ . (This figure was taken from [48])

### Tool Validation

We performed several squat jump experiments with HyQ. Figure 3.7 and 3.8 show the results of a jump of  $0.2m$  in height.

The three subplots of Fig. 3.7 (a) show the data of the experiment (red solid line) and of the simulation (black dashed line) for the knee joint angle (top), knee joint torque (middle) and vertical ground reaction force (bottom). The acceleration phase starts at  $0.1s$  and lasts till  $0.4s$  when the torques go to zero. The robot touches down again at  $0.78s$ . The simulation calculates values only during the acceleration phase.

Similarly, the three subplots of Fig. 3.8 (a) report the data for the knee joint angle on the top (to facilitate the comparison of the plots), and the knee and hip joint velocities in the middle and bottom plot, respectively.

The plots show that the simulation results match well for joint position, joint velocities and ground reaction forces. The simulated knee torques are slightly higher due to the above-mentioned assumptions.

Based on the simplified squat jump simulation presented in last section, we created three 3D plots illustrating estimations of knee joint torque, velocity, and power for a selection of leg segment lengths between  $0.1m$  and  $0.5m$  and jump heights ranging from  $0.02m$  to  $0.4m$ . Figure 3.7 (b) shows a plot of the maximum knee joint torques scaled in relation to body weight (BW). Figure 3.8 (b) shows a similar plot for the maximum knee joint velocities. As the jump height mentioned in (3.7) is independent of body weight and only related to the

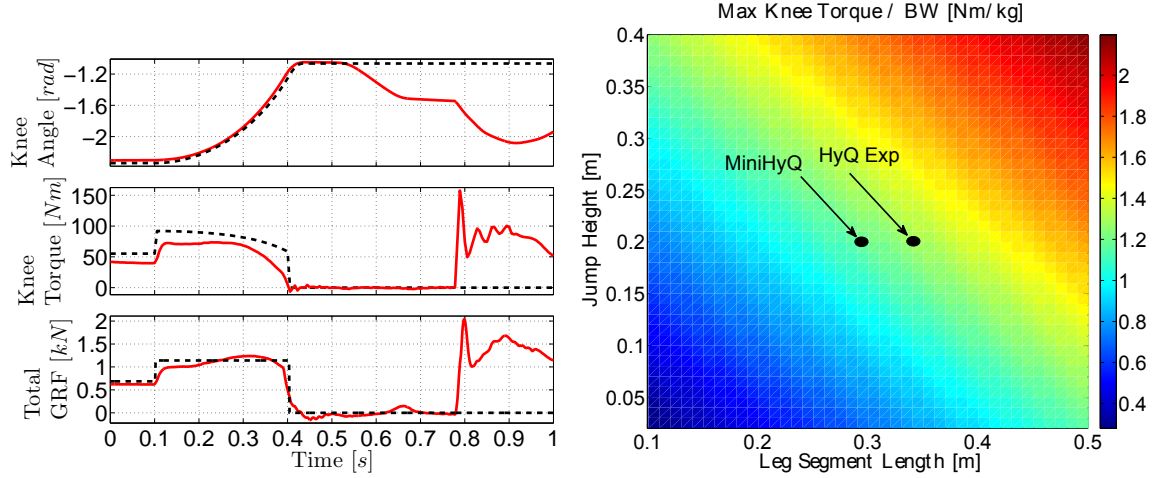


Fig. 3.7 (a) Plot of experimental data (red solid) and simulated data (black dashed) for a squat jump motion of 0.2m jump height. *Top*: knee joint angle  $\theta_2$ ; *middle*: knee torque  $\tau_2$ ; *bottom*: total ground reaction force  $4F_{zf}$ . (b) plot of maximum knee joint torque scaled by the robot's body weight (BW) for different leg segment lengths and jump heights. The arrow marked with *HyQ Exp* shows the experimental results obtained with HyQ as an example.

lift-off velocity, this plot does not need to be scaled by body weight. Finally, Fig. 3.9 shows the product of the knee joint torque and velocity plots resulting in the maximum required knee joint power scaled in relation to body weight.

As a reference, we added the results of the squat jump experiment with HyQ to each of the plots with an arrow marked *HyQ Exp*. A jump height of 0.2m and leg segment length of 0.35m results in a value of 1.3Nm/kg for the maximum knee torque. Multiplied by HyQ's weight of 70kg, this results in 91Nm, matching the peak value of the simulated torque shown in Fig.3.7 (a). In terms of joint velocities, we obtain 10rad/s. Figure 3.9 shows an estimated maximum knee joint power of 910W for HyQ (13W/kg \* 70kg).

### Estimation for MiniHyQ

- Jump height 0.20 m.
- Leg length is 0.6 m
- Robot mass is 25 kg
- Estimated MiniHyQ maximum KFE joint torque equals to 31.25 Nm ( $1.25\text{Nm/kg} * 25\text{kg}$ ).

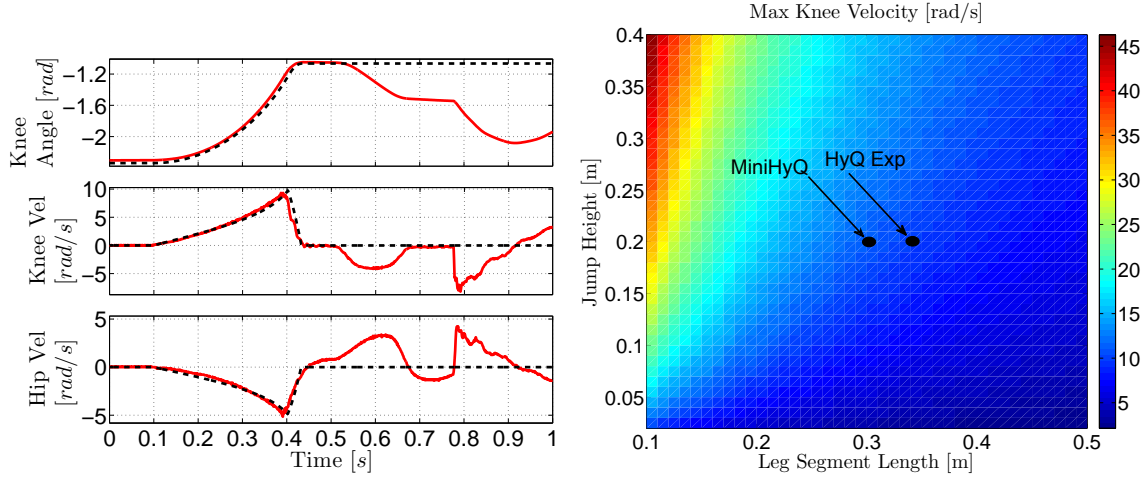


Fig. 3.8 (a) Plot of experimental data (red solid) and simulated data (black dashed) for a squat jump motion of 0.2m jump height. *Top*: knee joint angle  $\theta_2$ ; *middle*: knee joint velocity  $\dot{\theta}_2$ ; *bottom*: hip joint velocity  $\dot{\theta}_1$ . (b) plot of maximum knee joint velocity for different leg segment lengths and jump heights. The arrow marked with *HyQ Exp* shows the experimental results obtained with HyQ as an example.

Note that we only estimated the torque of the KFE joint but not of the HFE joint. Therefore, we continue our scaling study with running trot where the HFE joint is involved.

### 3.2.3 Running Trot

Desired joint torques are generated by placing a virtual linear spring between the hip and foot of each articulated robot leg [42] to control the motion of the leg during running. Each virtual spring of a diagonal leg pair is working synchronously in a trot and can be represented by one equivalent virtual spring, Fig. 3.11a. Blickhan and Full showed in one of their studies that the running motion for multilegged locomotion behaves like a bouncing monopod and they calculated the compression of a virtual monopod's leg and its stiffness from the animals' mechanical-energy fluctuation and ground-reaction force [8].

The center of mass (CoM) motion of any quadruped during a running trot can be approximated by a spring-loaded inverted pendulum (SLIP) model as it is observed in animals[7], Fig. 3.11b. A point mass  $m$  attached to a mass-less linear spring can be described as a SLIP model where  $k$  is the spring stiffness,  $l$  is the current length and  $l_0$  is the rest length. During stance phase, the spring force exerted on the ground is defined as  $k(l_0 - l)$ . During flight phase, the mass follows a parabolic trajectory under the law of gravitation. We define the spring rest length in relation to the leg segment length  $l_s$  (Fig. 3.12) of each articulated robot

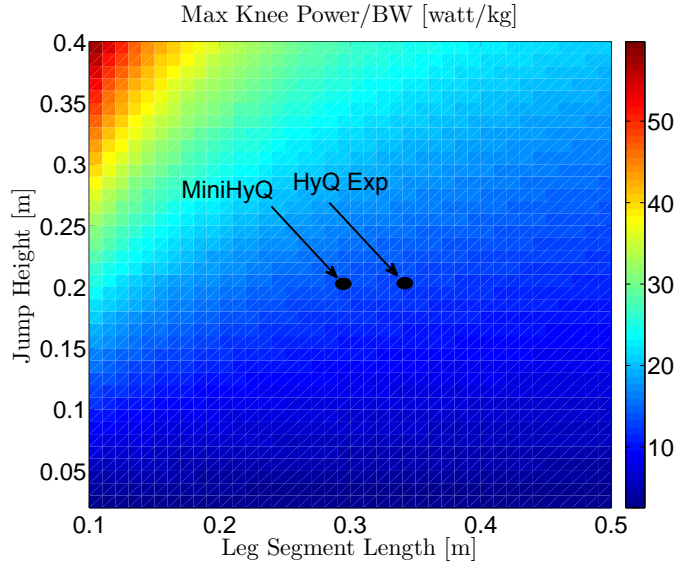


Fig. 3.9 Plot of maximum knee joint power scaled by body weight BW for different leg segment lengths and jump heights. The arrow marked with *HyQ Exp* shows the experimental results obtained with HyQ, as an example.

leg as follows:  $l_0 = K_l l_{ls}$ , where  $K_l$  is the ratio between the leg segment length and the spring rest length. In our simulation  $K_l$  is equal to 1.41, which we assume to be a good value based on our experience with HyQ. From the SLIP model, we know the foot trajectory in Cartesian coordinates of the equivalent virtual spring leg during stance. Using the leg Jacobian, we can calculate the angular position, velocity, and acceleration of hip and knee joints of the articulated robot leg. During the stance phase of a quadruped running trot, only two feet touch the ground. Therefore, the ground reaction forces (GRF) for each articulated robot leg can be defined as  $F = F_{vl}/2$ , assuming an evenly distributed load, where  $F_{vl}$  is the force for the equivalent virtual spring. The leg's GRF is then transformed into hip and knee joint torques with the Jacobian transpose.

### Tool Validation

Using the SLIP model, we performed a number of trotting simulations for a range of forward velocities and leg segment lengths. First of all, suitable SLIP parameters (spring stiffness and angle of attack) had to be calculated for each input pair based on the steps-to-fall map[39]. The SLIP parameters with the lowest spring stiffness that resulted in stable hopping of 50 or more steps were then selected, AS shown in Fig.3.13. This way, low impact peaks were obtained. A running trot experiment is performed on HyQ at forward velocity 1.6 m/s with 40% duty factor and it gives peak hip and knee joint torques equal to 24.3 N/m and 115.5

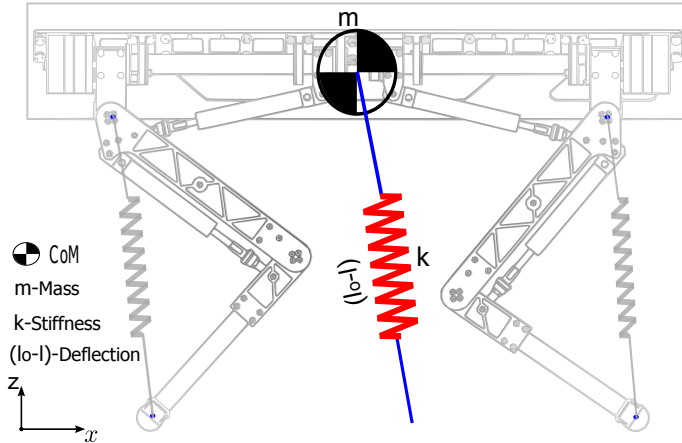


Fig. 3.10 (a) A quadruped robot with the equivalent virtual spring (connected to CoM) represents the virtual linear spring of a diagonal pair of legs.

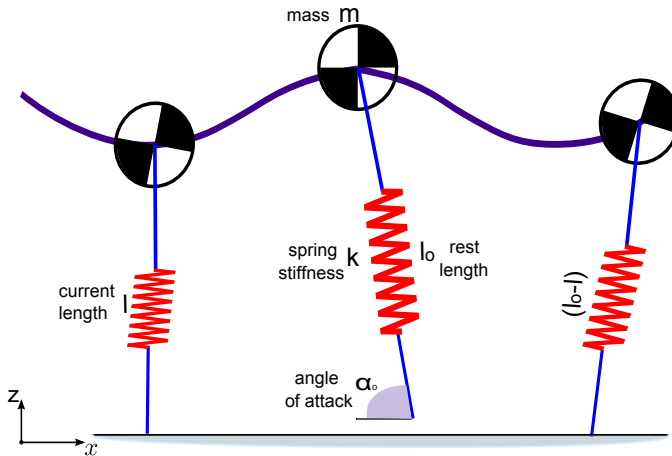


Fig. 3.11 A CoM trajectory (purple solid) of the legged robot during a running trot.

N/m respectively. 'HyQ Exp' arrows shown in Fig. 3.14 are the estimated peak hip and knee joint torques for a running trot at 1.6 m/s, equal to 21.9 Nm ( $0.3\text{Nm/kg} * 73\text{kg}$ ) and 116.8 Nm ( $1.6\text{Nm/kg} * 73\text{kg}$ ), respectively. Fig. 3.14 shows the peak joint torque scaled by the robot's body weight (BW) for different leg segment lengths and forward velocities. White areas indicate where the SLIP model failed to perform 50 steps for the given parameter range.

### Estimation for MiniHyQ

- Running at 2.5 m/s.
- Leg length is 0.6 m

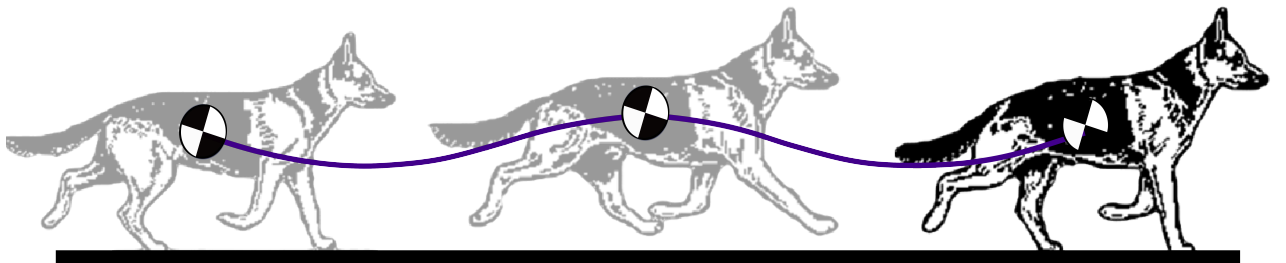


Fig. 3.12 A CoM trajectory (purple solid) of the legged robot during a running trot represented by the SLIP model.

- Robot mass IS 25 kg
- Estimated MiniHyQ maximum HFE joint torque equals to 10.25 Nm ( $0.41Nm/kg * 25kg$ ).
- Estimated MiniHyQ maximum KFE joint torque equals to 57.5 Nm ( $2.3Nm/kg * 25kg$ ).

### 3.2.4 The limitations of the scaling tool

To reduce the amount of tunable parameters, we made several assumptions: the legs are massless and that all weight is equally distributed in the robot's torso. Specifically for squat jump simulations, we assumed that the vertical acceleration is constant during the entire acceleration phase. *Massless legs*: If the mass of the legs is small in respect to the torso's weight, this first assumption does not significantly influence the results. However, Alexander[3] showed that increasing leg mass reduces the jump height, especially if the additional mass is located in the lower leg segment. *Equally distributed body weight*: If the body weight is not equally distributed, the joint torques in the four legs are not equal, however the average will match our simulation. A wise rule for the design of versatile, quadruped robots is an equal distribution of body mass, since it simplifies balancing during locomotion. *Constant vertical acceleration*: In reality, the acceleration and thus the pushing force does not follow the step input, this leads to a smaller jump height. *Hip joint axes vertically above feet*: In reality, the motion of the hip and knee joints are hard to perfectly synchronize. Therefore, the ground reaction forces will not always be only vertical, non-zero tangential components result in internal forces that might lead to foot slippage if the foot-ground friction coefficient is low. For this reason, the hip torque during the experiment is not zero. The torque plot of

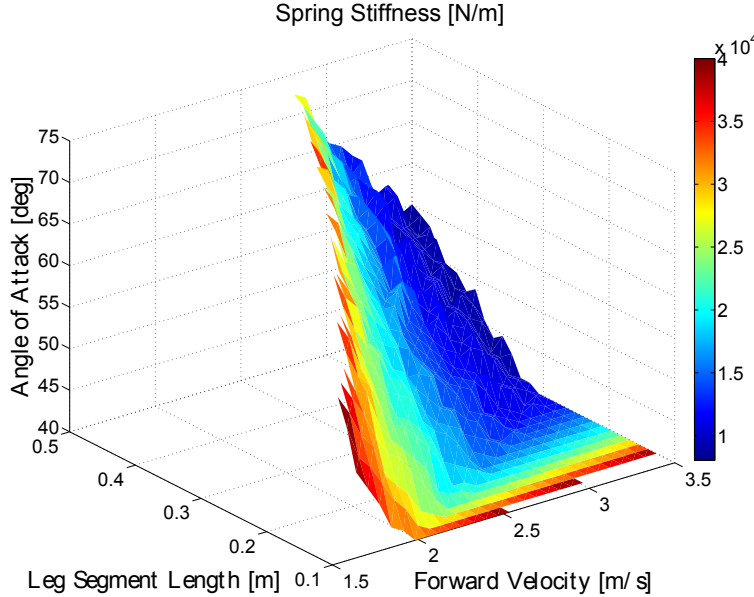


Fig. 3.13 Plot of stable SLIP parameters (Spring Stiffness and Angle of Attack) for different leg segment lengths and forward velocities at robot mass 73kg.

Fig. 3.7 (a) shows that our simulation results in an overestimation of required joint torques. In running trot simulation, it is assumed that the robot mass is evenly distributed and that the robot torso is always parallel to the ground. This assumption does not significantly influence the results even the biological studies have shown that all legged animals typically run with similar center of mass (CoM) motions relative to the (approximately) horizontal ground[57]. In this work, ground stiffness is assumed constant and the equivalent virtual spring stiffness and angle of attack is chosen from the stability domain of steps-to-fall map of the SLIP model.

### 3.3 MiniHyQ Actuator Selection

To keep it small and lightweight, we try to find the smallest hydraulic actuator in market.

#### 3.3.1 Actuators

The first version of HyQ is powered by a combination of electric and hydraulic actuators but MiniHyQ will only be powered by hydraulic actuators. Therefore, different hydraulic actuator technologies are studied.

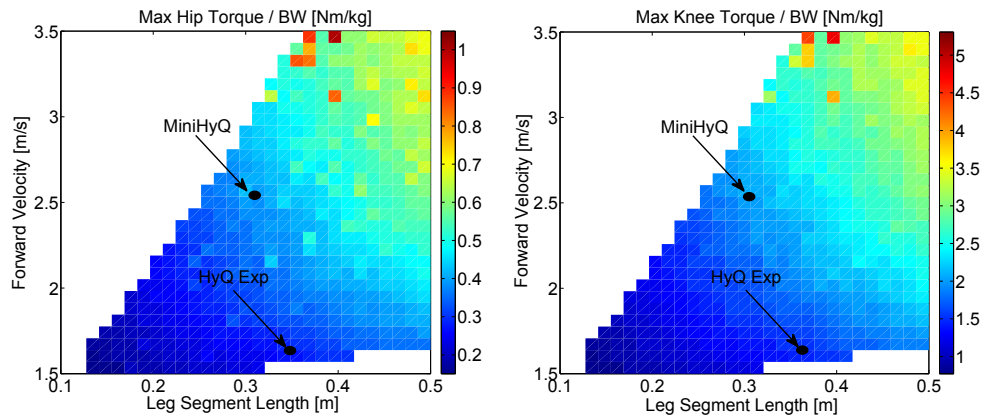


Fig. 3.14 (a) Plot of maximum hip joint torque scaled by BW for different leg segment lengths and forward velocities. (b) Plot of maximum knee joint torque. The arrows show the estimated result according to desired task specification for MiniHyQ .

### Hydraulic Rotary Actuator

Rotary hydraulic actuators are more compact when compared to linear hydraulic actuators. Therefore, rotary hydraulic actuators give more freedom in compact designing but rotary actuators have a lower power-to-weight ratio compared to linear hydraulic actuators. There are two types of hydraulic rotary actuators available in the market, single vane (shown in Fig. 3.15) or double vane (shown in Fig. 3.15). Due to their construction limitation, the single vane motors provide wider angle of rotation and smaller volumetric displacement. On the other hand, double vane motors give shorter angle of rotation and double the volumetric displacement. The double vane motors usually produce double the torque than single vane motors as higher the volume is displaced higher the torque is produced. Table 3.1 shows

Type of Motor	Dimension L x W x H	Range of Motion	Torque @ 20 Mpa	Weight
Single Vane	65 x 59 x 59	280°	60 Nm	778 g
Double Vane	65 x 59 x 59	100°	120 Nm	842 g

Table 3.1 Small size commercial rotary motors specifications

dimensions, weight and specifications of small rotary actuators.

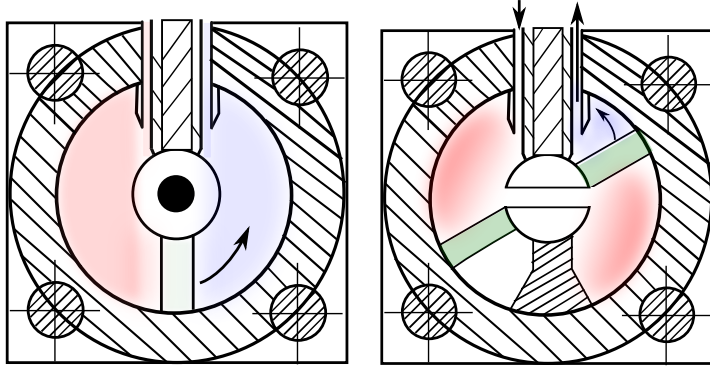


Fig. 3.15 Rotary motors

### Linear Hydraulic Actuator

Table 3.2 presents a comparison between the smallest linear hydraulic actuators on the market. Fluitronics AZ013 is a low-cost hydraulic cylinder that has a small offset length, where offset length is defined as the eye to eye length minus stroke length of a linear hydraulic actuator when it is completely retracted.

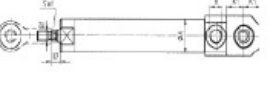
### 3.3.2 MiniHyQ actuator configuration

Due to their high mass-to-power ratio, linear actuators are preferable over hydraulic rotary actuators. It is challenging to generate a wide joint range of motion using linear actuators and at the same time keeping the joint torque output curve optimal for whole joint range of motion. We decided to use single vane rotary actuators for the HFE joint, which provides torque of 60Nm at 200 bars that is more than peak HFE joint torque estimated at 2.5 m/s running trot gait. This rotary motor is capable of providing joint range of motion equal to 280 °. For keeping the KFE joint lightweight and best possible solution to use fluitronics AZ013 cylinder. It provides peak force at 2653 N at 20 Mpa with highest A to B cambers cross section area ratio  $\alpha$  which equal to 0.79 (for symmetric cylinder this ratio equals to  $\alpha = 1$ ), and it is expressed as in (3.13), where area of chamber A at rod side is defined as  $Area_A = \frac{\pi}{4}(D_{bore}^2 - D_{rod}^2)$  and bore side area of chamber B is defined as  $Area_B = \frac{\pi}{4}D_{bore}^2$

$$\alpha = \frac{Area_A}{Area_B} \quad (3.13)$$

where for fluitronics AZ013 cylinder  $D_{bore} = 13\text{mm}$  and  $D_{piston} = 6\text{mm}$ . We decided to use the same cylinder for the HAA joint.

Table 3.2 A List of Commercial Hydraulic Cylinders

Type of linear Cylinder	HLK 14000	AZ013	LB6
Look			
Manufacturer	Hydro-Lek	Fluitronics	Hoerbiger
Bore/Rod Diameter(mm)	10/6	13/6	8/5
Offset Length(mm)	68	58	87
Operating Pressure(Mpa)	21	20	16

## 3.4 Conclusion

This chapter presented the robot specifications and the scaling tools to get estimated peak torques for MiniHyQ. The robot has an expected leg length of about 0.6 m and a weight up to 25 kg. The chapter then continued with the explanation of a series of scaling studies that build the foundation of the robot actuator selection. MiniHyQ (a smaller version of HyQ), whose actuators are sized and selected based on these estimations. These scaling tools are validated with the experimental tests performed on the HyQ robot. After getting the rough estimation of the maximum required torques, market surveys are made for the small rotary and linear hydraulic actuators. We concluded that it is most suitable for MiniHyQ

to use rotary actuators for the HFE joint to generate more than  $200^\circ$  and linear actuators for the other two joints (HAA and KFE). In the next chapter, we will propose special knee mechanism to get a wider range of joint angle and an optimized joint torque curve, since torque output is related to joint angle if linear actuators like pistons are used.

# Chapter 4

## Isogram Knee Joint

In this chapter, we focus on the knee joint and propose the adaptation and optimization of the isogram mechanism. It exhibits a changeable *instantaneous center of rotation* (CICR), similar to a human knee joint. Some part of this chapter is taken from our published paper on isogram knee joint mechanism [27]. This chapter is structured as follows: first, it discusses various possible knee joint kinematics and torque analyses which are actuated by linear cylinder. The isogram mechanism with the derivation of its kinematics. An optimization for the kinematic parameters of the isogram mechanism is also described in this chapter; isogram mechanism is compared with two traditional knee joint mechanisms (the hinge joint and four bar). This chapter also presents the comparison between the isogram knee joint with HyQ's hinge joint based knee. The chapter ends with a conclusion.

### 4.1 Knee Joint Mechanisms

The design goals are to achieve 1) a wide range of motion for bigger foot workspace which will increase rough terrain walking performance by increasing the number of reachable footholds for each step, 2) optimized joint torque curve since torque output is related to a joint angle if linear actuators like pistons are used. Here, we proposed an isogram mechanism, that is based on the crossed four-bar linkage [58]. It exhibits a changeable instantaneous center of rotation like a human knee joint. Our objective is not only to enhance the robot performance through the use of a knee joint having CICR but also to map the linear motion of a hydraulic cylinder (high power/weight ratio) into a revolute joint. Thanks to our new knee joint design, we achieve a  $180^\circ$  joint range and the desired torque profile. Due to our robust low level hydraulic control approach [10], we achieve linear hydraulic actuator active

compliance with smooth control. The kinematic and torque analysis of the traditional pin joint knee, four bar, and crossed four bar (isogram mechanism) are presented in this section. We study the influence of these mechanism's geometric parameters on knee joint torque profile and joint range of motion by assuming the same cylinder size in each case.

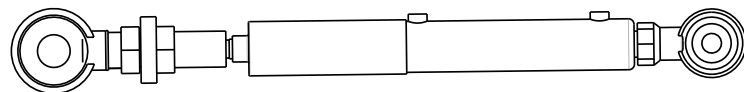


Fig. 4.1 Cylinder minimum eye-to-eye length configuration.

As shown in Fig. 4.1, minimum cylinder eye-to-eye length is defined as the combination of a fully retracted linear cylinder in series with load cell and both rod ends. The minimum eye-to-eye length is 205 mm assumed for these next studies while considering fluitronics AZ013 cylinder with stroke length  $X_{cyl}$  0-70 mm. It is the cheapest hydraulic cylinder in the market and it has a small possible offset length. It provides peak force at 2653 N at 20 Mpa.

#### 4.1.1 Hinge joint Knee Mechanism

Hinge joint knee mechanism are commonly found in the legged robots. HyQ's knee possesses a hinge joint shown in Fig.4.2 that uses a linear hydraulic actuator directly mounted between the upper and lower leg. The distance from the cylinder attachment point to the knee joint is 45mm, which results in a maximum joint torque of 145Nm at 16MPa. The knee range is  $120^\circ$  ( $q = 20^\circ$  to  $140^\circ$ ).

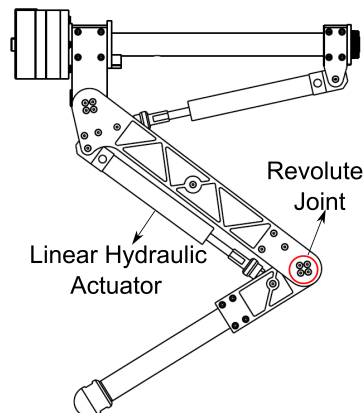


Fig. 4.2 HyQ: Hydraulic Quadruped robot, Drawing of HyQ's Leg with a red circle highlighting its revolute knee joint.

Figure 4.3 shows the configuration of the traditional hinge joint knee mechanism which is actuated by a linear actuator.

### 4.1.2 Knee Joint Angle $q$ and Joint Torque $\tau$

To obtain a definition of the knee joint angle  $q$  as a function of the cylinder extension  $x_{cyl}$ , we have to obtain an expression for  $L_{13}$ , as shown in Fig 4.3. The three side lengths of parallelogram 0123  $L_{01}$ ,  $L_{03}$  and  $L_{23}$  are fixed, while length  $C$  is the sum of the cylinder's fully contracted length  $L_{12}$  and the current cylinder extension  $x_{cyl}$ . From the known fixed parameters of  $\triangle 123$  we obtain

$$\eta = \arctan\left(\frac{L_{03}}{L_{01}}\right) \quad (4.1)$$

and

$$L_{13} = \sqrt{L_{03}^2 + L_{01}^2} \quad (4.2)$$

With the law of cosines applied to  $\triangle 123$  we obtain

$$q = 90^\circ - \eta + \arccos\left(\frac{(L_{13}^2 + L_{23}^2 - C^2)}{2L_{13}L_{23}}\right) \quad (4.3)$$

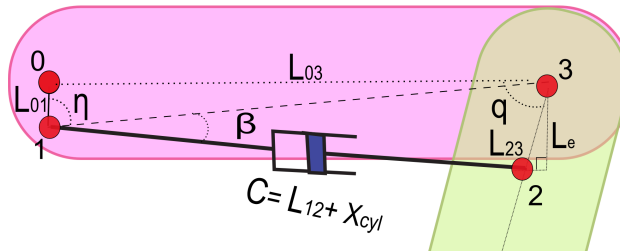


Fig. 4.3 Schematic representation of the hinge joint.

The knee joint torque  $\tau$  depends on the current cylinder extension  $x_{cyl}$  and cylinder force  $F$ .

$$L_{23}^2 = L_{13}^2 + (L_{12} + X_{cyl})^2 - 2L_{13}(L_{12} + X_{cyl})^2 \cos(\beta) \quad (4.4)$$

$$\beta = \arccos\left(\frac{L_{13}^2 + (L_{12} + X_{cyl})^2 - L_{23}^2}{2L_{13}(L_{12} + X_{cyl})^2}\right) \quad (4.5)$$

The effective lever arm  $L_e$  defined as

$$l_{el} = L_{13}\sin\beta = L_{13}\sin\left(\frac{L_{13}^2 + (L_2 + X_{cyl})^2 - L_{23}^2}{2L_{13}(L_2 + X_{cyl})^2}\right) \quad (4.6)$$

The hinge knee joint torque  $\tau$  is expressed as

$$\tau = F_{cyl}l_{el} = F_{cyl}L_{13}\sin\left(\arccos\left(\frac{L_{13}^2 + (L_2 + X_{cyl})^2 - L_{23}^2}{2L_{13}(L_2 + X_{cyl})^2}\right)\right) \quad (4.7)$$

### Effects of Design parameter

Fully retracted cylinder's eye-to-eye length  $L_{12}$  is fixed to 205 mm.

### Variation in Design parameter $L_{23}$

Figure 4.4 shows that the variation in  $L_{23}$  intensively affects cylinder extension distribution on the whole range of angle.

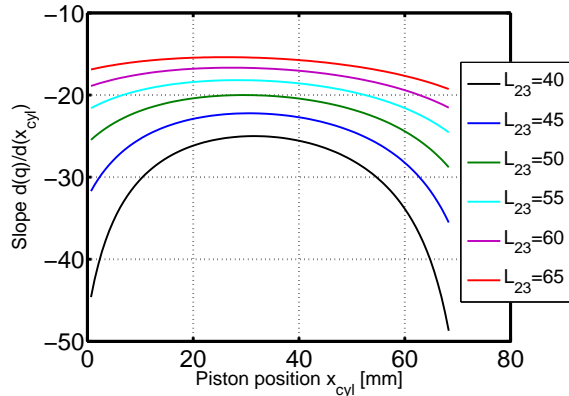


Fig. 4.4 The influence of design parameter  $L_{23}$  on joint slope while it varies from 40 mm to 60 mm, where  $L_{01}=10$  mm and  $L_{03}=240$  mm.

It can be seen in Fig. 4.5 that torque is directly proportional to  $L_{23}$ . However,  $L_{23}$  is inversely proportional to the range of joint angle. In this simulation, we kept  $L_{01}=10$  mm and  $L_{03}=240$  mm.

### Variation in Design parameter $L_{01}$

Figure 4.6 and 4.7 show that change in variation in  $L_{01}$  does not have a high effect on torque and range of motion

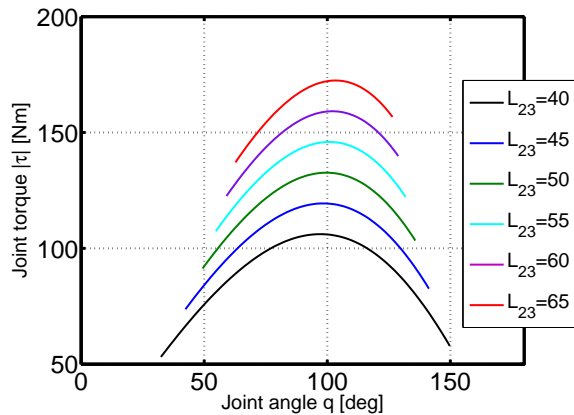


Fig. 4.5 The influence of design parameter  $L_{23}$  on joint torque while it varies from 40 mm to 60 mm. where  $L_{01}=10$  mm and  $L_{03}=240$  mm.

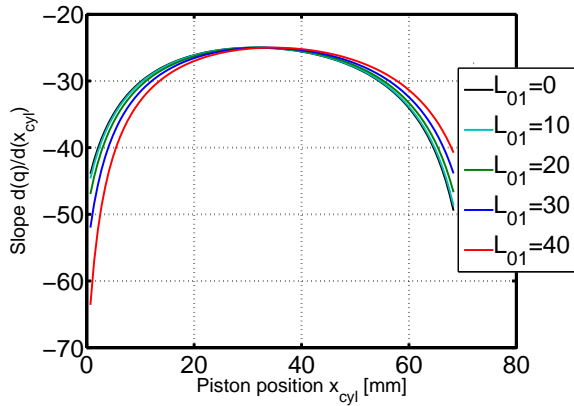


Fig. 4.6 The influence of design parameter  $L_{01}$  on joint slope while it varies from 0 mm to 40 mm. where  $L_{23}=40$  mm and  $L_{03}=240$  mm.

### Variation in Design parameter $L_{03}$

It can be seen in Fig 4.8 that the vibration in  $L_{03}$  does not effect on the range of joint angle.

However, the vibration of  $L_{03}$  shows in Fig. 4.9 that it brings shift in the fixed the range of joint angle.

#### 4.1.3 Four bar Knee Mechanism

In this section we will describe the kinematic analysis of the four bar mechanism based knee joint which mainly consists of four links: a *triangular* and a *cover* link which connect the upper and lower leg segments as shown in Fig. 5.27.

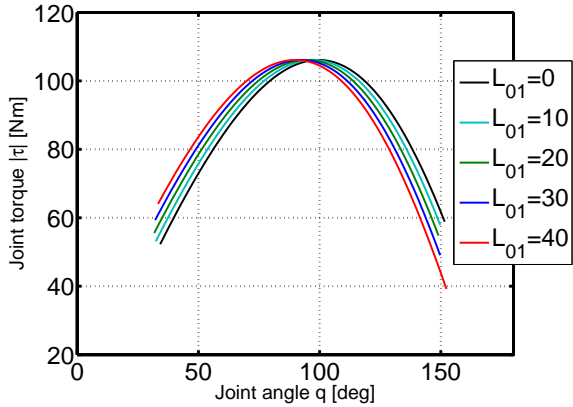


Fig. 4.7 The influence of design parameter  $L_{01}$  on joint slope while it varies from 0 mm to 40 mm. where  $L_{23}=40$  mm and  $L_{03}=240$  mm.

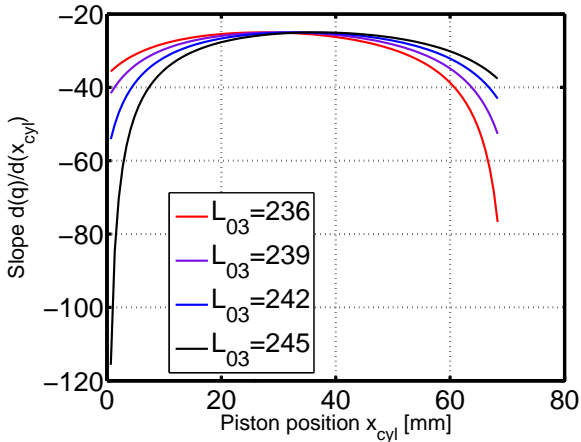


Fig. 4.8 The influence of design parameter  $L_{03}$  on a joint slope while it varies from 236 mm to 245 mm. where  $L_{23}=40$  mm and  $L_{01}=10$  mm.

#### 4.1.4 Knee Joint Angle $q$

The knee joint angle  $q$  is defined as

$$L_{14} = \sqrt{L_{01}^2 + L_{04}^2} \quad (4.8)$$

$$L_{42} = \sqrt{L_{14}^2 + (L_{12} + X_{cyl})^2 - 2L_{14}(L_{12} + X_{cyl})^2 \cos(\beta)} \quad (4.9)$$

$$\beta_2 = \arccos \left( \frac{L_{42}^2 + L_{14}^2 - (L_{12} + X_{cyl})^2}{2L_{42}L_{14}} \right) \quad (4.10)$$

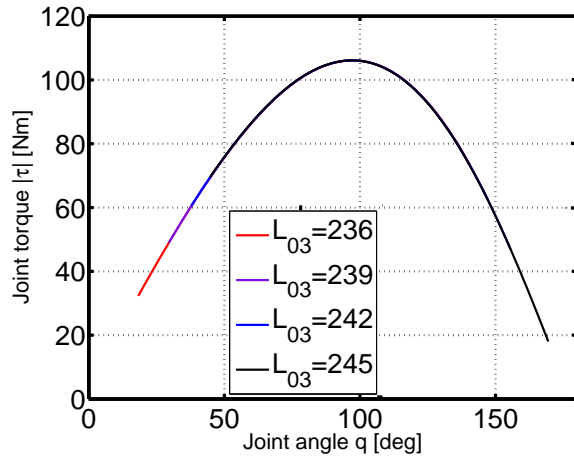


Fig. 4.9 The influence of design parameter  $L_{03}$  on a joint torque while it varies from 236 mm to 245 mm, where  $L_{23}=40$  mm and  $L_{01}=10$  mm.

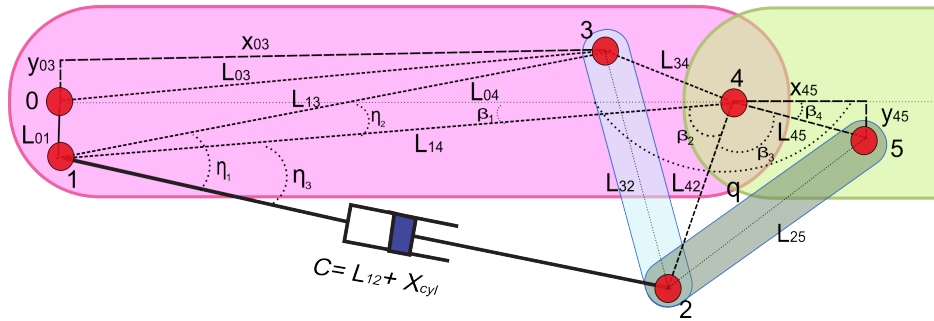


Fig. 4.10 Schematic representation of the four bar based knee mechanism.

$$\beta_3 = \arccos \left( \frac{L_{42}^2 + L_{45}^2 - L_{25}^2}{2L_{42}L_{45}} \right) \quad (4.11)$$

$$\beta_4 = \arctan \left( \frac{Y_{45}^2}{X_{45}} \right) \quad (4.12)$$

$$\beta_1 = \arctan \left( \frac{L_{01}^2}{L_{04}} \right) \quad (4.13)$$

By using Eq. (4.13), (4.10), (4.11) and (4.12), we can define four bar knee mechanism joint angel  $q$  as

$$q = \pi - (\beta_1 + \beta_2 + \beta_3 + \beta_4) \quad (4.14)$$

### 4.1.5 Knee Joint Torque $\tau$

$$\alpha = \frac{\pi}{2} + \arctan\left(\frac{L_{13}^2}{L_{23}^2}\right) \quad (4.15)$$

$$L_{13} = \sqrt{L_{03}^2 + L_{01}^2 - 2L_{03}L_{01}\cos(\alpha)} \quad (4.16)$$

$$\eta_1 = \arccos\left(\frac{L_{42}^2 + L_{14}^2 - (L_{12} + X_{cyl})^2}{2L_{42}L_{14}}\right) \quad (4.17)$$

$$\eta_2 = \arccos\left(\frac{L_{42}^2 + L_{45}^2 - L_{25}^2}{2L_{42}L_{45}}\right) \quad (4.18)$$

$$\alpha = \frac{\pi}{2} + \arctan\left(\frac{L_{13}^2}{L_{23}^2}\right) \quad (4.19)$$

$$\eta_3 = \eta_1 - \eta_2 \quad (4.20)$$

$$L_e = L_{14}\sin(\eta_3) \quad (4.21)$$

The four bar knee joint torque  $\tau$  is expressed as

$$\tau = F_{cyl}L_e \quad (4.22)$$

$$\tau = F_{cyl}L_{14}\sin(\eta_3) \quad (4.23)$$

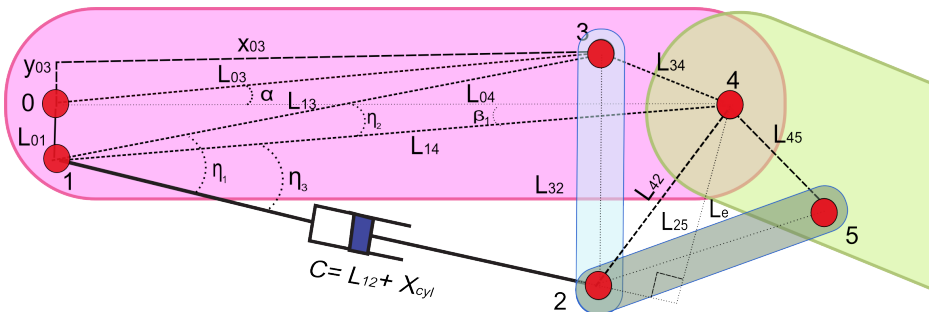


Fig. 4.11 Schematic representation of the four bar based knee mechanism.

## 4.2 Isogram Mechanism Based Knee Joint

The knee joint proposed in this work features a mechanism known as *Isogram Mechanism*. In this section, we will describe the kinematic analysis of the isogram mechanism based knee joint, which mainly consists of two links: a *triangular* and a *cover* link which connect the upper and lower leg segments as shown in Fig. 5.27.

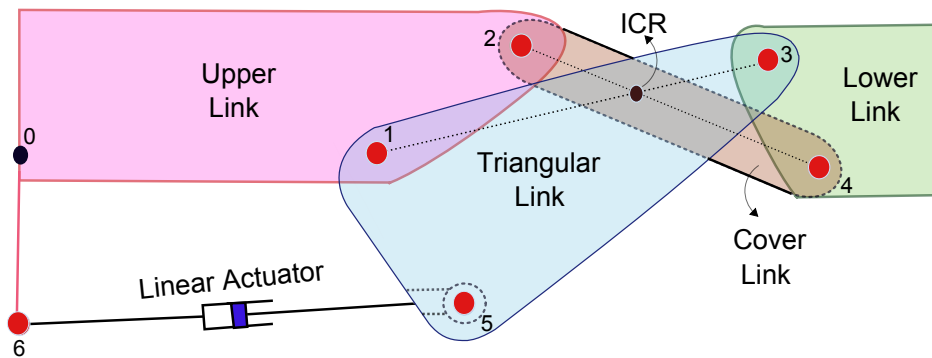


Fig. 4.12 Schematic representation of the isogram mechanism applied to a legged robot's knee joint. The joint is shown in the fully extended configuration (joint angle  $q = 0^\circ$ ).

The triangular link is directly connected to the linear actuator at node 5, which creates a rotation of node 5 about node 1 resulting in a knee joint rotation about the CICR with the help of a cover link. Its other two nodes, 1 and 3, are connected with the upper and lower leg segments, respectively. The cover link connects both upper and lower links through node 2 and 4. The black dot in Fig. 5.27 marked with *ICR* represents the instantaneous center of rotation (ICR), which is the intersection point of the cover and triangular link. Due to a changing center of rotation (polycentric rotation or CICR) of the proposed knee joint, the definition of the joint angle with respect to cylinder extension has to be derived as explained next.

### 4.2.1 Knee Joint Angle $q$

The knee joint angle  $q$  is defined as the angle between the longitudinal axis of the upper link and the longitudinal axis of the lower link. It can be expressed as the sum of the angle  $q_1$  (Fig. 4.13) and  $q_3$  (Fig. 4.14) as follows:

$$q = 180^\circ - (q_1 + q_3 - \varepsilon_1) \quad (4.24)$$

where  $\varepsilon_1$  is shown in Fig. 4.14. Equation (4.24) results in a knee angle equal to zero when the leg is fully extended (straight) and  $180^\circ$  when it is fully retracted. To obtain a definition of the knee joint angle  $q$  as a function of the cylinder extension  $x_{cyl}$ , we divided the mechanism into two parts.

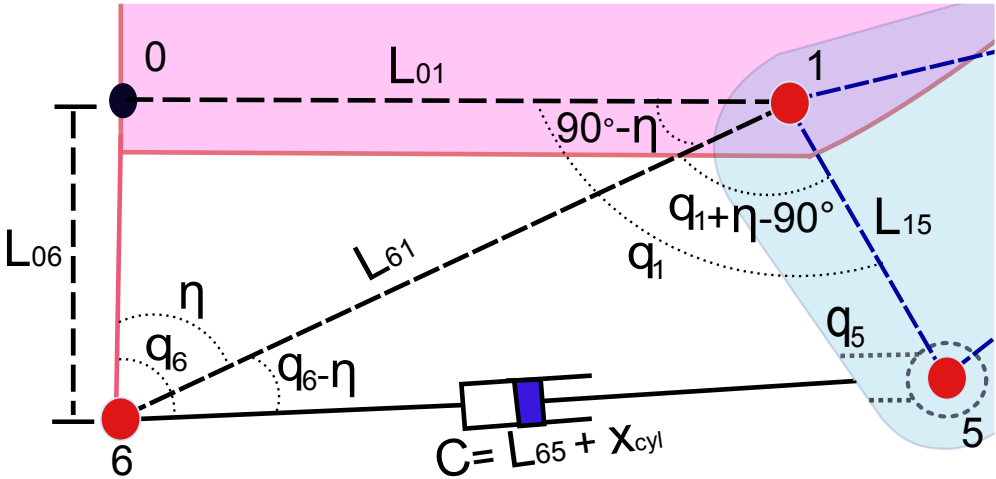


Fig. 4.13 Isogram mechanism: close-up view of the first half of the mechanism to illustrate angle  $q_1$

First, we have to obtain an expression for  $q_1$  considering only the first half of the mechanism, as shown in Fig 4.13. The three side lengths of parallelogram 0156  $L_{01}$ ,  $L_{06}$  and  $L_{15}$  are fixed, while length  $C$  is the sum of the cylinder's fully contracted length  $L_{65}$  and the current cylinder extension  $x_{cyl}$ . From the known fixed parameters of  $\triangle 016$  we obtain

$$\eta = \arctan\left(\frac{L_{01}}{L_{06}}\right) \quad (4.25)$$

and

$$L_{61} = \sqrt{{L_{01}}^2 + {L_{06}}^2} \quad (4.26)$$

With the law of cosines applied to  $\triangle 156$  we obtain

$$q_1 = 90^\circ - \eta + \arccos\left(\frac{(L_{61}^2 + L_{15}^2 - C^2)}{2L_{61}L_{15}}\right) \quad (4.27)$$

Let us now consider Fig. 4.14 to calculate  $q_3$ . It is defined as

$$q_3 = \beta - \varepsilon_3 - \phi + \lambda \quad (4.28)$$

where  $\lambda$  is defined as  $\lambda = \arccos\left(\frac{X_{34}}{L_{34}}\right)$  and we already know the dimensions of the triangular link, which are fixed lengths ( $L_{13}$ ,  $L_{15}$  and  $L_{35}$ ). Its angles ( $\varepsilon_1$ ,  $\varepsilon_2$  and  $\varepsilon_3$ ) can be expressed using the law of cosines. Using the law of cosines at  $\triangle 123$ , the virtual length  $L_{23}$  can be

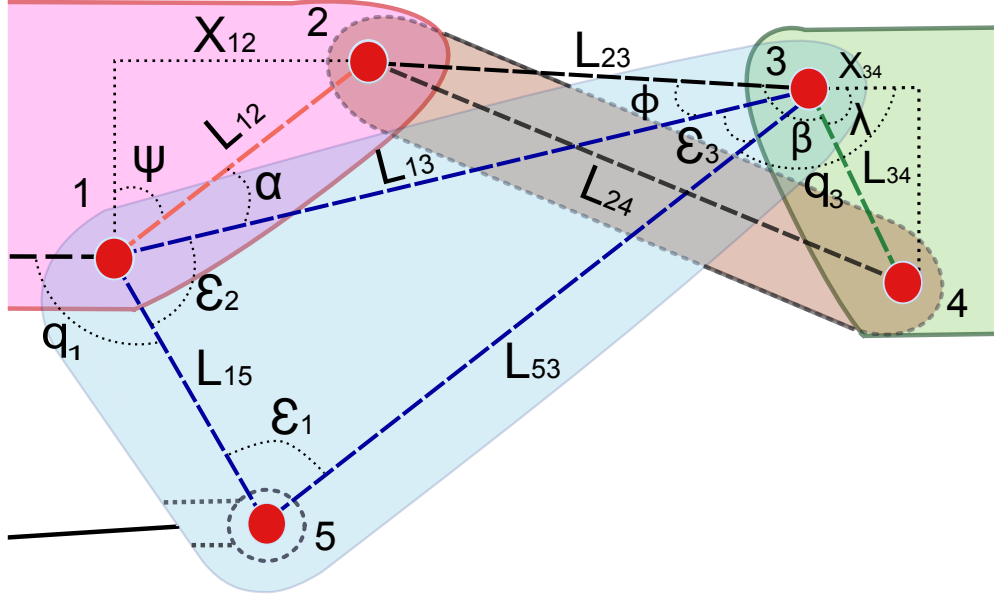


Fig. 4.14 Isogram mechanism: close-up view of the second half of the mechanism to illustrate angle  $q_3$

expressed as

$$L_{23} = \sqrt{L_{13}^2 + L_{12}^2 - 2L_{13}L_{12} \cos \alpha} \quad (4.29)$$

where  $\alpha$  is defined as

$$\alpha = 270^\circ - q_1 - \varepsilon_2 - \psi \quad (4.30)$$

and  $\psi$  is given  $\psi = \arcsin\left(\frac{L_{12}}{X_{12}}\right)$ . Once we calculated the virtual length  $L_{23}$ , we can express  $\phi$  as follows

$$\phi = \arccos\left(\frac{L_{23}^2 + L_{13}^2 - L_{12}^2}{2L_{23}L_{13}}\right) \quad (4.31)$$

Similarly, we obtain

$$\beta = \arccos\left(\frac{L_{23}^2 + L_{34}^2 - L_{24}^2}{2L_{23}L_{34}}\right) \quad (4.32)$$

Using (4.31) and (4.32), we can rewrite (4.28) as follows

$$q_3 = \lambda - \varepsilon_3 + \arccos\left(\frac{L_{23}^2 + L_{34}^2 - L_{24}^2}{2L_{23}L_{34}}\right) - \arccos\left(\frac{L_{23}^2 + L_{13}^2 - L_{12}^2}{2L_{23}L_{13}}\right) \quad (4.33)$$

At last, we obtain the analytical solution of the knee joint angle  $q$  in relation to piston position  $x_{cyl}$ :

$$\begin{aligned} q &= 90^\circ + \varepsilon_1 + \eta - \lambda + \varepsilon_3 \\ &- \arccos\left(\frac{(L_{61}^2 + L_{15}^2 - (L_{65} + x_{cyl})^2)}{2L_{61}L_{15}}\right) \\ &- \arccos\left(\frac{L_{23}^2 + L_{34}^2 - L_{24}^2}{2L_{23}L_{34}}\right) \\ &+ \arccos\left(\frac{L_{23}^2 + L_{13}^2 - L_{12}^2}{2L_{23}L_{13}}\right) \end{aligned} \quad (4.34)$$

### 4.2.2 Knee Joint Torque $\tau$

The knee joint torque  $\tau$  depends on the current cylinder extension  $x_{cyl}$  and cylinder force  $F$ . As the knee joint angle  $q$  is a function of the cylinder extension  $x_{cyl}$ ,  $q = f(x_{cyl})$ , the knee joint torque  $\tau$  be written as

$$\tau = \frac{dx_{cyl}}{dq} F \quad (4.35)$$

where

$$\frac{dx_{cyl}}{dq} = \frac{df(x_{cyl})}{dx_{cyl}}^{-1} \quad (4.36)$$

## 4.3 Optimization of Isogram Knee

### 4.3.1 Parametric optimization problem

The mechanism presented in the previous section has a set of 11 design parameters (namely the lengths  $L_{24}, L_{34}, L_{13}, L_{35}, L_{15}, L_{01}, L_{12}, x_{12}, x_{34}, L_{06}, L_{65}$ ) that have to be determined by the designer. This section explains how we optimized this parameter set to obtain a knee joint behavior that meets our requirements.

Such requirements are specified in terms of torque output profile and joint range. According to our group's experience in the development and control of versatile legged robots such as HyQ [5, 49, 50], the following joint range and torque profile are desirable for the knee joint design of agile and versatile quadruped robots (see Section 4.4 for more details on this choice): A smoothly distributed torque profile that provides high torque in a retracted joint configuration (i.e. flexed leg) and high velocity (but lower torque) when approaching the fully extended configuration is desired. Furthermore, a large knee joint range  $q$  from 0 to  $180^\circ$  is desired.

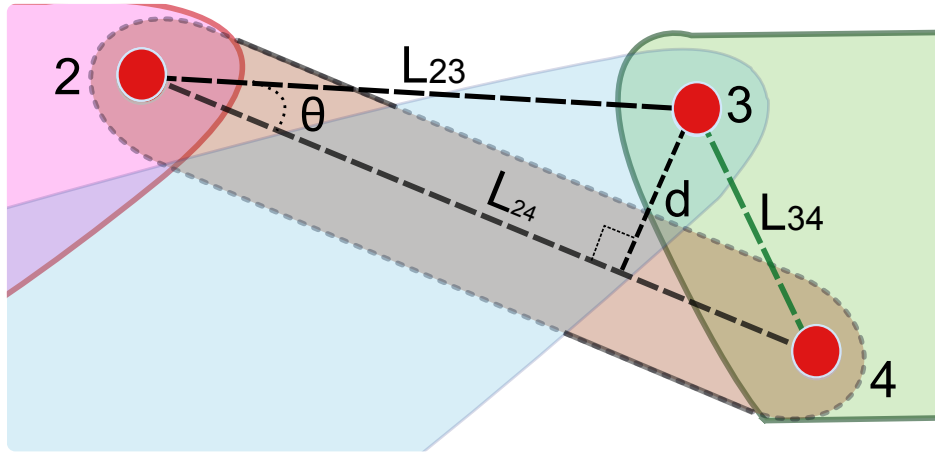


Fig. 4.15 Isogram mechanism: close-up view of the cover link.

### 4.3.2 The Objective Function

This section defines the objective function and gets an optimized set of design variables  $P = [L_{24}, L_{34}, L_{13}, L_{35}, L_{15}, L_{01}, L_{12}, x_{12}, x_{34}, L_{06}, L_{65}]$ . The objective function consists of two components: the first penalizes any design in which  $d$  gets too close to zero.  $d$  is the shortest distance between  $L_{24}$  and node 3 as shown in Fig. 4.15 and expressed as

$$d = L_{23} \sin(\theta) \quad (4.37)$$

where  $\theta$  is defined as

$$\theta = \arccos\left(\frac{L_{23}^2 + L_{24}^2 - L_{34}^2}{2L_{23}L_{24}}\right) \quad (4.38)$$

The second component rewards a smooth, gradual variation from cylinder extension to knee angle and favours a bigger Jacobian (4.36) at  $q = 0^\circ$  and a smaller one at  $q = 180^\circ$ .

This latter is achieved with a quadratic function as mentioned below. The objective function is defined as

$$Y(P) = W_1 * \frac{1}{\min(d)} + W_2 * \sum_{x_{cyl}=1}^{66} (q - q_l)^2 \quad (4.39)$$

We have an “ideal”  $q_l$  in mind, that is part of the optimization, but at the same time we need to keep the overall knee dimensions small. Therefore, we introduced the minimization of  $d$  in the objective function. Where  $\min(d)$  is the minimum value of variable  $d$  over the whole range of cylinder extension ( $x_{cyl}$  = 0 to 67 mm).  $q_l$  linearized knee joint angle is defined as a quadratic function  $q_l = a_2 * x_{cyl}^2 + a_1 * x_{cyl} + a_0$  that has to satisfy the following conditions:

- $x_{cyl} = 0$  when  $q = 180^\circ$  and  $x_{cyl} = 67mm$  when  $q = 0^\circ$
- its slope at  $x_{cyl} = 67mm$  is equal to twice the slope at  $x_{cyl} = 0mm$

which leads to  $a_0 = 180$ ,  $a_1 = -1.79$  and  $a_2 = -0.0134$  after solving the quadratic function.

### 4.3.3 The constraints

The equality constraints are defined on the basis of the following conditions:

- $Y(P) = K$  if a close loop kinematics solution does not exist
- $q = 180^\circ$  if  $x_{cyl} = 0mm$
- $q = 0^\circ$  if  $x_{cyl} = 67mm$

To obtain realistic design variables, we constrained the objective function so that if a close loop kinematics solution does not exist,  $Y(P) = K$ , where  $K$  is a large value (set to  $1e8$  here). This condition penalizes the sets of parameters  $P$  for which a geometric solution does not exist. The other two conditions make sure that the cylinder’s stroke length spans the entire range of desired knee joint angles.

### 4.3.4 Optimization result

The main goal of this optimization is to get a desired torque profile that is large for a flexed leg configuration and small when extended. Figure 4.16 shows the optimized knee joint torque profile (solid blue line) with respect to the knee angle. Its highest torque output lies where the knee is almost completely retracted ( $q= 150^\circ$  to  $180^\circ$ ). The red dashed line in

this figure shows the result of an initial guess for the values of the parameter set  $P$ . The Matlab function *fmincon* is used to minimize the cost function (4.39). We tried different initial conditions, which satisfy the constraints defined in Section 4.3.3. Table 4.1 shows the set of design variables.

Table 4.1 Optimized Design Variables

Design variables	Initial guess (mm)	Optimized values (mm)
$L_{24}$	67	75
$L_{34}$	32	28
$L_{13}$	69	75.5
$L_{35}$	75	70
$L_{15}$	45	38.7
$L_{01}$	211	205
$L_{12}$	36	35
$x_{12}$	12	18
$x_{34}$	15	22
$L_{06}$	43	0
$L_{65}$	fixed	180.5

The design of the knee joint mechanism is based on optimized results. For the optimization, we fixed one design variable ( $L_{65}$ ). The length  $L_{65}$  is the eye-to-eye distance of the fully retracted cylinder and given by the cylinder design, load cell, and rod end length. The initial guess for mechanism link lengths were found by trial and error. Reasonable upper and lower bound of each design variable were defined. Random initial guesses were chosen from these ranges to avoid local minimum. The results are shown in Fig. 4.16 to show the effectiveness of numerical optimization.

Figure 4.16 (right) shows the knee joint angle  $q$  with change in cylinder extension  $x_{cyl}$ . The torque profiles shown in Fig. 4.16 are based on a maximum actuator force  $F = 2653N$  that results from an extending cylinder at a pressure of  $20MPa$ . (The selected cylinder has a bore diameter of 13mm and a rod diameter of 6mm). The weights for the objective function are selected in a heuristic way and a priori knowledge is used to determine a best set of weights  $W_1 = 0.3$  and  $W_2 = 0.6$ .

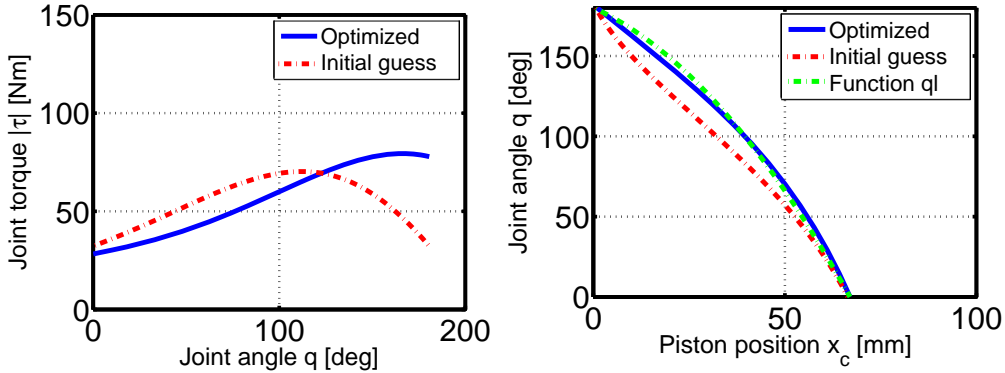


Fig. 4.16 (left) Isogram knee joint torque profile with respect to knee angle; (right) knee joint angle vs. piston position; where the blue solid line indicates the optimized results; the red dot dashed line is the result of an initial guess based on trial and error method; the green dashed line shows the quadratic function  $q_l$  with respect to piston position.

## 4.4 HyQ's knee vs Optimized Isogram knee vs Four Bar Knee

Here, we considered a squat jump as an example motion to demonstrate the importance of suitable knee joint torque profile for a highly dynamic robot. We used the experimental data of HyQ performing a squat jump with 0.2m jump height[50]. A squat jump is composed of several phases: first, a vertical *acceleration phase* from a squatting posture until lift-off; then, a parabolic *flight phase* with the legs moving to a suitable landing posture. The three subplots of Fig. 4.17 show the data of the experiment (red solid line) and of the simulation (black dashed line with 0.2m jump height where blue dashed line shows simulation results for 0.3m jump height) for the knee joint angle (top), knee joint torque (middle), and vertical ground reaction force (bottom). The acceleration phase of the experiment starts at 0.1s and lasts till 0.4s when the torques go to zero. The robot touches down again at 0.78s. The simulation calculates values only during the acceleration phase.

The comparison shown in Fig. 4.18 illustrates the advantages of the new knee mechanism over the existing HyQ knee. Here, the effective lever arm is obtained by scaling the joint torque profile by the maximum output force of the cylinder. The red dashed line shown in Fig. 4.18 represents HyQ's knee effective lever arm with respect to joint angle and the solid blue line indicates the scaled isogram knee joint angle vs. effective lever arm. The maximum force of the cylinder that drives HyQ's knee is 3217N (16 mm bore cylinder at 16MPa). p3 in Fig. 4.2 indicates HyQ's knee peak joint torque at 80° knee angle, which is 145Nm (3217N \* 0.045m).

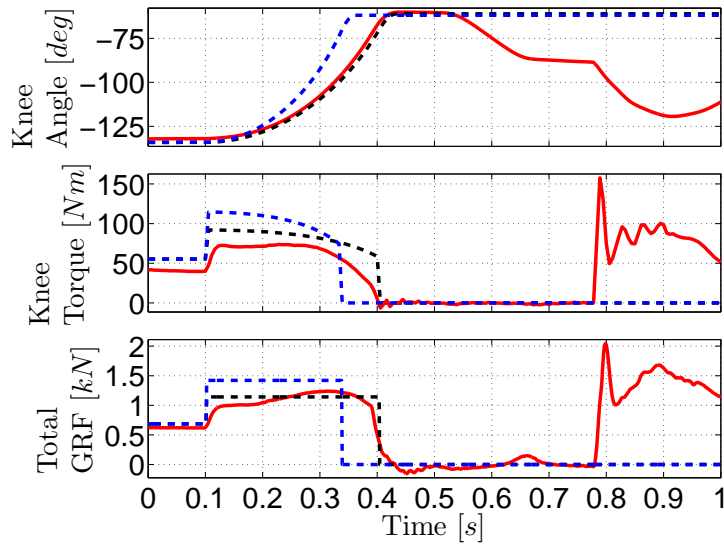


Fig. 4.17 Plot of experimental data of HyQ (red solid), simulated data (black dashed) for a squat jump motion of 0.2m jump height, where simulated data (blue dashed) is at 0.3m jump height. *Top*: knee joint angle; *middle*: knee torque; *bottom*: total ground reaction force. (Figure modified from [50])

It is shown in Fig. 4.17 that during a squat jump, HyQ requires the maximum torque in almost retracted knee configuration. It is marked as p1 in Fig. 4.18 at  $135^\circ$  joint angle. The effective lever arm is 25.5 mm, which gives 82Nm ( $3217\text{N} * 0.0255\text{m}$ ) joint torque. HyQ can safely perform a squat jump of 0.2m jump height with 70 kg body weight within its joint torque limit. However, simulation data (blue dashed) shown in Fig. 4.17 showed that HyQ's knee would need 117Nm at  $135^\circ$  knee angle to perform 0.3m high jump. Since its peak torque (at p3) lies in the center of HyQ's  $120^\circ$  range of motion, which tails out very quickly when the knee is almost retracted, HyQ is not capable of utilizing its maximum torque to perform a 0.3m high jump. However, in case, isogram knee joint is at  $135^\circ$  joint angle, it provides 137Nm ( $3217\text{N} * 0.0424\text{m}$ , scaled value), which is indicated by p2 shown in Fig. 4.18. The solid blue curve shows optimized torque profile of isogram knee joint where its torque distribution is close to the desired shape. While HyQ's knee joint range of motion is restricted to  $120^\circ$  ( $q = 20^\circ \text{to} 140^\circ$ ), the isogram knee provides  $180^\circ$  ( $q = 0^\circ \text{to} 180^\circ$ ). From the shown torque profiles, it can be concluded that the optimized isogram knee mechanism exhibits a larger range of motion and the desired torque profile.

The comparison shown in Fig. 4.19 illustrates the advantages of the new knee mechanism over the existing HyQ knee and four bar mechanism. Here, the effective lever arm is obtained by scaling the joint torque profile by the maximum output force of the cylinder. The red

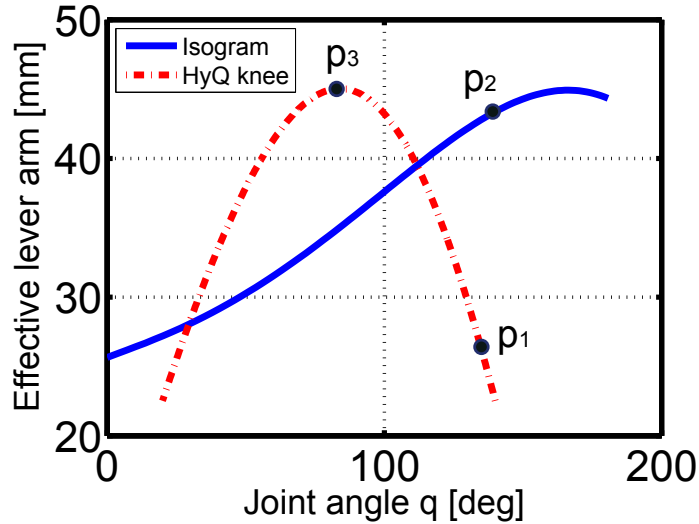


Fig. 4.18 Shows the comparison of the effective lever arm between HyQ's knee joint and scaled optimized isogram knee joint during knee extension

dashed line shown in Fig. 4.18 represents HyQ's knee effective lever arm with respect to the joint angle and the solid blue line indicates the scaled optimized isogram knee joint angle vs. the effective lever arm. The solid black line indicates the four bar mechanism- the maximum force of the cylinder that drives HyQ's knee.

## 4.5 Conclusion

A hydraulic cylinder that is suitable for agile and versatile legged robot joints due to high power/weight ratio. The objective of this study on the knee mechanisms is to use a linear actuator for the rotational joint, which results in a large angular range and gives desired distribution of joint torque over whole the range of motion. We have shown in detail the kinematic and torque analysis of the traditional pin joint knee, four bar, and crossed four bar (isogram mechanism). Each is actuated by a linear actuator. We have seen each mechanism's design parameters behavior on its torque and joint range of motion. Even despite its higher complexity, the isogram mechanism is superior to the traditional designs, because its many kinematic parameters can be fine-tuned to achieve an optimal torque profile. Such profiles should preferably lead to a robotic leg that is strong in a flexed configuration and fast when almost extended.

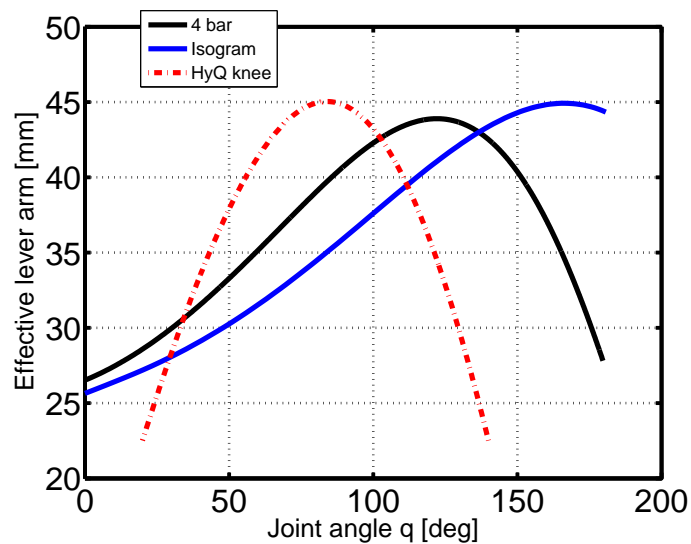


Fig. 4.19 Shows the comparison of the effective lever arm between HyQ's knee joint, four bar, and scaled optimized isogram knee joint during knee extension



# Chapter 5

## Design of MiniHyQ

This chapter presents the development of the lightweight hydraulic quadruped robot-*MiniHyQ*. The robot has almost the same leg length as the previous robot (HyQ [49], built by our group), but MiniHyQ has changeable instantaneous virtual upper and lower link lengths due to the CICR of its knee joint. It gets almost 15% shorter when it is fully retracted. MiniHyQ significantly achieved its physical requirements, which are

- MiniHyQ is easily manageable and lightweight in its category of robots. MiniHyQ is light and powerful at the same time. Its weight is only 35kg (24kg with offboard pump unit), considerably less than HyQ, which makes it portable by one person.
- Each of MiniHyQ leg has 3 DoF and its each joint must give wide range of motion which allows motion like self righting.

To keep MiniHyQ lightweight, the miniature hydraulic actuators were carefully selected, allowing us to reduce the required pump size inside the torso. By using a hydraulic rotary actuator for the hip and the linear actuators with the isogram mechanism for the knee joint, a wider range of motion is achieved allowing a self-righting motion. The torso and the power pack of the MiniHyQ robot were designed with the help of visiting student Satoshi Kitano of Tokyo Institute of Technology. Most of this chapter is taken from our published and already submitted papers [28] [29] and [31] [30], respectively.

This chapter is structured as follows: it starts with introduction to MiniHyQ and its torso design. It follows by design of MiniHyQ's leg and continued with MiniHyQ's leg configuration. Next, it shows the development of a new innovative design of a strain gauge based torque sensor with a high degree of linearity, symmetry, and scalability (both in dimension and measuring range). An overview of the MiniHyQ's control system is described

next. The chapter also describes the design of MiniHyQ's compact power pack. This chapter concludes with the final design of the MiniHyQ robot and conclusion.

## 5.1 Introduction

Hydraulic actuation is robust against impact, allowing high-bandwidth control and the application of very large forces. For these reasons, most mainstream dynamic legged robots like HyQ [49] and the robots from Boston Dynamics (BigDog [44], LS3, Cheetah and ATLAS) use hydraulics. However, the conventional hydraulic quadrupeds are currently facing four main issues and MiniHyQ provides solutions.

- The hydraulic robots tend to be bulky. This makes it difficult to conduct experiments with hydraulic quadruped robots. In addition, appropriate safety procedures require a large number of people. A comparison of existing hydraulic quadruped robots has been made (Table 5.1) demonstrating how MinihyQ lines up against the rest of the existing hydraulic quadruped robots.

Table 5.1 A comparison of Hydraulic Quadruped Robots

Name	Mass (offboard, onboard pump)	Dimensions (LxWxH)	DoF ( per leg)	Joint Torque Controlled
SCalf[46]	78kg,123kg	1.1m x 0.49m x 1m	3	Yes
HyQ[49] [17]	75kg,98kg	1m x 0.5m x 1m	3	Yes
Baby Elephant [17]	90kg,130kg	1.2m x 0.6m x 1m	3	No
BigDog [44]	N.A,110kg	1.1m x 0.4m x 1m	4	Yes
JINPOONG[32]	80kg,120kg	1.1m x 0.4m x 1.2m	4	No
RLA-1[25]	60.2kg,N.A	1.1m x 0.67m x 1m	3	No
LS3	N.A	bigger than BigDog	3	N.A
Wildcat	N.A	N.A	3	N.A
Spot	N.A,74kg	smaller than BigDog	3	N.A
MiniHyQ	24kg,35kg	0.85m x 0.35m x 0.77m	3	Yes

- The most commercial hydraulic components are focused on heavy industrial applications, for example excavators and bulldozers. Small scale hydraulics are still largely absent from the mainstream hydraulic industry and can normally only be found in niche markets. MiniHyQ utilizes the smallest possible commercial hydraulic actuators found in the market.

- The external hydraulic power hoses can negatively affect the dynamics of the robots causing unpredictable disturbances and restricting the working range of robot to remain inside a circumference around the pump. We designed a compact power pack for the MiniHyQ robot which is enough to fulfill its required flow needs and its finishes the need of an external hydraulic hoses.
- The existing legged hydraulic robots often lack versatility to perform a wide range of different motion. This is because of limited joint range of motion and its torque limits. From our experience with HyQ, for example during one of our recent experiments where HyQ walked over obstacles with planned footholds on a 3D map [61], when stepping onto a pallet, stairs or over obstacles, the limited hip joint range made it difficult to retract the leg enough to avoid collisions. MiniHyQ has 40% wider joint range of motion in the leg-sagittal plane compared to the HyQ robot.

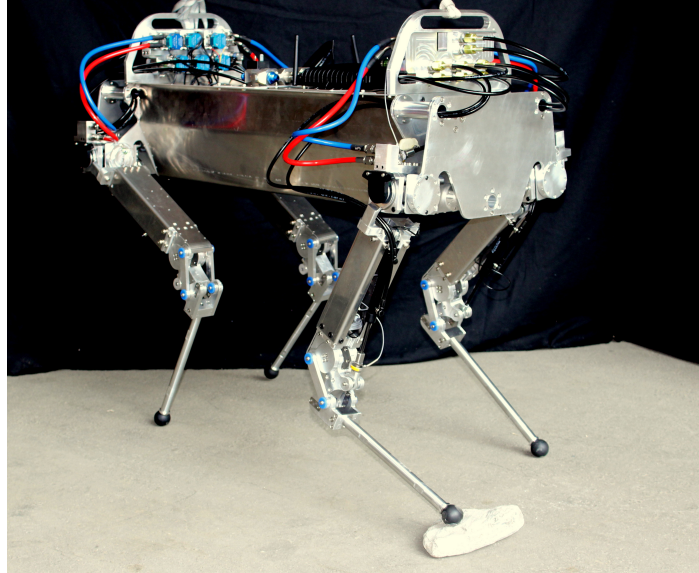


Fig. 5.1 Picture of the lightweight hydraulically actuated quadruped robot MiniHyQ.

## 5.2 MiniHyQ's Torso

MiniHyQ has an 0.85m long torso as shown in Fig. 5.2. It is made of a 2 mm thick folded aluminum sheet and contains the computing system, IMU (inertia measurement unit) sensor, hydraulic manifolds and compact power pack. The torsional movements within the torso are avoided by screwing two 10 mm thick supporting plates at its both ends. The thickness of

these plates is decided after performing the FEM analysis simulation on this torso. These plates are not only to connect the front and hind legs frames but also to hold the front and hind centralized manifolds. All components within torso are separated by 1.5 mm thick folded aluminum sheets.

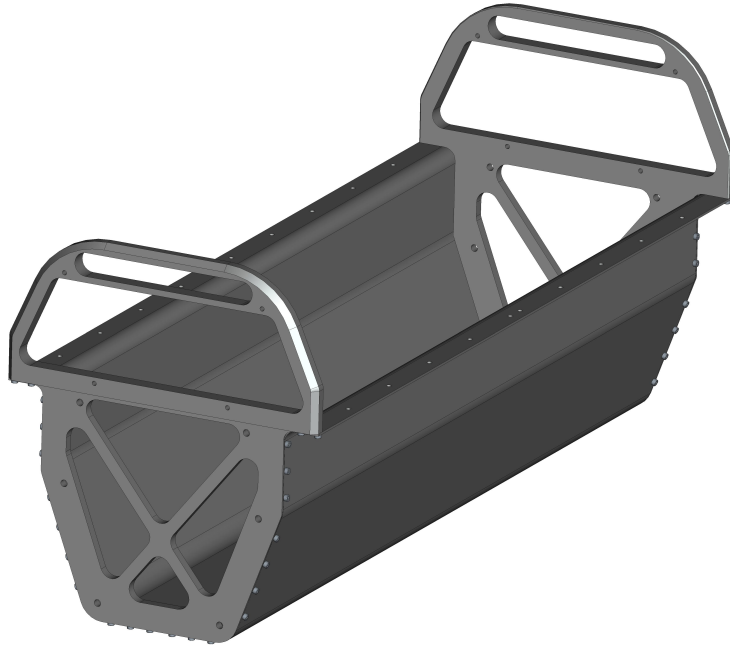


Fig. 5.2 CAD of the MiniHyQ's Torso.

### 5.3 Mechanical Design Of The Leg

Each leg of MiniHyQ is completely modular and consists of 3 active joints. Hip Flexion/Extension (HFE) and Knee Flexion/Extension (KFE) are the joints which work in the leg-sagittal plane. They are responsible for generating the main forward and upward motion of the robot. Most tasks like walking straight and running on flat terrain are accomplished by these joints. Rotary hydraulic actuators have a wide range of motion and constant torque. However, they are heavier than linear actuators. For MiniHyQ's HFE joint, we used a rotary actuator. However, if we put a rotary actuator inside the KFE joint, it would increase the inertia of leg significantly. Therefore, for KFE we used a linear actuator with a special knee mechanism, which does not only provide wider range of motion but also provides an optimized torque profile. The third joint named as hip Abduction/Adduction (HAA) is less involved in the creation of forward propulsion, but rather responsible for the balance of

the robot. Linear actuators are used for the HAA actuation. A CAD Model of MiniHyQ's leg design is shown in Fig. 5.3 and the definition of MiniHyQ's joint angles are shown in Appendix B.

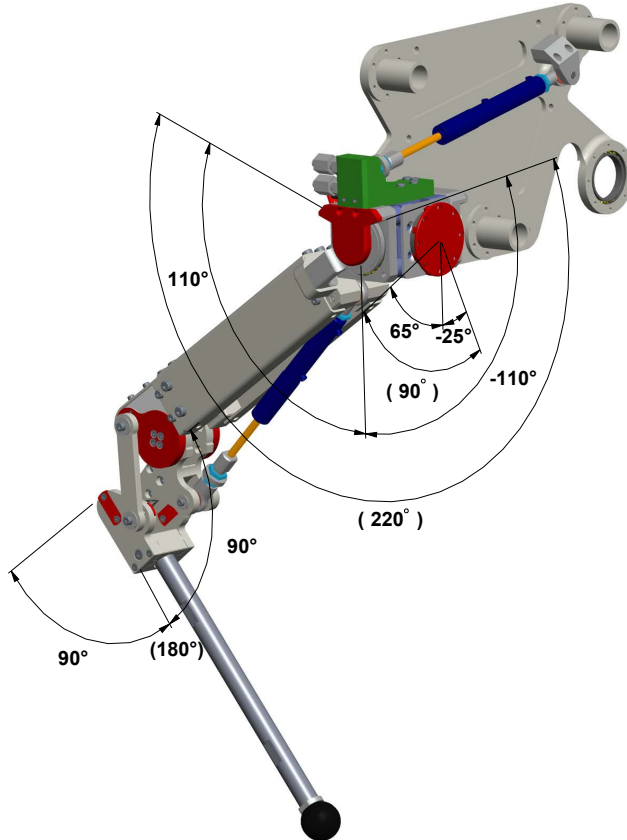


Fig. 5.3 CAD model of MiniHyQ Leg which is consist of 3 active DoF i.e HAA, HFE and KFE.

### 5.3.1 Hip Abduction/Adduction (HAA)

HAA is an important joint in a quadruped robot to support robot's weight (mostly in cases when the robot's legs are not parallel to their leg-sagittal plane). The HAA joint always needs to react quickly to keep the robot's balance. It requires a reasonable joint torque and velocity. An asymmetric hydraulic cylinder is used, which has a bore diameter of 13mm and a rod diameter of 6mm with 69 mm stroke length. It weighs 0.11kg and one end of the cylinder is attached on the top surface of Hip Flexion/Extension (HFE) joint motor and the other end is attached to a torso plate, as shown in Fig. 5.4. To measure the joint torque, we installed a load cell in series with the cylinder rod that measures the cylinder force that can then be

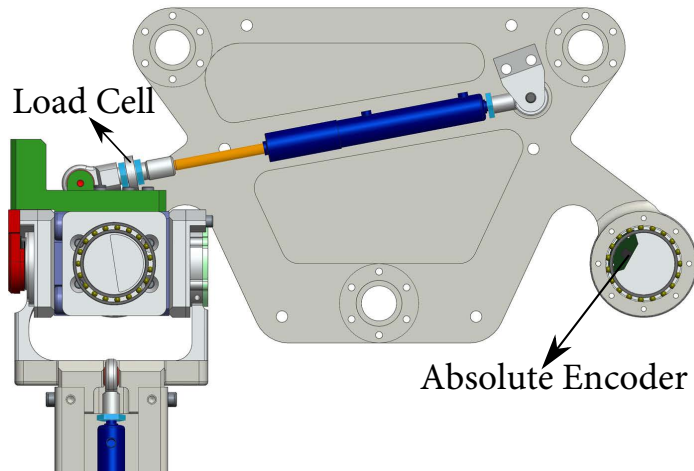


Fig. 5.4 CAD model of HAA joint. The cylinder is connected on top of rotary actuator).

mapped into a torque. The torque profiles shown in Fig. 5.5 are for cylinder extension and retraction.

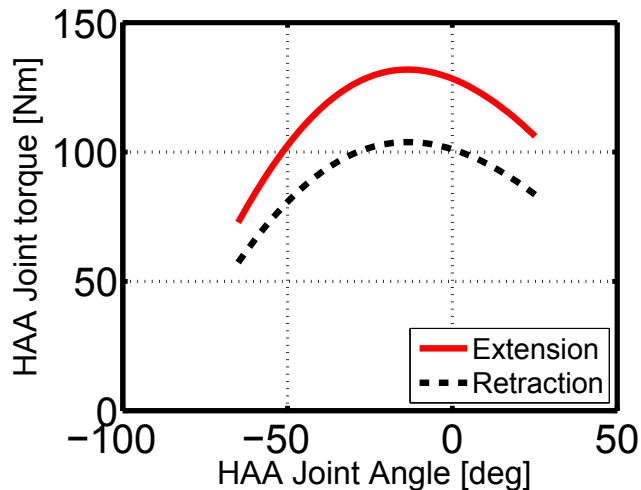


Fig. 5.5 Torque profile of HAA joint for cylinder extension(red solid line) and retraction(black dashed line).

### 5.3.2 Hip Flexion/Extension (HFE)

MiniHyQ's HFE joint is based on a hydraulic rotary actuator. It has joint range of motion of  $220^\circ$ ( $-110^\circ$  to  $110^\circ$ ) and it provides constant joint torque 60 Nm at 20MPa. High resolution absolute encoder is used for position sensing, as shown in Fig 5.6 (left) and strain gauge based custom designed torque sensor is displayed in Fig 5.6 (right).

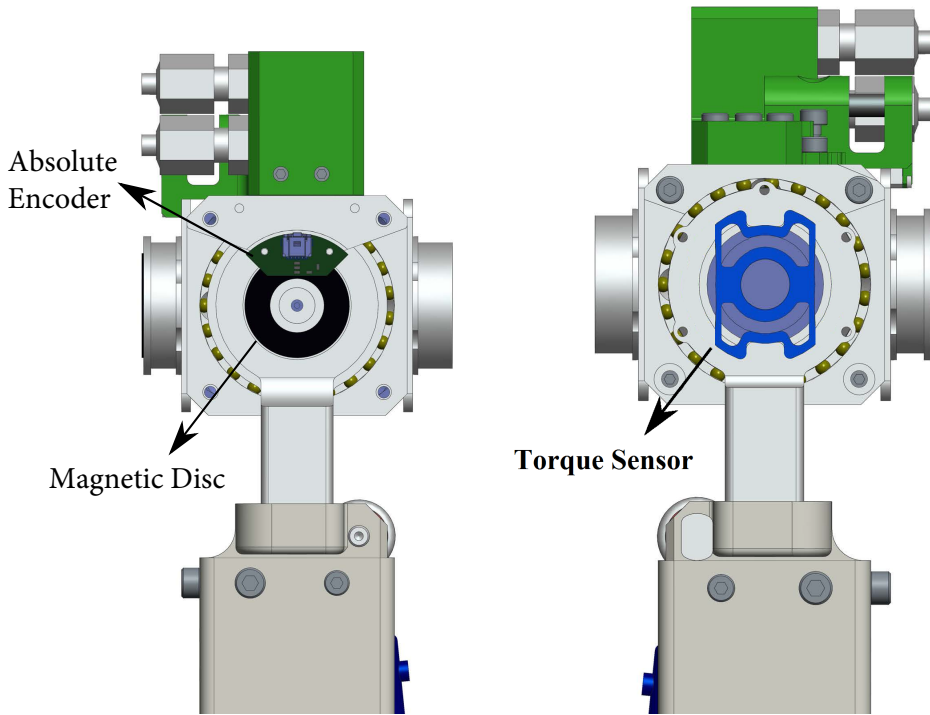


Fig. 5.6 CAD model of HFE joint showing the mounting of absolute magnetic encoder and magnetic disk (left) and the other side of the motor with a custom designed strain gauges based torque sensor fitted onto the HFE motor spline shaft (right).

### 5.3.3 Knee Flexion/Extension (KFE)

The implementation of the isogram mechanism based KFE joint of MiniHyQ is shown in Fig. 5.7. We optimized a set of design parameters to obtain a smoothly distributed torque profile that provides high torque in a retracted joint configuration (i.e. flexed leg) and high velocity (but lower torque) when approaching the fully extended configuration. Furthermore, a large knee joint range  $q$  from 0 to 180°.

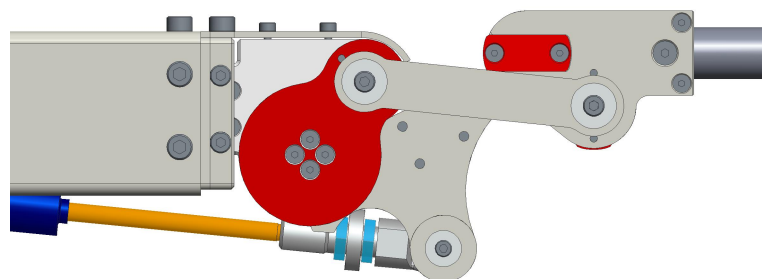


Fig. 5.7 The CAD model of MiniHyQ KFE joint.

The knee joint angle  $q$  (seen in Fig. 5.8) is defined as the angle between the long axis of the upper link and the long axis of the lower link. It can be expressed as the sum of the angle  $q_1$  and  $q_3$  as follows:

$$q = 180^\circ - (q_1 + q_3 - \varepsilon_1) \quad (5.1)$$

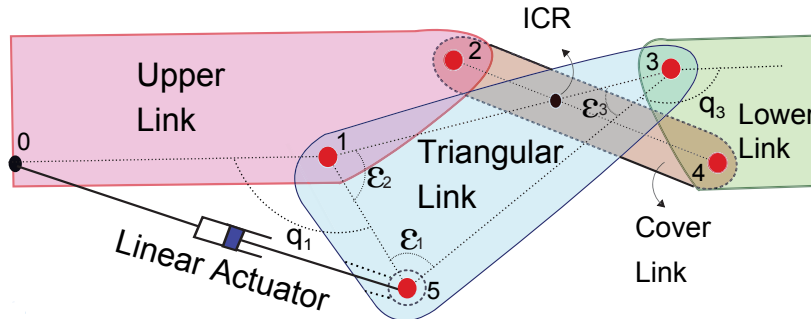


Fig. 5.8 Schematic representation of the isogram mechanism based MiniHyQ's knee joint.

where  $\varepsilon_1$  is fixed angle of triangular link shown in Fig. 5.8. Equation (5.1) results in a knee angle equal to zero when the leg is fully extended (straight) and  $180^\circ$  when it is fully retracted.

MiniHyQ has changeable instantaneous virtual upper and lower link lengths due to the CICR. It gets almost 15% shorter when it is fully retracted, which can be seen in Fig. 5.9 (right). As shown in one of our most recent works [50], the quadruped with the shorter link lengths in a squat position requires less desired torque for performing a squat jump. Figure 4.16 (left) shows the knee joint angle  $q$  with change in cylinder extension  $x_{cyl}$ . Due to the CICR, it is

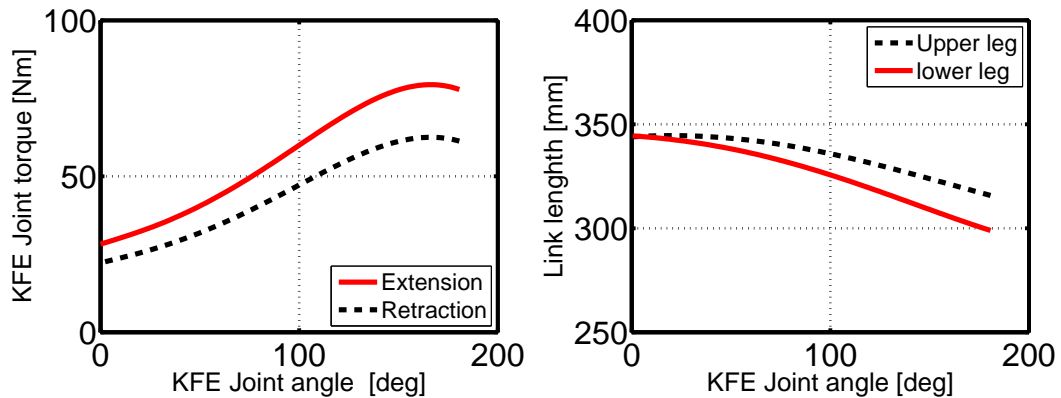


Fig. 5.9 (left) Isogram knee joint torque profile with respect to knee angle. (right) The instantaneous virtual upper and lower link lengths with respect to knee angle.

not possible to install position sensors that directly measure the joint angle. Therefore, we

installed an absolute (high-resolution) encoder at node 1 (see Fig. 5.8) to measure  $q_1$  which can then be mapped into a joint angle  $q$ .

### 5.3.4 Leg Configuration on Torso

By default, MiniHyQ is configured as forward/backward (inward-pointing) leg configuration but it is reconfigurable, which can be seen in Fig 5.10. Several studies [34, 36, 63] indicated that this configuration is suitable for quadruped robots. It reduces slippage between the feet and the ground, which improves motion performance in general [63].

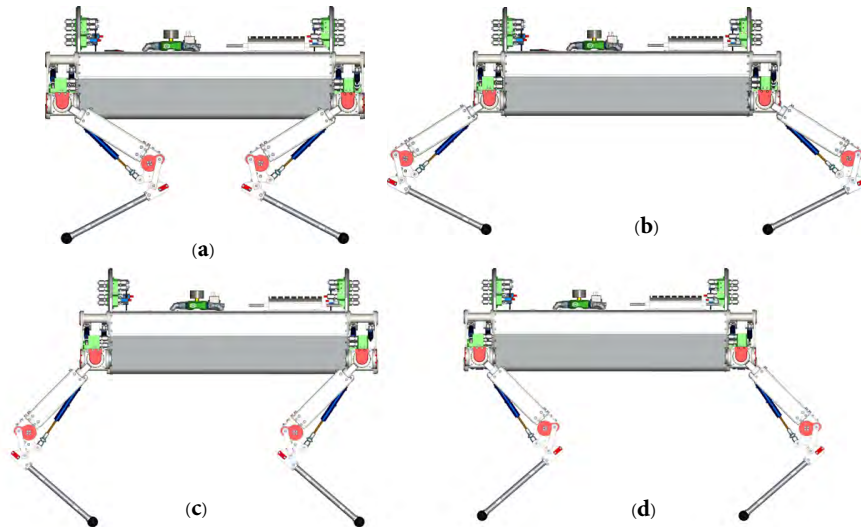


Fig. 5.10 Leg configurations of MiniHyQ with forward walking direction to the right: (a) forward/backward; (b) backward/forward; (c) backward/backward; (d) forward/forward.

## 5.4 Torque sensor design

High-performance legged robots that are required to navigate on unstructured and challenging terrain benefit from torque-controlled joints. High-fidelity torque measurements are crucial for proper joint torque control. Commercially available torque sensors are expensive and often hard to integrate into compact and light-weight robot leg designs. Custom-made sensors on the other hand often suffer from asymmetric behavior with respect to the direction of rotation or poor linearity, especially for small and compact applications. We developed a new innovative design of a strain gauge based torque sensor (seen in Fig. 5.11) with a high degree of linearity, symmetry, and scalability (both in dimension and measuring range). Furthermore,

the gluing and wiring of the strain gauges were easy thanks to the geometry of the sensor that allowed direct access to the mounting surfaces, even in compact dimensions. We show the design's symmetric (clockwise and counterclockwise rotation) and linear behaviour through virtual prototyping and experimental tests. A detailed sensitivity analysis is also done on

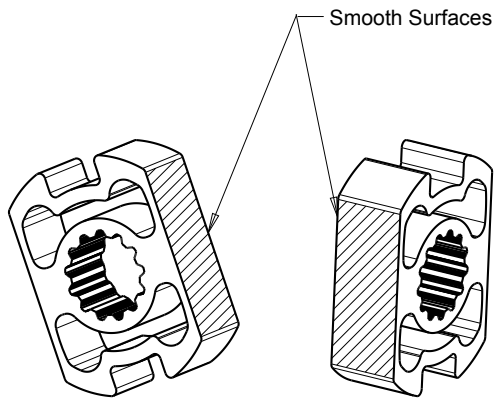


Fig. 5.11 A drawing of easily customizable and compact strain gauge based joint torque sensor. Smooth surfaces show where strain gauges are to be glued on both wings.

proposed design with the help of my colleague, Mariapaola D'Imperio at IIT. It is done by changing the overall size, the material and/or "wings" width and thickness it is possible to modify torque sensor performances in terms of full scale and sensitivity without affecting its linearity and symmetry. The experimental results are compared with the simulation results for the design validation. This small-scale instance of the sensor design is successfully installed on the MiniHyQ robot.

#### 5.4.1 Design

In order to find a compact solution due to limited space, we started with scaling down and investigating the traditional strain gauge based designs. **Four spokes based torque sensor** It is a classic example of strain gauge based torque sensor. The main drawback of this design, due to four spokes it is not easy or possible to glue and wire strain gauges on it. It provides reasonable output for medium-sized applications, but it is not feasible for compact applications.

**Two spokes based torque sensor** Design with two spokes, seems promising for gluing strain gauges and symmetric output. However, due to size constraints, it was not possible to bring peak strain or stress in the middle of spoke to act like beam. Even though it is brought in the middle by changing spoke thickness and its round size, it reduced the horizontal flat surface

to less than 5mm (in our case, recommended horizontal length for mounting strain gauge is a minimum of 5 mm). So, both of the previous torque sensors already in use in the HyQ [49] were not suitable to be scaled. A new design was necessary.

The structure was designed following the linearity, the symmetry, the high sensitivity, and easy access requirements: to do that, the pros and cons of previous designs were analyzed. The main issues were the low sensitivity and the symmetry: the limit of first one depended on the access to the high strain areas, which was prevented by narrow spaces inside sensors, as shown in the Fig 5.12 (left). With this kind of shape, it is not possible to improve the strain too much, because the maximum stress arises close to the connection between the circular section and the spokes and it exceeds the yield point of the material. While the second one depends on machining tolerance and/or asymmetric shapes, as shown in the Fig. 5.12 (left). To overcome these two limits, the new sensor was designed with two “twin-wings”, which were stretched or compressed depending on the torque clockwise or counterclockwise rotation, as shown in the Fig. 5.13.

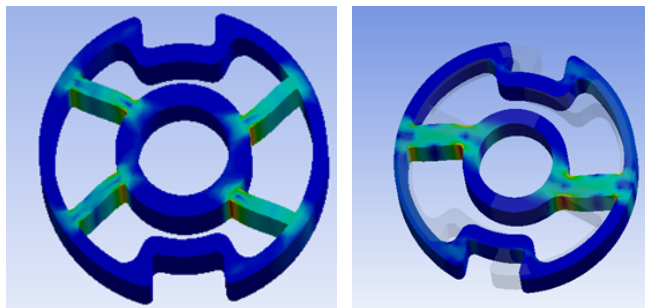


Fig. 5.12 Torque Sensor with (*left*) four spokes; (*right*) two spokes.

Another fundamental improvement given by these “twin-wings” is that this torque sensor has a linear behavior and high strain, as not only are they stressed within small displacements, that guarantees the linear strain, but also the strain-gauges can be attached to the highest value strain spot. To make the access easier, the smoothed surface where to glue the strain-gauges were designed outside the torque sensors, as shown in the Fig. 5.13, moreover the high quality of gluing guarantees the sensor reliability. Last but not least, the strain-gauges were connected via half-bridge in order to maximize the signal and temperature compensation. That structure, moreover, permits the elimination of the residual differences between clockwise and counterclockwise application torque (due to machining and geometrical tolerances, material properties etc.): the strain-gauges were connected to sum the signal from two specular “wings”, as shown in the Fig 5.13. That means the behavior becomes symmetric, as shown in the Fig. 5.14 and Fig. 5.15.

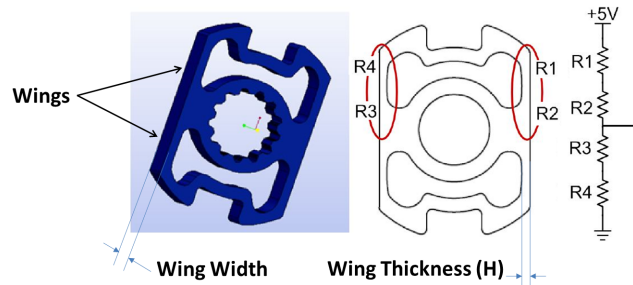


Fig. 5.13 Drawing of Torque Sensor. (left) CAD drawing, (right) Strain Gauges Positions

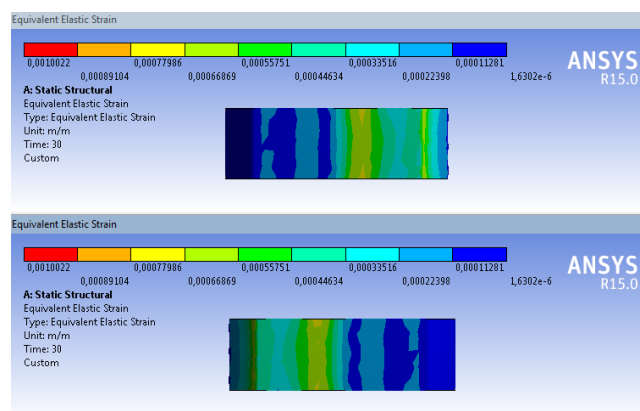


Fig. 5.14 Simulated strain with counter clockwise applied torque at maximum value (60Nm): (top) upper surfaces, (bottom) lower surface

### 5.4.2 Simulations

Virtual prototyping design (in particular finite element analysis) was applied to envisage the torque sensors behavior and to perform a sensitivity analysis with respect to four parameters: material, size, “wing” width and thickness.

CASE NUMBER	MATERIAL	SCALE	W	H
0	39NiCrMo3	1:1	1:1	1:1
1	Ergal	1:1	1:1	1:1
2	Titanium	1:1	1:1	1:1
3	39NiCrMo3	<b>1:1.25</b>	1:1	1:1
4	39NiCrMo3	<b>1:0.75</b>	1:1	1:1
5	39NiCrMo3	1:1	<b>1:1.25</b>	1:1
6	39NiCrMo3	1:1	<b>1:0.75</b>	1:1
7	39NiCrMo3	1:1	1:1	<b>1:1.25</b>
8	39NiCrMo3	1:1	1:1	<b>1:0.75</b>

Table 5.2 Simulations Plan

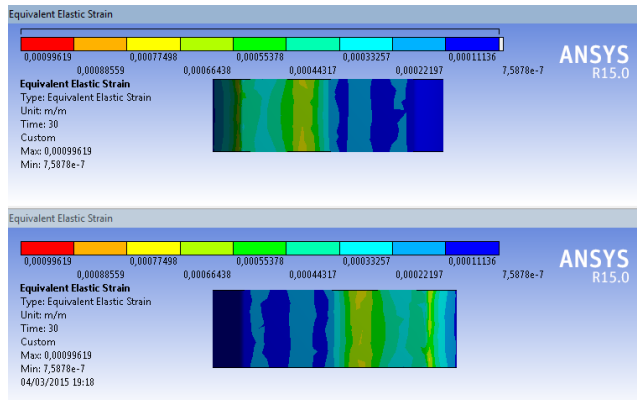


Fig. 5.15 Simulated strain with clockwise applied torque at maximum value (60Nm): (top) upper surfaces, (bottom) lower surface

### Numerical Model

The numerical analysis carried out in this work has the purpose of investigating how much the torque sensor behavior could be affected from the variation of some parameters like material, scale, wing width and wing thickness, as shown in the Fig. 5.13. Table 5.2 resumes all the simulation characteristics, all the ratios are referred to the dimension of the physical prototype. Two materials were analyzed: aluminum and titanium. Both of them behave weakly if compared to the original material (steel: 39NiCrMo3). The torque sensor was 1:0.75 and 1:1.25 scaled. Then the wing width (W) and wing thickness (H) were investigated, changing one values higher and one lower, as shown in the Table 5.3 . All the simulations were carried out using the commercial program ANSYS r15.

CASE NUMBER	Number of elements
0	13137
1	13137
2	13137
3	13112
4	13119
5	14405
6	10293
7	13552
8	12492

Table 5.3 Simulations Plan

The mesh was realized by using a quadratic element with six degrees of freedom for each node, suitable both for linear and for non-linear applications (SOLID 189, Ansys user's manual), as shown in the Fig. 5.16.

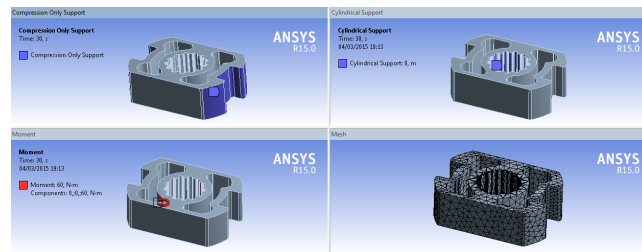


Fig. 5.16 Finite Element Model: (top left) the contact constraint between the Sensor and the case, (top right) the fix constraint, (bottom left) the applied torque, (bottom right) the mesh.

The constraint and the load applied aim to reproduce the experimental tests conditions. More in detail, the device was fixed to the external environment through a joint applied on the external surface (a contact constraint that takes into account the unidirectional interaction between the torque sensor and the external case) and it was subjected to a tangential ramped torque (from 0 to 60 Nm) both in clockwise and in counterclockwise direction applied in the internal hole.

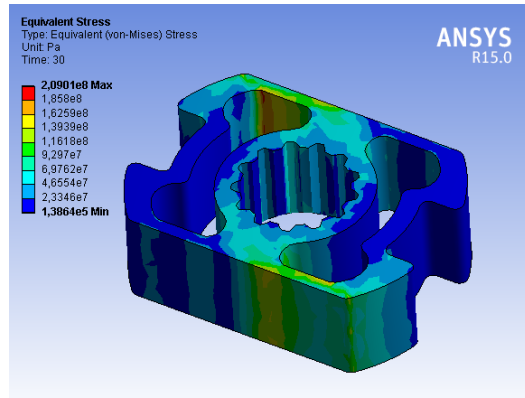


Fig. 5.17 The Simulated Von Mises Stress at maximum load (60Nm) demonstrates that the maximum stress value of Torque Sensor is more than 25% under the yield point (260MPa).

The simulations were run and the results were carried out. First, the stress was checked in order to ensure that the torque sensor was far from the yield point, as shown in the Fig. 5.17. Then the parameters were investigated. The first overall observation is that the torque sensor is linear and symmetric, because all the charts show that in CWR and CCWR the behavior is straight and with the same inclination.

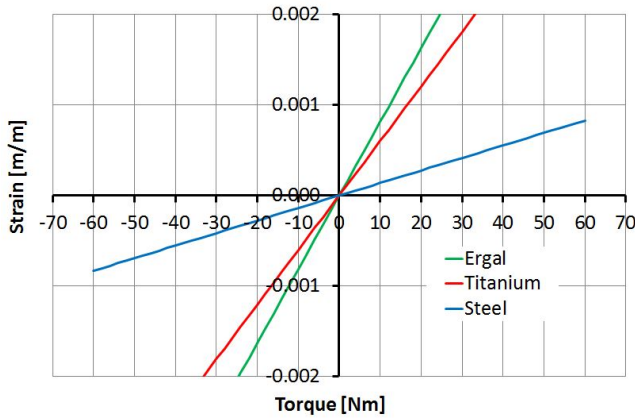


Fig. 5.18 Relationship between the Torque and the Strain depending on the Material: the 25% of variation influences Torque Sensor behavior. The Titanium and even more the Ergal are weaker than the original material (steel) and therefore, as expected, the strain increases several times. It is possible to notice that, more than 0.002 of strain, the materials were close to the yield point, so it was not anymore possible to increment the torque further.

### Effects of Material

Two materials were investigated in order to check their effect on the strain measurement. The Ergal(7000 series) was so stressed that got the yield point at 25Nm of torque and the titanium around 33Nm. This meant they are not suitable for this load. This result permits to the range of the material characteristics for building a torque sensor suitable for 60Nm, as shown in the Fig. 5.18.

### Effects of Scaling

The scale was incremented and decremented of 25% and the results demonstrate that this parameter influences the strain significantly: the strain was doubled or an half, as shown in the Fig. 5.19. That means it is possible to have some noticeable modification of the full scale of the torque sensor, changing just a few percentages of the size.

### Effects of Wing Width and Thickness

As expected, “wing” width and thickness influenced the torque sensor strain rate significantly. In particular, the increment of 1.25 of width is less sensitive than 1.25 of thickness, it was expected according to the applied design rules [41] as shown in Fig. 5.20 and 5.21.

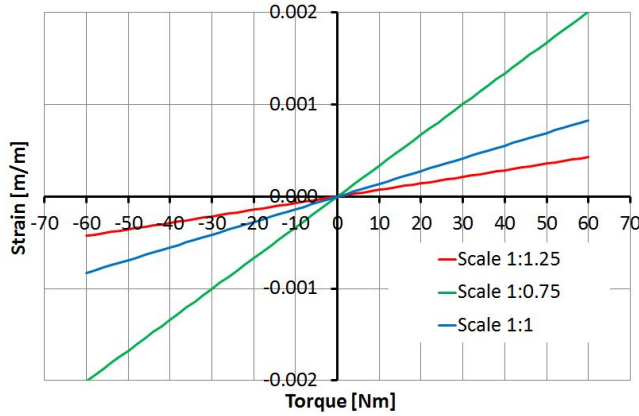


Fig. 5.19 Relationship between the torque and the Strain depending on the Size Scale parameter: the 25% of variation influences Torque Sensor behavior. The reduction increases more than double the strain and the increment of the scale reduces it about an half.

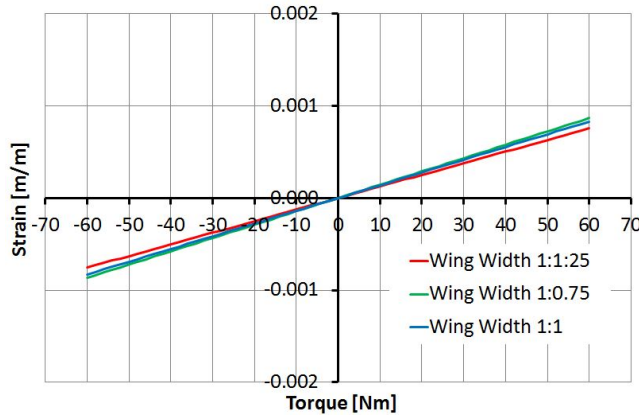


Fig. 5.20 Relationship between the torque and the strain depending on the Wing Width parameter: the 25% of variation is almost negligible. It is possible to notice that the reduction of the width has more influence than the increment.

### 5.4.3 Validation

The experimental results are compared with the simulation results, as shown in the Fig. 5.22. The good agreement between the two outputs demonstrate that both the physical and numerical model are well designed: they are linear and symmetric. Moreover, the small difference of between the two models means that the finite element model can be used for further investigation with high reliability.

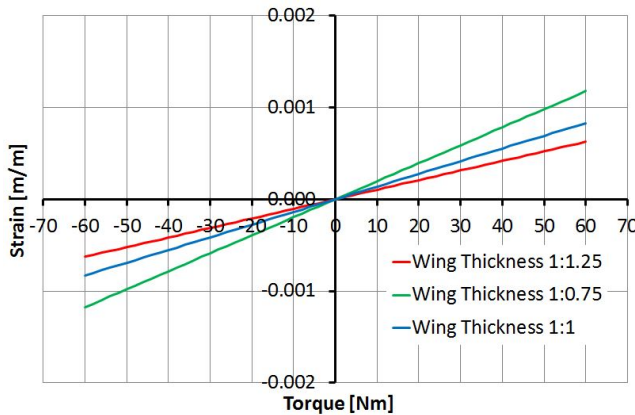


Fig. 5.21 Relationship between the torque and the strain depending on the wing thickness parameter: the 25% of variation influences torque sensor behavior. The reduction increases more than 40% the strain and the increment of the thickness reduces it about that 25%. That means the width reduction has more influence than the width increment.

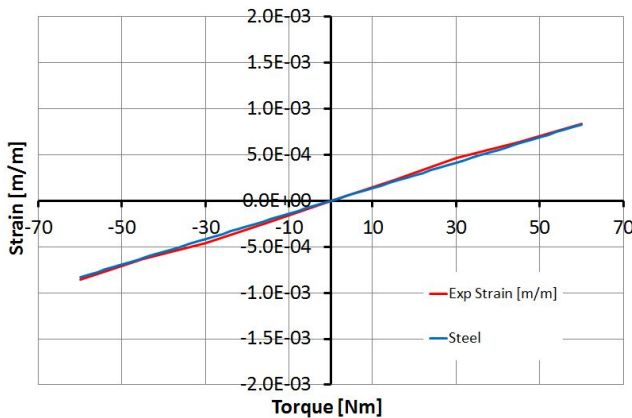


Fig. 5.22 Experimental result vs FEM

## 5.5 MiniHyQ Control System

The control system architecture of miniHyQ is shown in Fig. 5.23. It basically consists of a main unit and 4 leg units. In the main unit, the control PC running Linux kernel patched with real-time Xenomai takes care of all low level control of servo valves via main I/O board and high level control such as leg trajectory. Leg units collects input signal from 3 magnet encoders (19 bit, absolute type), 2 force sensors ( $\pm 4448\text{N}$ ) and 1 custom designed torque sensor, and sends these data to the main unit. For communication between each unit, EtherCAT bus is used and gives the system high speed real time communication. Additionally power for the leg units is supplied via LAN cables which construct EtherCAT bus i.e. Power over EtherCAT. For simulation and real-time control software, SL(Simulation Laboratory)

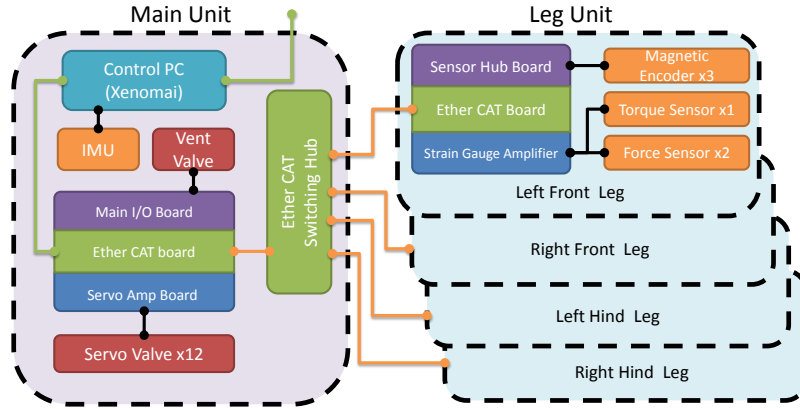


Fig. 5.23 MiniHyQ’s control system architecture

developed by Stefan Schaal [47] is used. Since SL can be used for both simulation and real robot controller, we can conduct an experiment and a simulation seamlessly. As a low level controller, each joint is fully torque controlled based on the HyQ’s torque controller [10]. Full torque control allows the robot to perform active compliance, which is essential to cope with impact during dynamic motions. Furthermore, inverse dynamics can be used for improving control of locomotion[5].

## 5.6 Power Pack

In this section, we explain the step by step designing procedure of the hydraulic system of MiniHyQ. Table 5.4 shows the specification of the designed power pack. MiniHyQ’s power pack schematic and its implementation are shown in Fig. 5.24 and Fig. 5.25 respectively. The hydraulic system consists of a power pack, which includes a pump and an electric motor and manifolds, which include vent valve and relief valve for safety. This power pack is detachable and it can be replaced by an external pump if it is available. Before designing a hydraulic system, the maximum pressure of a hydraulic system was decided by the actuator’s maximum pressure, which is 20MPa. In following the design, we use this value as maximum pressure.

### 5.6.1 Estimation of required flow rate

First of all, we estimated required flow rate for each actuator. In order to estimate required flow rate, we used the experimental data of the quadruped robot HyQ. Since MiniHyQ and HyQ have almost the same length of leg segments, we assumed that required angular

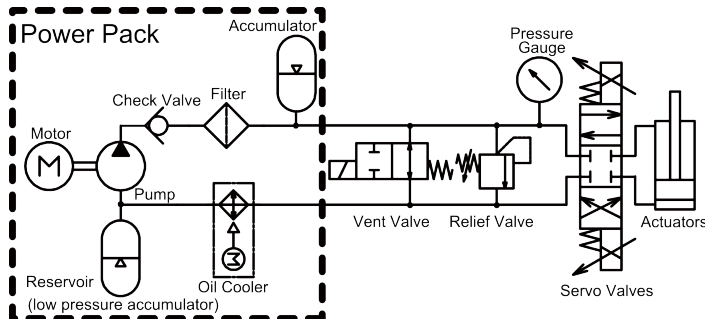


Fig. 5.24 Schematic of a hydraulic system.

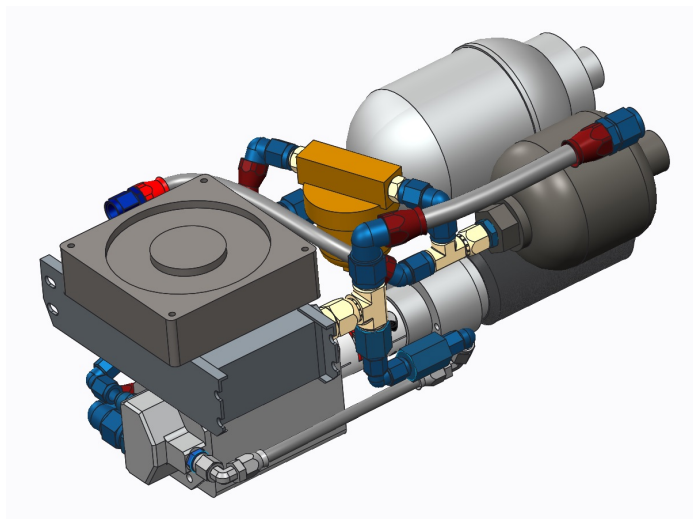


Fig. 5.25 CAD model of MiniHyQ Power pack.

velocity of each joint is same for MiniHyQ and HyQ. As a template motion that determines the maximum performance of the robot, 2m/s running trot and 0.2 m squat jump were chosen. As we explained in Section 5.3, MiniHyQ has different leg mechanism compared to HyQ. Required flow rate for each joints is calculated by multiplying required angular velocity and volumetric displacement of each actuator. In case of a rotary actuator for HFE, volumetric displacement is constant. However in case of linear actuator with linkage mechanism for HAA and KFE, volumetric displacement varies with each position and the volumetric displacement is calculated by inverse kinematics. Figure 5.26 shows the sum of the required flow rate of all of the actuators and leakage flow of servo valve.

### 5.6.2 Selection of Servo Valve

MiniHyQ has 12 active joints and its each actuator is controlled by the high performance servo valve. Valve mass, flow leakage, bandwidth, and price are the most critical parameters for

Table 5.4 MiniHyQ Power Pack

Size(L x W x H)	0.59 x 0.20 x 0.19 m
Weight	12 kg
Max Flow Rate	13 L/min
Max System Pressure	20 MPa
Max Power Consumption	5.5 kW

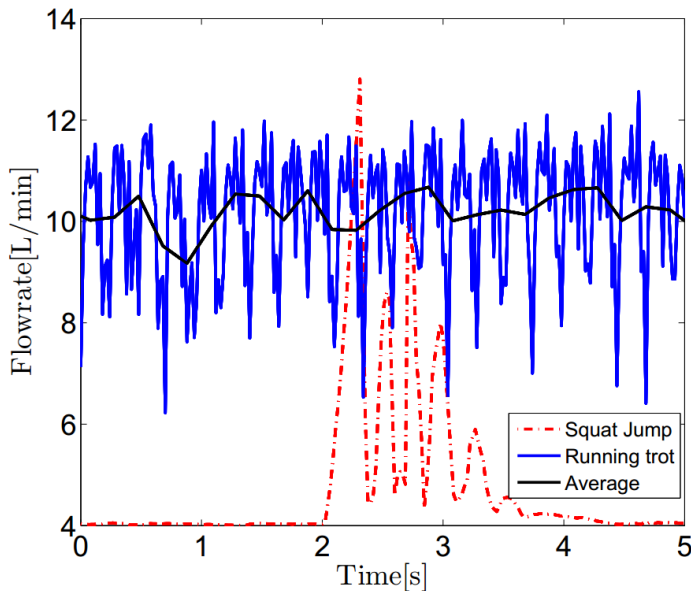


Fig. 5.26 Estimated flow rate, blue line shows the total required flow rate of the robot for a running trot, red dotted line shows the total required flow rate for a squat jump, and the black line shows the average flow rate while running tort.

valve selection. Table 5.5 shows the comparison of the three smallest servo valves available on the market. Moog E024 is the lightest and offers the highest frequency bandwidth among them. Star ST-200 servo valve offers high flow leakage as compared to Moog E024 and E242. MiniHyQ used 12 Moog E024 servo valves due to its small size, light weight, and high frequency control bandwidth. In order to control the dynamic walking of a robot such as MiniHyQ, a quick response and lightweight servo valve is required. We chose MOOG E024, which is also used for HyQ.

### 5.6.3 Selection of pump and motor

According to Fig 5.26, the required average flow rate which pump need to supply is 10 L/min. However, to have a margin in the system we selected a pump and motor to fulfill the

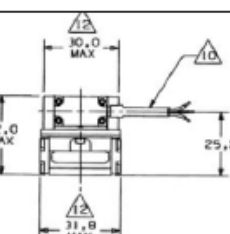
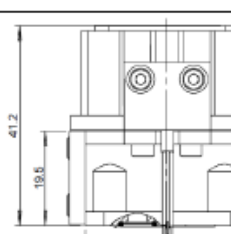
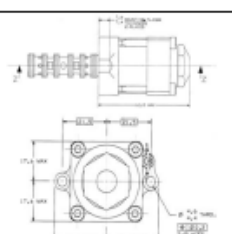
Servo valve type	MOOG E024	STAR ST-200	MOOG E242	
				
Mass	92g	230g	380g	
Max Pressure	210 bar	NBR 315 bar FPM 280 bar EPDM 210 bar (NBR FPM EPDM Seal materials)	210 bar	
Rated flow options @70 bar	.4,1,1.5,2,3.8,5,7 and 7.4 l/min	2 , 4 & 7 l/min	5,7 , 10 & 18 l/min	
Leakage flow	standard Low leakage Ultra low leakage	0.3l/min@210bar 0.18l/min@210bar 0.12l/min@210bar	≤ 0.7 l/min@140bar	@140 bar 5 l/min version: 0.05l/min 7 l/min version:0.07l/min 10 l/min version:0.1l/min 18l/min version:0.15l/min
Band width in 25%	standard Low leakage Ultra low leakage	-3dB attenuation >250Hz -3dB attenuation >120Hz -3dB attenuation >80Hz	-3dB attenuation>120Hz	-3dB attenuation>150Hz
Temp range	0 to 135 °C	-29 to 135 °C	0 to 135 °C	
Dimensions				

Table 5.5 Miniature Hydraulic valves comparison

maximum flow rate of 13 L/min. The important points of pump selection are lightweight, low volumetric displacement, and high input speed. Lightweight is always important for a mobile robot. However, the requirement of low volumetric displacement and high input speed

come from an electric motor which runs efficiently at a high speed and low torque region. Considering the above points, we chose TAKAKO micro pump (axial piston pump with constant volumetric displacement) and high power brushless DC motor originally designed for a hobby air plane by Neu motor (maximum output power is 10 kW and weight is 1.36 kg without gearbox). The motor has a one stage planetary gear box to match the maximum input speed of the pump and reduce the required torque of the motor to achieve 20 MPa. Additionally, the motor has a cooling fan to keep itself working fine in a static situation. We chose a motor driver for the hobby air plane developed by Astroflight. This motor driver can handle up to 10 kW.

#### 5.6.4 Accumulator

To absorb a sudden change of flow rate and deviation of flow rate because of the pump, an accumulator is required. In this case, a diaphragm accumulator was chosen to compensate the 3 L/min, which is the difference between the maximum flow rate 13 L/min and the average flow rate 10 L/min. To select appropriate accumulator we assume adiabatic change, actuation time of accumulator is 0.2s and the minimum operation pressure is 18 MPa. If we want to sustain 3 L/min, the accumulator needs to provide 0.1 L. Pre-charged pressure 14.4 MPa is calculated by using the recommended compression ratio of 0.8. From these values required pre-charged nitrogen gas volume is calculated by the equation below.  $V_i$  and  $P_i$  means the volume and the pressure of nitrogen gas of each state.  $i=0$  is pre-charged state,  $i=1$  is minimum hydraulic pressure state, and  $i=2$  is the maximum hydraulic pressure state. The efficiency of the accumulator is assumed to be 0.95.

$$V_0 = \frac{(V_1 - V_2)}{\left( \left( \frac{P_0}{P_1} \right)^{1.4} - \left( \frac{P_0}{P_2} \right)^{1.4} \right)} \times \frac{1}{\eta} \quad (5.2)$$

We searched the accumulator, which has a gas volume of more than 0.17 L and found HYDAC 0.32 L diaphragm accumulator to be the smallest and lightest one.

#### 5.6.5 Filter and Oil cooler

The servo valves require NAS 3 or lower. We choose a line filter as lightweight filter among the one fulfilling this requirement and the maximum operation pressure of 20 MPa. The estimated pressure drop is 0.15 MPa at a flow rate of 13 L/min, thus we considered this pressure drop to be acceptable. We chose an oil cooler that has an aluminum honeycomb

shape and its cooling capacity is estimated at 2300 W with 9.0m/s air flow. Since we use a constant volumetric pump, if the robot does not consume kinetic energy e.g. standing, most of energy will be turned into heat and it is difficult to cool such an amount of heat by the oil cooler and also a lot of heat dissipation decreases the energy efficiency of the robot. In order to avoid these problems, we will control the rotation speed of the pump depending on the movement of the robot.

### 5.6.6 Reservoir

In the case of legged robots, their torso is always vibrating and the air can enter into the oil because of walking motion, although conventional reservoir is usually open to the atmosphere. In order to solve this problem, some aircraft use self-pressurizing reservoirs (boot strap reservoirs). However, a commercial self-pressurizing reservoir is too bulky for a mobile robot, thus we use an accumulator as a reservoir. The maximum system oil difference was estimated at 0.19 L (linear actuator  $x8 = 0.06L$ , accumulator = 0.1 L, temperature variation = 0.03L). By following the same procedure as section 5.6.4, if we assume maximum pressure = 0.5MPa, minimum pressure = 0.2MPa and pre-charged pressure = 0.17MPa, the required gas volume is calculated as 0.47 L.



Fig. 5.27 Picture of Micro Pump used for the MiniHyQ's power pack.

### 5.6.7 Manifold

Two separate centralized manifolds are used for the front and hind legs. Both manifolds are identical and each has a capacity of six valves. It is shown in Fig. 5.28. A centralized manifold is placed in the torso rather than using distributed manifolds on each leg and this design is validated by FEM analysis.



Fig. 5.28 MiniHyQ's centralized manifold.

## 5.7 Final Design of MiniHyQ

Table 5.6 shows the specification of MiniHyQ and its CAD model with exposed view that can be seen in Fig. 5.29. MiniHyQ is fully torque controlled and measured directly at the joint. High performance miniature hydraulic connectors are used to ensure that there is 0% oil leakage. We made sure that Minihyq have high torque density and a wide range of motion that allows it to preform extreme tasks like self righting and high jumping. MiniHyQ self-righting sequence is demonstrated in Fig 5.30.

Table 5.6 Specifications of MiniHyQ Robot

Dimensions (LxWxH) (Fully stretched legs)	0.85 m x 0.35 m x 0.77 m
Weight (off-board/ on-board Power Pack)	24 kg, 35 kg
Degrees of Freedom	12 (3 per leg (2-linear 1-rotary hydraulic actuator))
Joint Torque/ Range of motion	75 Nm, 90° Hip AA 60 Nm, 220° Hip FE 75 Nm, 180° Knee FE
Sensors per Leg	2 Load cells, 1 Torque sensor 3 Absolute encoders
Hydraulic Valves	12 High performance servo valves
On-board Computing	1 computer (real time Linux)
Operating Pressure	20 MPa
Peak Flow Rate	13 l/min

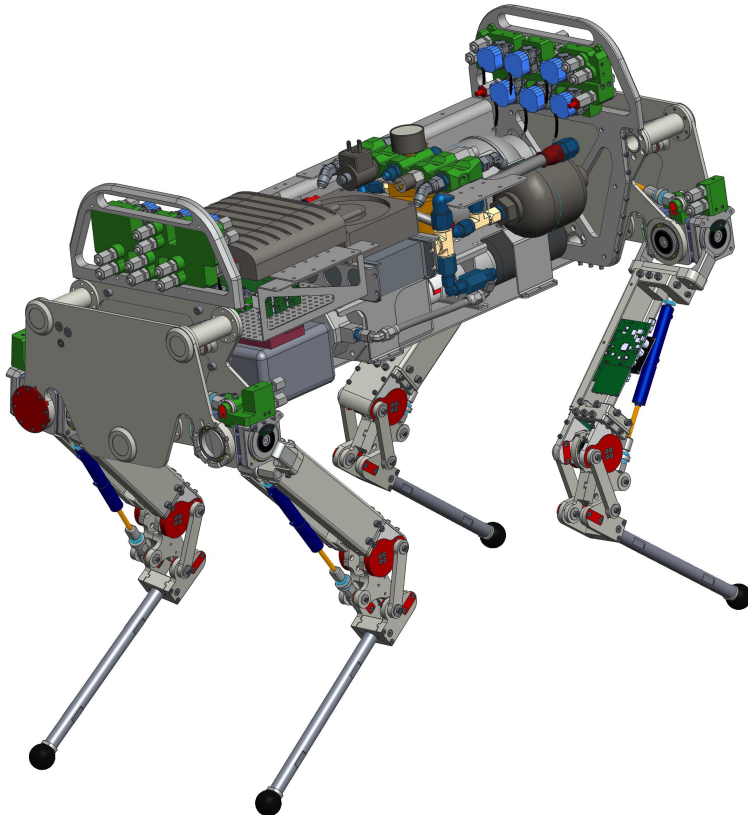


Fig. 5.29 The CAD model of MiniHyQ with an exposed view of the onboard power pack, magnetic encoder disks, and EtherCat control PCB in upper leg link.

## 5.8 Conclusion

This chapter presents the design of the development of the lightweight hydraulic quadruped robot '*MiniHyQ*'. To the authors best knowledge, MiniHyQ is the lightest and smallest hydraulic quadruped robot that has been built so far. MiniHyQ is a fully torque controlled robot. It has reconfigurable leg configurations. It has a wide joint range of motion and an onboard compact power pack. The robot with fully stretched legs has the following dimensions 0.85m x 0.35m x 0.77m (LxWxH) and weighs 25 kg with an external hydraulic power supply and 34 kg with a complete hydraulic system onboard. We discussed the mechanical structure of the robot torso and legs in detail. We have also shown the development of a new innovative design of a strain gauge based torque sensor with a high degree of linearity, symmetry, and scalability (both in dimension and measuring range). The chapter ends with the detailed development of the MiniHyQ powerpack.

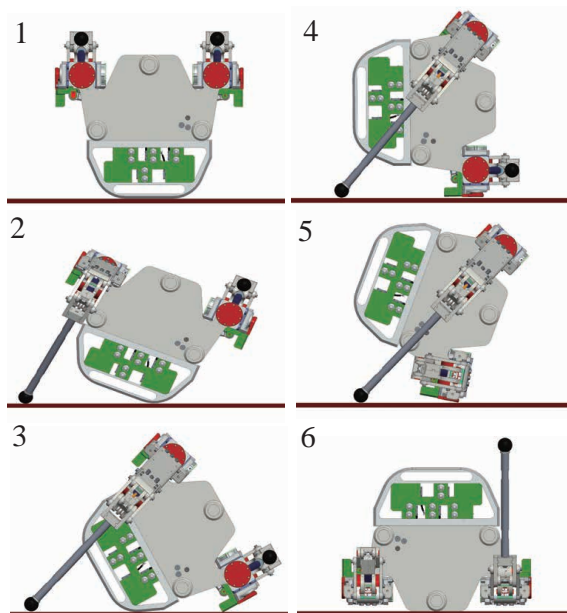


Fig. 5.30 Self-righting sequence, front view. From 1 to 6: After a fall, the robot lies on its top. To right itself, the robot first has to move the feet of the two legs at one side and push to the ground up to turn its torso. The HAA will then rotate to push the robot up until the Center of gravity (CoG) passes the pivot point of the frame. As a consequence, the robot will then roll back onto the bottom of the torso. The retracted legs will then extend to move the robot back onto its feet.

# Chapter 6

## Results and Discussion

This chapter discusses the experimental tests which were performed for the design and hardware validation. It includes the testing of first prototype isogram knee joint and its comparison with the final version of isogram knee joint. This chapter also presents the testing on the final version of MiniHyQ's single leg. This chapter ends with experimental testing and the validation of MiniHyQ's torque sensor.

### 6.1 Experimental testing of First Prototype of Isogram Knee

As proof of the concept, we built and tested an early design of the knee joint mechanisms, as shown in Fig. 6.1. The implemented design is in accordance with the optimization results. The upper link is built with a folded 1.5 mm aluminium sheet and the lower link with a square-section carbon fiber rod. The knee mechanism is constructed with machined aluminium parts and ball bearings with tight tolerances to avoid backlash in the mechanism. To check the stability of the hardware, we performed a *push up* motion. The experimental setup is shown in Fig 6.1, where the upper leg is attached to a revolute hip joint. A Push ups task is preformed by moving the foot in a vertical trajectory below the hip joint at 0.5 Hz with a 12 kg payload. Results are shown in Fig. 6.2. Figure 6.3 shows a picture sequence of an experimental motion through the whole joint range of motion.

#### 6.1.1 First Prototype vs. Final Prototype Isogram knee Joint

We demonstrated that despite its higher complexity, the isogram mechanism is superior to the traditional design, because its many kinematic parameters can be fine-tuned to achieve an optimal torque profile. Such profiles should preferably lead to a robotic leg that is strong in

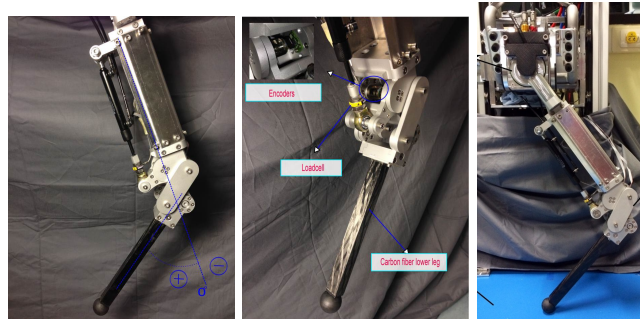


Fig. 6.1 Hardware implementation. *Left:* Side view of the *isogram mechanism* based knee joint; *center:* close up view of load cell and encoders; *Right:* Experimental setup for performing push ups.

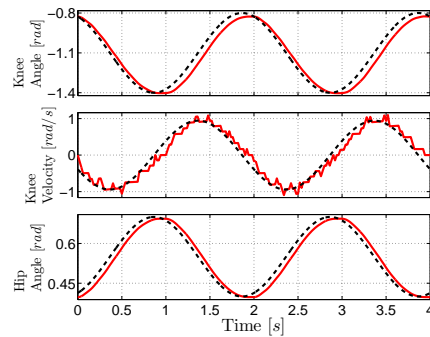


Fig. 6.2 Plot of experimental measured data of isogram knee (red solid), reference data (black dashed) for push ups at 0.5Hz (with 12Kg payload). *Top:* knee joint angle; *middle:* knee velocity; *bottom:* Hip joint angle.

a flexed configuration and fast when almost extended. We demonstrated how smooth and optimized torque profiles can be obtained by parameter optimization. The weights  $W_1$  and  $W_2$  are currently selected in a heuristic way. A more detailed study of the influence of these weights is required. Furthermore, we noticed that if we penalize  $d$  in the objective function we might end up with solutions that favor larger overall sizes of the mechanism. Since we aim for compact and lightweight designs, instead of penalizing small  $d$ , an objective function that keeps the angle  $\beta$  away from  $180^\circ$  might be more suitable since it does not lead to larger designs.

In the first version, it was decided that a manifold in upper link would be used, so we fixed  $L_{06}$  at a certain value. The variable  $L_{06}$  is the distance between the reference node 0 to cylinder mounting node 6, as shown in Fig. 5.27. We fixed  $L_{06}$  to keep some space for leg electronics and hydraulic manifold, which has to fit inside the upper link. In the second version, we decided to use a centralized manifold within the torso to keep the leg lightweight and then the optimized parameters resulted in  $L_{06}$  being equal to zero. Besides an improved

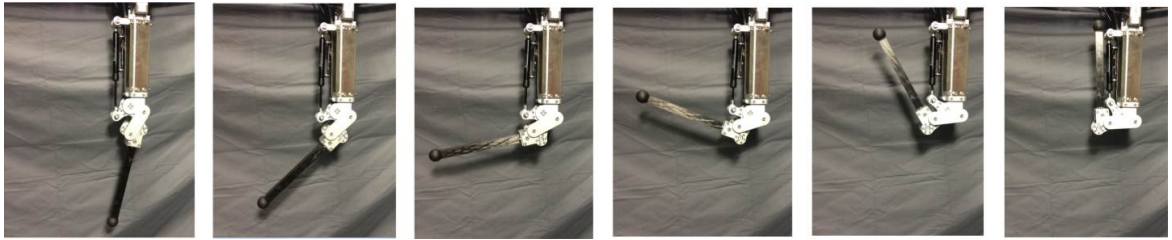


Fig. 6.3 Picture sequence of the prototype leg during an experiment that moves the knee joint from extended to a completely retracted position.

torque profile (shown in Fig 6.5), the mechanical design also benefited from L06 being zero since it enabled a more compact and lighter design. The resulting mechanical design of the upper and lower leg of the final design (see CAD model in Fig. 6.4 (right)) is 28% lighter.

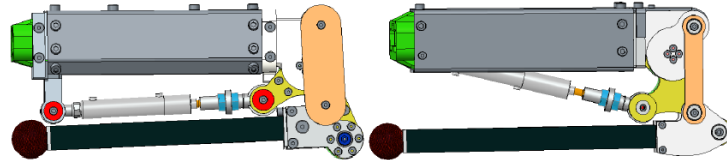


Fig. 6.4 CAD models (left). Full view CAD model of implemented knee joint. Its total mass is 1.43 Kg; (right) a CAD model of final design. Its total mass is 1.05 Kg and it is also noticeable that the link length L06 is equal to zero.

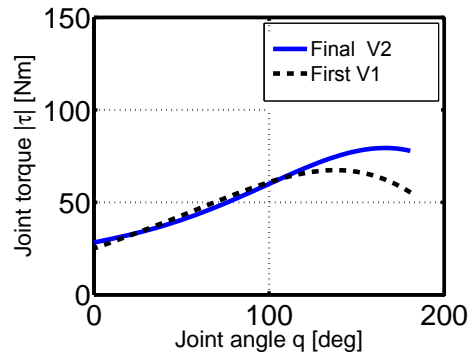


Fig. 6.5 Torque Profile: First prototype vs Final MiniHyQ's Isogram knee joint .

## 6.2 Experimental testing of final version of MiniHyQ Leg

For the design validation, the initial experiments are performed on MiniHyQ's single leg connected to a slider, which only allows the leg to move in vertical direction. The experimental

setup can be seen in Fig. 6.7 for the initial leg testing, where the electronics hub board is attached to the outside of the upper link. For the initial testing of the leg, we attached the 3 kg load to its foot and swung it through the air at 1.2 Hz. Figure 6.6 shows its results, with reasonable torque tracking and poor position tracking. These preliminary results are taken by using a very simple low level hydraulic controller without taking into account the velocity and pressure compensation terms [10]. PID gain are not properly for hardware validation.

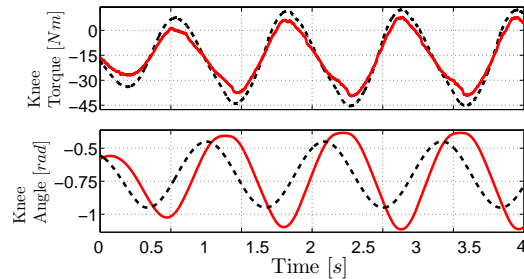


Fig. 6.6 Plot of experimental measured data(red solid), and reference data (black dashed) for the leg swinging through the air at 1.2 Hz with a 3kg load attached to the foot. *Top*: knee joint torque ; *bottom*: knee joint angle.

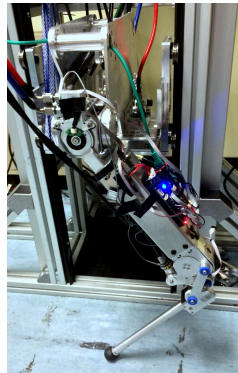


Fig. 6.7 Experimental setup; Single MiniHyQ leg is connected to a slider slider which allows it to move freely up and down (vertically).

### 6.3 Experimental validation of Torque Sensor Design

The torque sensor was machined and the half bridge strain gauges was easily glued on the both sides, to maximize the signal. To verify the design performances, an experimental test was carried out by loading the torque sensor with a force in order to reproduce the working conditions. The torque was applied with a beam and the masses hanged on its ends, as shown

in the Fig. 6.8. The beam length and the masses  $m$  varies according to the desired torque requirement. As such, the applied torque is defined as  $\tau = m * g * b$ , where  $g$  is the gravity acceleration.

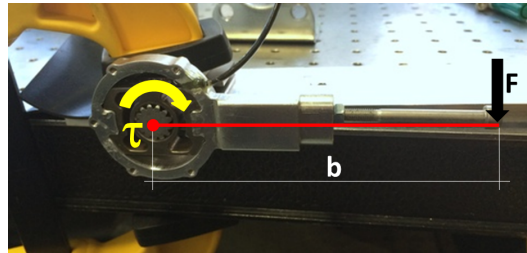


Fig. 6.8 Experimental Set Up. The Force (F) was applied at distance (b) in order to obtain the Torque ( $\tau$ ) on the Sensor

The experimental output of the half bridge strain gauges against applied torque is shown in Fig. 6.9.

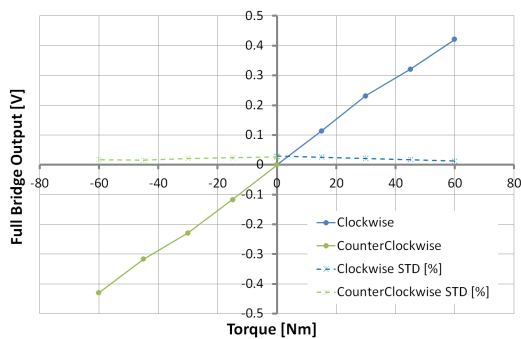


Fig. 6.9 Experimental results of torque sensor while varying torque CWR and CCWR.



# Chapter 7

## Conclusion and Future Work

### 7.1 Conclusion

MiniHyQ is a pioneer and is a slightly smaller in size than the previous robot, HyQ [49], built by our group (the DLS lab). However, MiniHyQ is the lightest among all the existing hydraulically actuated quadruped robots [46] [17] [44] [32] [25] [49]. The development of this robot is a significant step forward in miniature hydraulics in robotics. The ultimate goal of MiniHyQ is that it should be able to cope with all sorts of rough terrain and work power-autonomously for several hours. The objective of this dissertation is to make a significant contribution to the development of a lightweight, highly dynamic, and versatile hydraulic quadruped robot MiniHyQ with a compact on-board power pack. The following goals have been reached to meet the final objective:

- The development of 34 kg lightweight hydraulically actuated quadruped with a compact on-board power pack. It is designed to have a high joint torque density and a wide joint range of motion.
- Several scaling design studies for the development of a quadruped robot with a focus on hydraulic joint actuation design and kinematics. Based on these scaling studies, actuators have been selected according to the joint's specifications and requirements.
- A novel knee joint is implemented for the MiniHyQ robot. Despite its higher complexity, the isogram mechanism is superior to the traditional design, because its many kinematic parameters can be fine-tuned to achieve an optimal torque profile. Such profiles should preferably lead to a robotic leg that is strong in a flexed configuration and fast when almost extended.

- An innovative compact torque sensor design is proposed and implemented. It is shown to have a high degree of linearity, symmetry, and scalability (both in dimension and measuring range). Furthermore, the gluing and wiring of the strain gauges are easy thanks to the geometry of the sensor that gives direct access to the mounting surfaces, even in compact dimensions. We show the design's symmetric (clockwise and counterclockwise rotation) and linear behavior through virtual prototyping and experimental tests. A detailed sensitivity analysis of the proposed design is presented by changing the overall size and the material and/or “wings” width and thickness. It is possible to modify torque sensor performances in terms of full scale and sensitivity without affecting its linearity and symmetry. The experimental results are compared with the simulation results for the design validation.
- A compact on-board power pack is designed for the MiniHyQ robot. The step by step procedure is demonstrated for component selection for its on-board hydraulic system. In order to keep MiniHyQ’s legs as lightweight as possible, a centralized manifold is placed in the torso rather than using distributed manifolds on each leg.
- For the design validation and hardware testing, a series of experiments are conducted on a single leg of the MiniHyQ robot. It includes its range of motion, joint velocities at different speeds, leg swing in air with a weighted load attached to the foot, and push up action when the leg is under the load.

## 7.2 Future Work

The development of a lightweight hydraulic quadruped robot MiniHyQ with a compact on-board power pack is only the first step. Currently, debugging and system testing of the MiniHyQ robot is in process. Once MiniHyQ is fully tested and operational, then a number of research goals can be achieved in the future. MiniHyQ’s future to-do list is given below:

- The versatility of MiniHyQ will be demonstrated in future work by performing different motions and gaits using MiniHyQ’s wide range of joint angles. It includes experiments such as MiniHyQ’s self-righting, walking, and running on an indoors treadmill and on rough terrains. These experimental tests will be started with the reimplementation of already existing HyQ’s locomotion algorithms.
- Future experiments will be performed on MiniHyQ using the on-board power pack.

- The effects of a CICR knee joint on the performance of the MiniHyQ robot locomotion will be studied.
- The application of a proposed torque sensor will be done on the other robots and then new requirements will be permitted to verify this torque sensor flexibility.



# Appendix A

## Publications

- **H. Khan**, M. D'Imperio, F. Cannella, D. G. Caldwell, and C. Semini. "**A design of customizable and compact strain gauge based joint torque sensor for robots**". In International Conference on Intelligent Robots and Systems (IROS), 2015. (under review)
- **H. Khan**, F. Cannella, D. G. Caldwell, and C. Semini. "**An innovative torque sensor design for the lightest hydraulic quadruped robot**". In International Conference on Climbing and Walking Robots (CLAWAR), 2015.
- **H. Khan**, S. Kitano, M. Frigerio, V. Barasuol, R. Featherstone, D. G. Caldwell, and C. Semini. "**Development of the lightweight hydraulic quadruped robot - MiniHyQ**". In The IEEE International Conference on Technologies for Practical Robot Applications (TePRA), 2015.
- **H. Khan**, R. Featherstone, D. G. Caldwell, and C. Semini, "**Bio-inspired Knee Joint Mechanism for a Hydraulic Quadruped Robot**", International Conference on Automation, Robotics and Applications (ICARA), 2015.
- **H. Khan**, S. Kitano, D. G. Caldwell, and C. Semini, "**Development of a lightweight on-board hydraulic system for a quadruped robot**", Scandinavian International Conference on Fluid Power (SICFP), 2015.
- **H. Khan**, C. Semini, V. Barasuol, D. G. Caldwell, "**Actuator sizing for highly-dynamic quadruped robots based on squat jumps and running trots**", International Conference on Climbing and Walking Robots (CLAWAR), 2013.

- **H. Khan**, C. Semini, D. G. Caldwell, "**Scaling of versatile quadruped robots for running trot**", Proceedings 6th International Symposium in Adaptive Motion of Animals and Machines (AMAM), 2013.
- C. Semini, **H. Khan**, M. Frigerio, T. Boaventura, M. Focchi, J. Buchli and D. G. Caldwell, "**Design and Scaling of Versatile Quadruped Robots**", Int. Conf. on Climbing and Walking Robots (CLAWAR), 2012
- J. Iqbal, **H. Khan**, N.G. Tsagarakis and D.G. Caldwell, "**A novel exoskeleton robotic system for hand rehabilitation - Conceptualization to prototyping**", Biocybernetics and Biomedical Engineering, 2014, 34(2) PP:79-89

## **Appendix B**

### **Definition of Joint Frames**

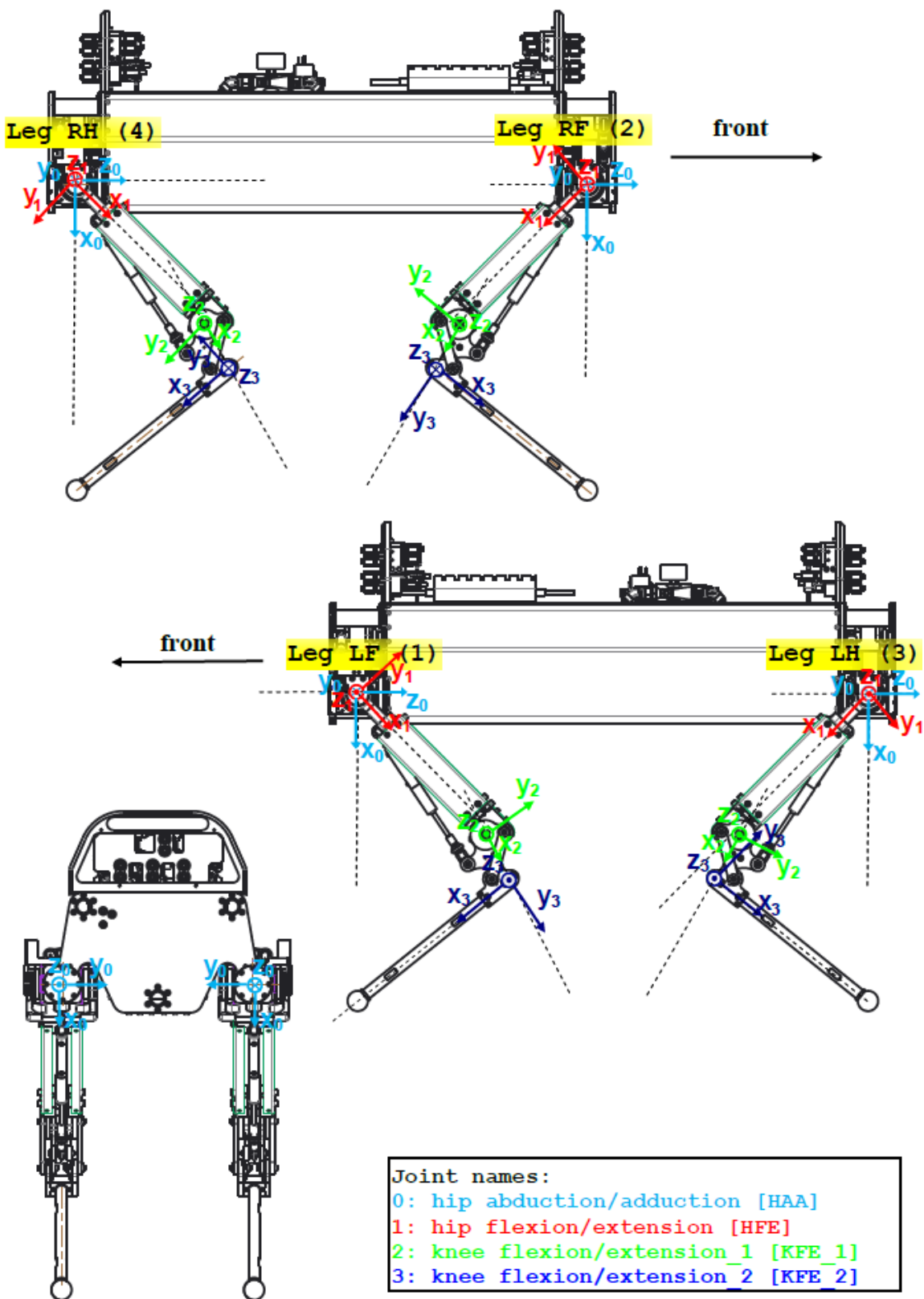


Fig. B.1 Definition of link coordinate systems and joint names.

# References

- [1] F. Aghili, M. Buehler, and J. M. Hollerbach. A joint torque sensor for robots. In *ASME International Mechanical Engineering Congress & Exposition*, 1997.
- [2] R. M. Alexander. The gaits of bipedal and quadrupedal animals. *The International Journal of Robotics Research*, 3(2):49–59, 1984.
- [3] R. M. Alexander. *Principles of Animal Locomotion*. Princeton University Press, 2003.
- [4] R. M.. Alexander and A. S. Jayes. A dynamic similarity hypothesis for the gaits of quadrupedal mammals. *Journal of Zoology*, 201(1):135–152, 1983.
- [5] V. Barasuol, J. Buchli, C. Semini, M. Frigerio, E. R. De Pieri, and D G. Caldwell. A reactive controller framework for quadrupedal locomotion on challenging terrain. In *IEEE International Conference on Robotics and Automation (ICRA)*, 2013.
- [6] Andrew A. Biewener. Allometry of quadrupedal locomotion: The scaling of duty factor, bone curvature and limb orientation to body size. *J. of Experimental Biology*, 105: 147–171, 1983.
- [7] R. Blickhan. The spring-mass model for running and hopping. *Journal of Biomechanics*, 22:1217–1227, 1989.
- [8] R. Blickhan and R.J. Full. Similarity in multilegged locomotion: bouncing like a monopode. *Journal of Comparative Physiology*, 173:509–517, 1993.
- [9] T. Boaventura, M. Focchi, J. Frigerio, M.and Buchli, C. Semini, G. A. Medrano-Cerda, and D. G. Caldwell. On the role of load motion compensation in high-performance force control. In *IEEE/RSJ International Conference on Intelligent Robots and Systems*, 2012.
- [10] T. Boaventura, G. Medrano-Cerda, C. Semini, J. Buchli, and D G. Caldwell. Stability and performance of the compliance controller of the quadruped robot hyq. In *IEEE/RSJ International Conference on Intelligent Robots and Systems (IROS)*, 2013.
- [11] D G. Caldwell, G. A. Medrano-Cerda, and M. Goodwin. Control of pneumatic muscle actuators. *IEEE Control Systems*, pages 40–48, 1995.
- [12] F. Caricchi, F. Crescimbini, F.G. Capponi, and L. Solero. Study of bi-directional buck-boost converter topologies for application in electrical vehicle motor drives. *APEC '98 Thirteenth Annual Applied Power Electronics Conference and Exposition*, 1998.

- [13] P. Chatzakos and V. Papadopoulos. The influence of dc electric drives on sizing quadruped robots. In *IEEE ICRA Conference*, 2008.
- [14] M. DiImperio, F. Cannella, C. Semini, D. G. Caldwell, D. Catelani, and R. Bernetti. Finite element analysis within component design process of hydraulic quadruped robot. In *ASME International Design Engineering Technical Conferences and Computers and Information in Engineering Conference*, 2014.
- [15] W. J. Duncan. *Physical similarity and dimensional analysis*. Arnold (London), 1953.
- [16] A. C. Etoundi, R. Vaidyanathan, and S. C. Burgess. *A bio-inspired condylar hinge joint for mobile robots*, pages 4042–4047. Institute of Electrical and Electronics Engineers, Sep 2011. ISBN 978-1-61284-456-5. doi: 10.1109/IROS.2011.6094924. URL <http://dx.doi.org/10.1109/IROS.2011.6094924>.
- [17] G. Feng, Q. Chenkun, S. Qiao, C. Xianbao, and T. Xinghua. A quadruped robot with parallel mechanism legs. In *2014 IEEE International Conference on Robotics & Automation (ICRA)*, 2014.
- [18] I. Fujii, T. Inoue, Dzung Viet Dao, S. Sugiyama, and S. Hirai. Tactile perception using micro force/moment sensor embedded in soft fingertip. In *Sensors, 2006. 5th IEEE Conference on*, pages 558–562, Oct 2006. doi: 10.1109/ICSENS.2007.355529.
- [19] D. Gouaillier, V. Hugel, P. Blazevic, C. Kilner, J. Monceaux, P. Lafourcade, B. Marnier, J. Serre, and B. Maisonnier. Mechatronic design of nao humanoid. In *2009 IEEE International Conference on Robotics and Automation*, pages 769–774, May 2009. ISBN 978-1-4244-2788-8.
- [20] P. Gregorio, M. Ahmadi, and M. Buehler. Design, control, and energetics of an electrically actuated legged robot. *IEEE Transactions on Systems Man and Cybernetics*, 27:626–634, 1997.
- [21] N.C. Heglund and C.R. Taylor. Speed, stride frequency and energy cost per stride: how do they change with body size and gait? *J. of Experimental Biology*, 138(1):301–318, 1988.
- [22] J.W. Hurst, J.E. Chestnutt, and A.A. Rizzi. An actuator with physically variable stiffness for highly dynamic legged locomotion. In *ICRA 04*, volume 5, pages 4662–4667, 2004. URL 10.1109/ROBOT.2004.1302453.
- [23] M. Hutter, C. Gehring, M. Bloesch, M. A. Hoepflinger, C. D. Remy, and R. Siegwart. StarlETH: A compliant quadrupedal robot for fast, efficient, and versatile locomotion. In *15th International Conference on Climbing and Walking Robot - CLAWAR 2012*, 2012.
- [24] M. Hutter, C. D. Remy, M. A. Hoepflinger, and R. Siegwart. Efficient and versatile locomotion with highly compliant legs. *IEEE/ASME Transactions on Mechatronics*, 18(2):449–458, Apr 2013.
- [25] N.I Kentaro, K.and Takuki, K. Yuki, K. Kota, and H. S. Hyon. Development of hydraulic quadruped walking robot -rl-a1. *The Robotics and Mechatronics Conference (ROBOMECH)*, 2014.

- [26] H. Khan, C. Semini, and D. G. Caldwell. Actuator sizing for highly-dynamic quadruped robots based on squat jumps and running trots. *Int. Conf. on Climbing and Walking Robots (CLAWAR)*, Jul 2013. doi: 10.1142/9789814525534\_0065.
- [27] H. Khan, R. Featherstone, D. G. Caldwell, and C. Semini. Bio-inspired knee joint mechanism for a hydraulic quadruped robot. In *International Conference on Automation, Robotics and Applications (ICARA)*, 2015.
- [28] H. Khan, S. Kitano, D. G. Caldwell, and C. Semini. Development of a lightweight on-board hydraulic system for a quadruped robot. In *The Scandinavian International Conference on Fluid Power -SICFP*, 2015.
- [29] H. Khan, S. Kitano, M. Frigerio, V. Barasuol, R. Featherstone, D. G. Caldwell, and C. Semini. Development of the lightweight hydraulic quadruped robot - minihyq. In *The 7th Annual IEEE International Conference on Technologies for Practical Robot Applications (TePRA)*, 2015.
- [30] H. Khan, F. Cannella, D. G. Caldwell, and C. Semini. An innovative torque sensor design for the lightest hydraulic quadruped robot. In *International Conference on Climbing and Walking Robots (CLAWAR)*, 2015 (under review).
- [31] H. Khan, M. DImperio, F. Cannella, D. G. Caldwell, and C. Semini. A design of customizable and compact strain gauge based joint torque sensor for robots. In *International Conference on Intelligent Robots and Systems (IROS)*, 2015 (under review).
- [32] J. T Kim, J. S. Jung, B.-Y. Park, S. Park, and Y. Lee. Experimental investigation on the design of leg for a hydraulic actuated quadruped robot. In *44th International Symposium on Robotics (ISR)*, 2013.
- [33] Zhibin L., N.G. Tsagarakis, and D.G. Caldwell. A passivity based admittance control for stabilizing the compliant humanoid coman. In *IEEE-RAS International Conference on Humanoid Robots (Humanoids)*, pages 43–49, Nov 2012.
- [34] D.V. Lee and S.G. Meek. Directionally compliant legs influence the intrinsic pitch behaviour of a trotting quadruped. *Proc Biol Sci*, 272(1563):567–572, 2005.
- [35] L. Maes, M. Herbin, R. Hackert, V. Bels, and A. Abourachid. Steady locomotion in dogs: temporal and associated spatial coordination patterns and the effect of speed. In *Journal of Experimental Biology*, 2008.
- [36] S. Meek, J. Kim, and M. Anderson. Stability of a trotting quadruped robot with passive, underactuated legs. In *Proceedings of the 2008 IEEE International Conference on Robotics and Automation (ICRA)*, 2008.
- [37] K. Oberg. Knee mechanisms for through-knee prostheses. In *Prosthetics and orthotics international*, 1983.
- [38] A. Parmiggiani, M. Randazzo, L. Natale, G. Metta, and G. Sandini. Joint torque sensing for the upper-body of the icub humanoid robot. In *Humanoid Robots, 2009. Humanoids 2009. 9th IEEE-RAS International Conference on*, pages 15–20, Dec 2009. doi: 10.1109/ICHR.2009.5379525.

- [39] F. Peuker, A. Seyfarth, and S. Grimmer. Inheritance of slip running stability to a single-legged and bipedal model with leg mass and damping. In *BioRob*, pages 395–400, june 2012.
- [40] S. Pfeifer, R. Riener, and H. Vallery. An actuated transfemoral prosthesis with optimized polycentric knee joint. In *2012 4th IEEE RAS & EMBS International Conference on Biomedical Robotics and Biomechatronics (BioRob)*, pages 1807–1812, Jun 2012.
- [41] W. D. Pilkey. *Analysis and Design of Elastic Beams: Computational Methods*. Wiley, July 2002.
- [42] J. Pratt, C.M. Chew, A. Torres, P. Dilworth, and G. Pratt. Virtual model control: An intuitive approach for bipedal locomotion. *The International Journal of Robotics Research*, 20(2):129–143, 2001.
- [43] CW. Radcliffe. Four-bar linkage prosthetic knee mechanisms: Kinematics, alignment and prescription criteria. In *Prosthetics and orthotics international*, 1994.
- [44] M. Raibert, K. Blankespoor, G. Nelson, R. Playter, and the BigDog Team. Bigdog, the rough-terrain quadruped robot. In *IFAC*, 2008.
- [45] C. D. Remy, O. Baur, M. Latta, A. Lauber, M. Hutter, M. A. Hoepflinger, C. Pradalier, and R. Siegwart. Walking and crawling with alof: a robot for autonomous locomotion on four legs. *Industrial Robot: An International Journal*, 38(3):264 – 268, 2011.
- [46] Xuewen Rong, Yibin Li, Juhong Ruan, and Bin Li. Design and simulation for a hydraulic actuated quadruped robot. *Journal of Mechanical Science and Technology*, 26(4):1171–1177, Apr 2012.
- [47] Stefan Schaal. The SL simulation and real-time control software package. Technical Report, (Online) Accessed February 2011 at <http://www-clmc.usc.edu/publications/S/schaal-TRSL.pdf>, 2006.
- [48] C. Semini. *HyQ – Design and Development of a Hydraulically Actuated Quadruped Robot*. PhD thesis, Italian Institute of Technology and University of Genoa, 2010.
- [49] C. Semini, N G. Tsagarakis, E. Guglielmino, M. Focchi, F. Cannella, and D G. Caldwell. Design of HyQ - a hydraulically and electrically actuated quadruped robot. *IMechE Part I: J. of Systems and Control Engineering*, 225(6):831–849, 2011.
- [50] C. Semini, H. Khan, M. Frigerio, T. Boaventura, M. Focchi, J. Buchli, and D. G. Caldwell. Design and scaling of versatile quadruped robots. In *CLAWAR Conference*, 2012.
- [51] C. Semini, V. Barasuol, T. Boaventura, M. Frigerio, and J. Buchli. Is active impedance the key to a breakthrough for legged robots? In *International Symposium of Robotics Research (ISRR)*, 2013.
- [52] S. Seok, C. D. Onal, K. Cho, R. J. Wood, D. Rus, and S. Kim. Meshworm: A peristaltic soft robot with antagonistic nickel titanium coil actuators. *IEEE/ASME Transactions on Mechatronics*, 18(5):1485–1497, Oct 2013.

- [53] S. Seok, A. Wang, Meng Y. C., D. Otten, J. Lang, and S. Kim. Design principles for highly efficient quadrupeds and implementation on the MIT cheetah robot. *2013 IEEE International Conference on Robotics and Automation*, May 2013.
- [54] S. Shams, Dongik Shin, Jungsoo Han, Ji Yeong Lee, Kyoosik Shin, and Chang-Soo Han. Compact design of a torque sensor using optical technique and its fabrication for wearable and quadruped robots. *2011 IEEE/RSJ International Conference on Intelligent Robots and Systems*, Sep 2011. doi: 10.1109/iros.2011.6094590. URL <http://dx.doi.org/10.1109/IROS.2011.6094590>.
- [55] A. Sproewitz, T. Alexandre, M. D’Haene, R. Mockel, J. Degrave, M. Vespignani, S. Gay, A Mostafa, B. Schrauwen, and A. J. Ijspeert. Towards dynamically running quadruped robots: Performance, scaling, and comparison. In *AMAM Conference*, 2013.
- [56] A. Sprowitz, A. Tuleu, M. Vespignani, M. Ajallooeian, E. Badri, and A. J. Ijspeert. Towards dynamic trot gait locomotion: Design, control, and experiments with cheetah-cub, a compliant quadruped robot. *The International Journal of Robotics Research*, 32(8):932–950, Jul 2013.
- [57] M. Srinivasan and P. Holmes. How well can spring-mass-like telescoping leg models fit multi-pedal sagittal-plane locomotion data? *Journal of Theoretical Biology*, 255: 1–7, 2008.
- [58] A. G. Steven, S. C. Dudley, and E. U. Jack. The influence of four-bar linkage knees on prosthetic swing-phase floor clearance. *Journal of Prosthetics and Orthotics*, 8(2): 34–40, 1996.
- [59] D. Tsetserukou, R. Tadakuma, H. Kajimoto, N. Kawakami, and S. Tachi. Development of a whole-sensitive teleoperated robot arm using torque sensing technique. pages 476–481, 2007. URL <http://www.scopus.com/inward/record.url?eid=2-s2.0-34548128352&partnerID=40&md5=beed94e557099d0012535a4bb2a79cab>. cited By 3.
- [60] D. Vischer and O. Khatib. Design and development of high-performance torque-controlled joints. *IEEE T. Robotics and Automation*, 11(4):537–544, 1995. URL <http://dblp.uni-trier.de/db/journals/trob/trob11.html#VischerK95>.
- [61] A. Winkler, I. Havoutis, S. Bazeille, J. Ortiz, M. Focchi, R. Dillmann, D. G. Caldwell, and C. Semini. Path planning with force-based foothold adaptation and virtual model control for torque controlled quadruped robots. In *IEEE International Conference in Robotics and Automation*, 2014.
- [62] S. Wolf and G. Hirzinger. A new variable stiffness design: Matching requirements of the next robot generation. In *ICRA*, pages 1741–1746. IEEE, 2008. URL <http://dblp.uni-trier.de/db/conf/icra/icra2008.html#WolfH08>.
- [63] X. Zhang, H. Zheng, X. Guan, Z. Cheng, and L. Zhao. A biological inspired quadruped robot: structure and control. In *IEEE International Conference on Robotics and Biomimetics*, 2005.

